

**NPS ARCHIVE**  
**1963**  
**CRISP, H.**

Thesis  
C867

Library

U. S. Naval Postgraduate School

Monterey, California





ADDITIONAL STUDIES: FIXED BLADE PLANING OF  
ROCKS IN THE BRITTLE STRESS STATE

APPROVED:



ADDITIONAL STUDIES: FIXED BLADE PLANING OF  
ROCKS IN THE BRITTLE STRESS STATE

by

HUGH ALBERT CRISP

B.S. in Mining Engineering

THESIS

Presented to the Faculty of the Graduate School of  
The University of Texas in Partial Fulfillment  
of the Requirements

For the Degree of  
Master of Science in Petroleum Engineering

THE UNIVERSITY OF TEXAS  
JUNE, 1963

DUDLEY KNOX LIBRARY  
NAVAL POSTGRADUATE SCHOOL  
MONTEREY CA 93943-5101

NPS ARCHIVE  
963  
CRIST, H.

Thesis  
~~C 67~~



## ABSTRACT

This thesis describes fixed blade planing tests performed on Leuders limestone at atmospheric pressure using six different tip geometries. Tool-to-rock and rock-to-rock friction coefficients are measured with the planing apparatus, for W-31 tungsten carbide and Leuders limestone. Force measurements of vertical and horizontal components were taken by means of strain gages and Wheatstone bridge circuits, and displayed on an oscilloscope.

In general it was found that (1) friction has a more pronounced effect on the vertical forces than on the horizontal forces developed on a drag bit; (2) lubrication of the tip reduced the vertical forces but had little or no effect on the horizontal forces; (3) increasing the flat width on a drag bit decreases the impact forces transmitted to the rock by the bit; and (4) small negative clearance angles have little or no effect on the forces developed on a drag bit during the planing operation.



## ACKNOWLEDGEMENTS

The author wishes to acknowledge herein assistance received from others in the process of acquiring Petroleum Engineering education at The University of Texas and more directly in the completion of this thesis project. First to Dr. Carl Gatlin, Dr. Sylvain Pirson, Dr. Frank Jessen, and Dr. Kenneth Gray is due appreciation for a comprehensive introduction to Petroleum Engineering in a limited period of time. The assistance and advice of fellow graduate students Farrile Young, Martin Chenevert, Aldon Hagedorn, Norman Garner, and Ben Caudle is also acknowledged and appreciated. Appreciation is also extended to Mr. William Maurer of the Jersey Production Research Corporation for ideas expressed concerning the formulation of the problem.

Particular appreciation is due the United States Navy for providing both the opportunity and financial support for the author's postgraduate education, and to the Department of Petroleum Engineering, and the Jersey Production Research Corporation for providing, through The University of Texas Bureau of Engineering Research, equipment



and supplies used in the experimental portion of the research.

The author's thanks and "well done" are extended to Mr. Howard Webb and Mr. Herman Haydon for fabricating the friction head used in the experiments.

To his supervising professor, Dr. Kenneth Gray, for assistance, direction, and encouragement throughout the project, and to the members of the thesis committee, Dr. Carl Gatlin, and Dr. Kermit Brown, for timely and pertinent criticism, is due the author's sincere appreciation.

And finally, in token appreciation for the love and understanding tendered, and the time relinquished so that the project could be completed, this thesis is dedicated to Grace, the author's wife, Kathy, his daughter, and Mike, his son.

Hugh Albert Crisp

LT, CEC, USN

Austin, Texas  
June, 1963



## TABLE OF CONTENTS

	Page
ABSTRACT . . . . .	iii
ACKNOWLEDGEMENTS . . . . .	iv
LIST OF TABLES . . . . .	viii
LIST OF FIGURES . . . . .	ix
CHAPTER	
I. FORMULATION OF THE PROBLEM . . . . .	1
1.1 Introduction . . . . .	1
1.2 Survey of the Literature . . . . .	3
1.3 The Appl Rowley Model for Rock Failure in Drag Bit Drilling . . . . .	7
1.4 Friction . . . . .	15
1.5 Purpose . . . . .	22
II. EXPERIMENTAL WORK . . . . .	24
2.1 Apparatus . . . . .	24
2.2 Experimental Procedure . . . . .	32
2.3 Discussion of the Cutting Trial Results . . . . .	38
2.4 Discussion of the Friction Trial Results . . . . .	55
2.5 Conclusions . . . . .	59
III. IMPACT, HOLE GEOMETRY, AND RECOMMENDATIONS FOR FUTURE STUDY . . . . .	61
3.1 Impact . . . . .	61
3.2 Bore Hole Geometry . . . . .	64
3.3 Recommendations for Future Study . . . . .	67
BIBLIOGRAPHY . . . . .	71
NOMENCLATURE . . . . .	73





	Page
APPENDICES	
I. EXPANSION OF THE APPL AND ROWLEY DERIVATIONS	76
II. CALIBRATION OF THE FRICTION HEAD . . . . .	81
III. CUTTING TRIAL DATA . . . . .	83
IV. FRICTION TRIAL DATA . . . . .	104



## LIST OF TABLES

Table	Page
I. Maximum Force Components and Operating Data for the Cutting Trials . . . . .	83
II. Oscilloscope Traces for the Cutting Trials	92
III. Maximum Force Components and Operating Data for the Friction Trials . . . . .	104
IV. Oscilloscope Traces for the Friction Trials	107



## LIST OF FIGURES

Figure		Page
1	Effect of Wear on Bit Forces . . . . .	6
2	Two-dimensional Rounded Chisel Penetrating a Rigid-plastic Material . . . . .	8
3	Two-dimensional Drag Bit Blade with Rounded Edge at Low Drilling Rate . . . . .	8
4	Two-dimensional Representation of Drag Bit Operation (Dull Blade) . . . . .	11
5	Schematic Representation of Stresses Acting to Form Chip . . . . .	11
6	Real vs. Apparent Contact Area . . . . .	17
7	Variation of Friction with Load for Copper on Copper . . . . .	19
8	Friction of a Steel Ball on Copper as a Function of Sliding Speed . . . . .	20
9	Schematic Diagram of Rock Cutting Apparatus .	25
10	Cutting Head Assembly . . . . .	26
11	Location of Strain Gages on Dynamometer Ring and Wiring Diagram . . . . .	27
12	Friction Head Assembly . . . . .	29
13	Location of Strain Gages on Friction Head and Wiring Diagram . . . . .	30
14	Tip Geometries . . . . .	33
15	Force vs. Side Contact . . . . .	35
16	Maximum Vertical Force per Inch of Bit Width vs. Depth of Cut for All Bits . . . . .	41



Figure		Page
17	Maximum Horizontal Force per Inch of Bit Width vs. Depth of Cut for All Bits . . . .	42
18	Maximum Forces per Inch of Bit Width vs. Depth of Cut for the "A" Bit . . . . .	44
19	Maximum Forces per Inch of Bit Width vs. Depth of Cut for the "B" Bit . . . . .	46
20	Maximum Forces per Inch of Bit Width vs. Depth of Cut for the "C" Bit . . . . .	47
21	Maximum Forces per Inch of Bit Width vs. Depth of Cut for the "D" Bit . . . . .	49
22	Maximum Forces per Inch of Bit Width vs. Depth of Cut for the "E" Bit . . . . .	50
23	Maximum Forces per Inch of Bit Width vs. Depth of Cut for the "F" Bit . . . . .	51
24	Horizontal Forces per Inch of Bit Width vs. Depth of Cut for the "D" Bit, Lubricated and Dry . . . . .	53
25	Vertical Forces per Inch of Bit Width vs. Depth of Cut for the "D" Bit, Lubricated and Dry . . . . .	54
26	Typical Friction Trial Force Traces . . . .	56
27	Effect of Vertical Load on Tool-Rock Friction Factor . . . . .	57
28	Effect of Vertical Load on Rock-Rock Friction Factor . . . . .	58
29	Vertical Section of Slabbing Caused by Reflected Tension Waves in a Steel Plate .	63
30	Participation of Reflected Waves in the Planing Operation . . . . .	64
31	Stepped Hole Produced by Christensen Bit .	67
32	Linear Failure Envelope for $\sigma_c \neq \sigma_t$ . . . .	68





Figure		Page
33	The Appl and Rowley Graphical Solution for Shear Angle, $\delta$ , with the Proposed Simplification . . . . .	78
34	Calibration Chart for Friction Head . . . . .	82



## CHAPTER I

### FORMULATION OF THE PROBLEM

#### 1.1 Introduction

The problem of determining what factors affect the penetration rate of a drilling tool is severely complicated by the environment in which such tools normally operate. In the hole, inaccessability of the bit, high temperatures, high pressure, vibration, dust, and moisture combine to preclude direct measurement of forces on the bit. In order to compile design information for improved tools or better utilization of existing ones, the engineer is forced to rely on measurements taken on the derrick floor or to duplicate in the laboratory certain basic drilling operations. He must then attempt to interpret them so that similarities with actual drilling are accentuated, but such that phenomena associated with the laboratory apparatus do not adversely affect the interpretation.

Since 1955, several authors have published data derived from laboratory experiments in which rock was broken by various methods, and the forces required to accomplish



this were recorded. A brief summary of the methods reported would include impacting with a chisel in a drop tester, planing, drilling with a rotary drill press, and loading to failure in conventional materials testing machines. In the beginning most of these tests were conducted at atmospheric pressure, and no control was exercised over pore pressure in the rock. Recently, pressure cells have been constructed in which both confining pressure and pore pressure can be controlled while basic drilling operations are executed therein. Instrumentation has progressed from the simple stop watch, measuring stick and tachometer, to the more sophisticated strain gage, thermocouple, and transducer circuits. Some experimenters have used the photoelastic effect to display actual stress patterns around a point of interest.

In order to make this ever-improving laboratory data applicable to the field drilling problem someone must reduce the experimental findings to tables and simple empirical relationships, which the tool designer and the drilling superintendent can translate into improved drilling equipment and/or technique, and hence into lower costs per foot. Drilling rate formulas have been published by Simon [1], Hartman [2], Appl and Rowley [3], Maurer [4], and others. These formulas have focused attention on



parameters which affect drill performance, but have not provided fool-proof empirical means for predicting same. Improvement of these formulas will require the efforts of many individuals performing investigations of limited scope to test the validity of small portions of the proposed relationships. This thesis reports the results of one such limited research project covering additional investigation of the planing process at atmospheric pressure.

## 1.2 Survey of the Literature

Several investigators have studied aspects of rock failure as produced by planing. Goodrich [5] performed tests with a laboratory planer. Chip formation was projected for study by means of a Jones and Lamson comparator, which permitted him to record and observe the activity at the bit-rock contact with 36 magnifications. Goodrich observed a cyclic failure with fine and coarse chips being formed alternately. The size and geometry of the large chips seemed to be quite reproducible as the bit advanced across the material. He explained these phenomena in terms of a critical angle existing between the rock face being cut and the tool surface doing the planing, the idea being that crushing action would occur permitting the tool to advance and achieve this angle, but that as soon as the angle





was achieved the large chip would be formed and the cycle would repeat. Bit movement was tied to chip formation by postulating that crushing occurred as the bit rebounded after the formation of a large chip, and that chips were formed as the bit built up elastic energy, deforming without advancing.

Fairhurst and Lacabanne [6] described the mechanics of rock failure due to planing in the following manner:

- (1) Build-up of forces and deflection of bit as the bit contacts the rock, until fracture suddenly occurs from the bit tip to the rock surface.
- (2) Rapid release of energy stored in deflection of the bit to impact the rock.
- (3) Build-up of forces again, with slight falling off as minor fractures occur along lines connecting with the previous fracture line. This action continues until a further major fracture occurs, and the cycle is repeated.

These authors also recognized that impact plays a part in the planing mechanism. They further stated that the resultant force on the cutting tool was determined principally by friction conditions between the rock and the front face of the cutting tool and by the compressional strength of the rock. They analyzed the forces developed on the tool by the bit-rock contact as follows:



As the bit advances into the rock a contact pressure develops normal to the front cutting face and the rock is constrained to move upwards across the face, thus developing in the rock a frictional force acting downwards parallel to the bit front face. The opposite and equal reaction force on the bit tends to push the bit up out of the rock. The important practical factor to note is that it is this frictional effect that results in the necessity to use heavy axial thrusts in rotary drilling to maintain bit contact with the rock. . . . Measurement of the inclination of the resultant force on the bit indicates that the coefficient of friction is highly variable, as would be expected from the heterogeneous nature of most rocks, and assumes high values sometimes greater than unity. The effective downward force caused by friction develops a contact pressure on the underface of the bit which, as the bit advances, results in frictional drag and abrasive wear. The stress effective in causing fracture is confined to a small area around the tip and, as the width of flat increases, the downward thrust required to produce the necessary resultant stress must be increased proportionally. The friction drag will also increase with thrust. . . . Thus, whilst the thrust for a given penetration rate varies directly with the state of wear the torsional force is only partly affected.

Figure (1) copied from reference [6] illustrates these findings.

In 1961 and 1962, Gray and co-workers [7, 8, 9] performed extensive drag bit tests in which rake angle, clearance angle, cutting speed, and depth of cut were studied to determine if a critical angular relationship existed between rock and tool faces. They found that some rake angles produced a more efficient cutting action than others, but that local bit-to-rock contact was so small that very minor wear of the cutting element drastically



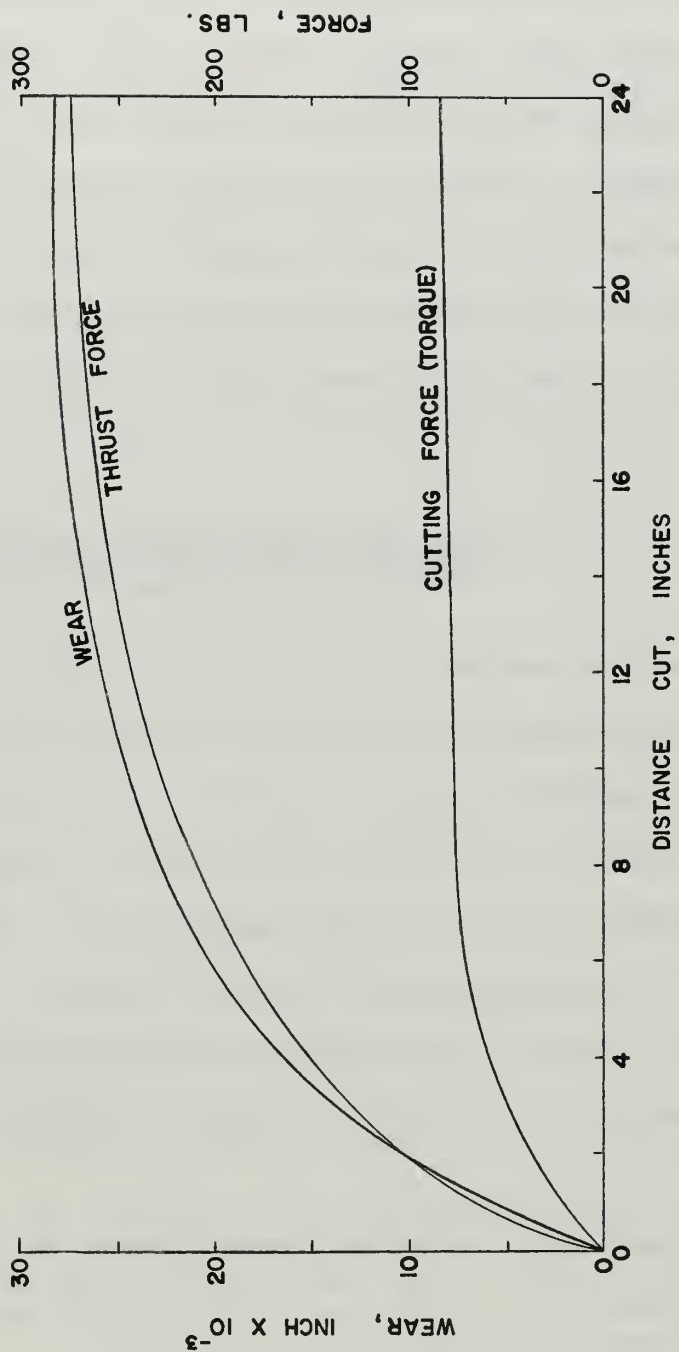


FIG. 1 EFFECT OF WEAR ON BIT FORCES.



changed the local rake angle. Therefore, a simple critical angle hypothesis did not adequately explain all of their experimental observations. Gray's high speed photography confirmed that planing action produced large and small chips alternately; however, contrary to Goodrich's findings that the volume of large chips and dust were approximately equal, his photography and cutting-size analyses indicated that the volume of chips was much greater than that of the dust.

### 1.3 The Appl Rowley Model for Rock Failure in Drag Bit Drilling

Appl and Rowley [3] proposed an analytical solution for the stresses acting on a drag bit during the planing operation. Their analysis handles the entire planing problem in two parts; the first a plastic solution for depths of cut less than radius of the cutting edge, and the second an elastic, shear failure solution for depths of cut greater than the cutting edge radius. Quoting directly from the paper the derivations are as follows:

On the basis of Prandtl's work for the penetration of wedge shaped chisels, Cheatham has worked out the stress distribution on a rounded chisel penetrating a rigid plastic material. The two-dimensional case is considered as shown in figure (2). According to Cheatham, the expression for this pressure,  $p(\gamma)$ , is





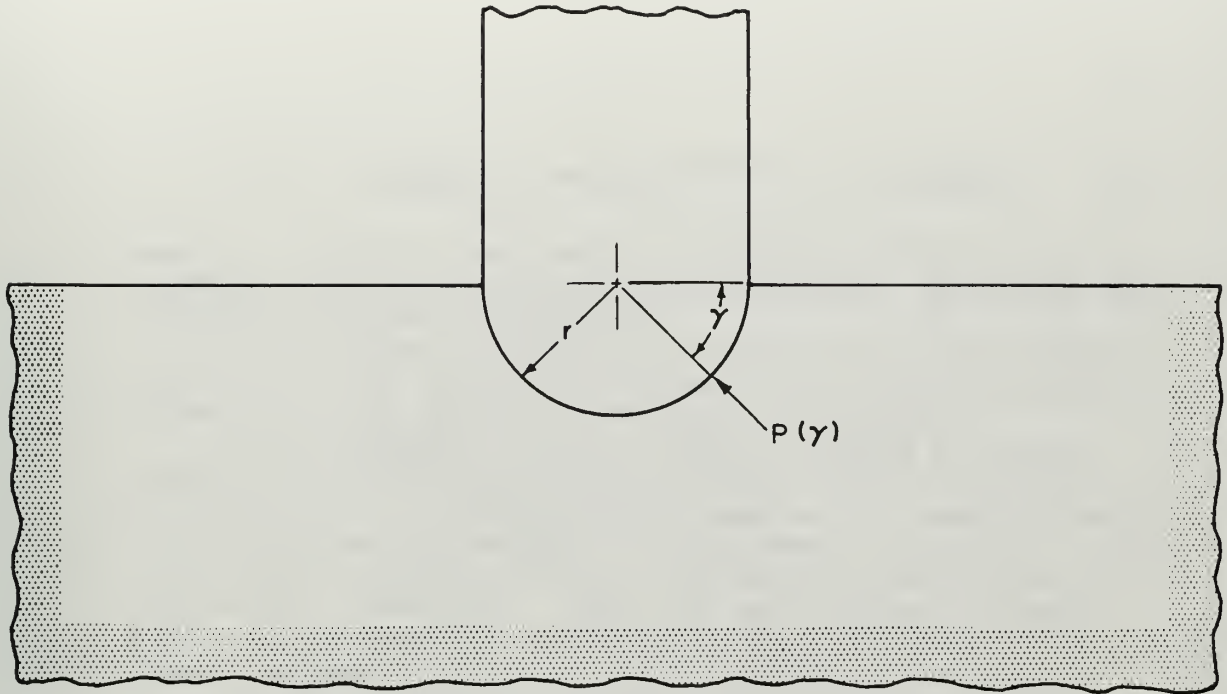


FIG. 2: TWO-DIMENSIONAL ROUNDED CHISEL PENETRATING A RIGID-PLASTIC MATERIAL (After Appl and Rowley)

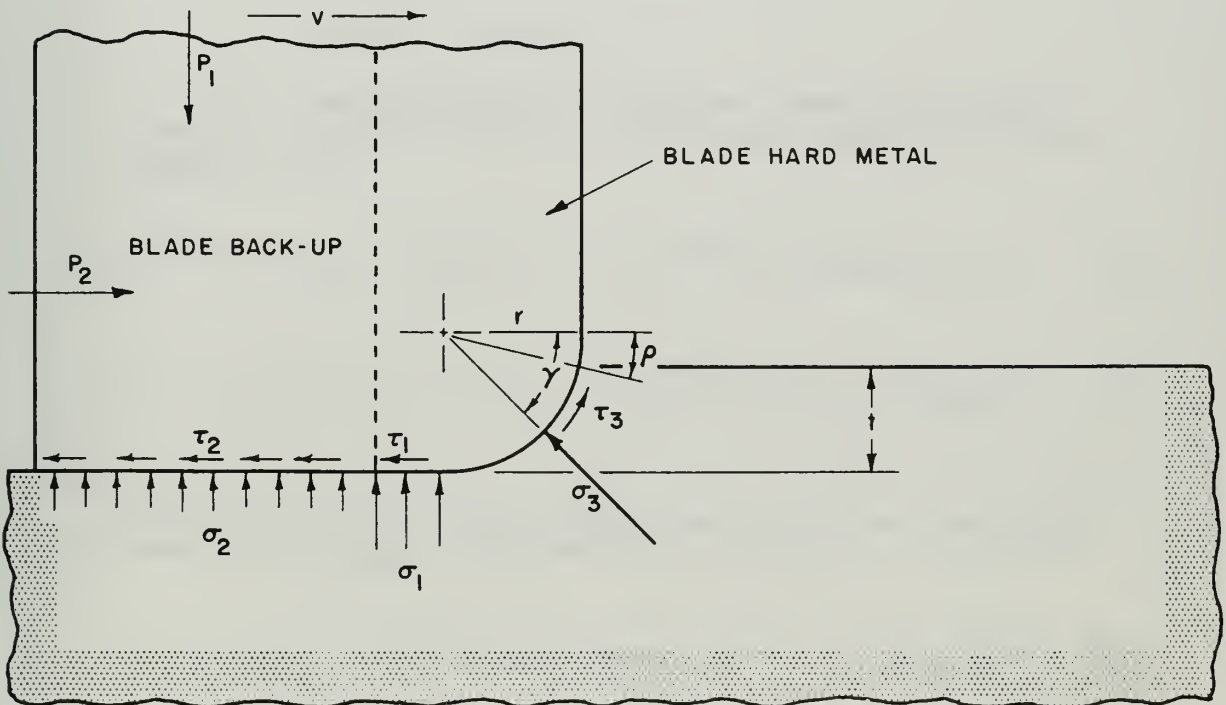


FIG. 3: TWO-DIMENSIONAL DRAG BIT BLADE WITH ROUNDED EDGE AT LOW DRILLING RATE (After Appl and Rowley)



$$p(\gamma) = \frac{\sigma_c}{2 \sin \phi} [(1 + \sin \phi) e^{2\gamma \tan \phi} - (1 - \sin \phi)] \quad (1)$$

where  $\sigma_c$  is the compressive strength of the rock, including effects of hydrostatic pressure, and  $\phi$  is the angle of internal friction.

This stress distribution will be a good approximation to that existing in the vicinity of a drag bit blade when the formation behaves as a plastic.

The situation for the drag bit blade is represented two-dimensionally in figure (3). The friction is included in an approximate manner by considering the effect on bit weight of the shear stress  $\tau_3$ , which is assumed proportional to the theoretical value of the normal stress  $\sigma_3$ . This is not entirely correct since  $\sigma_3$  is derived by Cheatham on the basis of no shear stress.

Using Cheatham's equation for  $\sigma_3$  and assuming that  $\mu$  is the effective coefficient between tool and rock gives

$$\sigma_3(\gamma) = p(\gamma)$$

$$\tau_3(\gamma) = \mu \sigma_3(\gamma)$$

The expressions for vertical and horizontal load per inch of radial width can then be written respectively

$$P_1 = (Z-z)\sigma_2 + (z-r)\sigma_1 + r \int_{\rho}^{\pi/2} (\sin \gamma + \mu \cos \gamma) \sigma_3 d\gamma \quad (2)$$

$$P_2 = (Z-z)\tau_2 + (z-r)\tau_1 + r \int_{\rho}^{\pi/2} (\cos \gamma - \mu \sin \gamma) \sigma_3 d\gamma \quad (3)$$

These forces are then separated into the components due to "cutting stresses"  $P_{11}$  and  $P_{21}$ .

$$P_{11} = r \int_{\rho}^{\pi/2} (\sin \gamma + \mu \cos \gamma) \sigma_3 d\gamma \quad (4)$$



$$P_{21} = r \int_0^{\pi/2} (\cos \gamma - \mu \sin \gamma) \sigma_3 d\gamma \quad (5)$$

Substituting for  $\sigma_3$  and integrating the expressions for  $P_{11}$  and  $P_{21}$  gives

$$\begin{aligned} \frac{P_{11}}{r\sigma_c} = & [A_1 \left( \frac{e^{\pi \tan \phi}}{4 \tan^2 \phi + 1} \right) (2 \tan \phi + \mu) - \mu A_2] \\ & - [A_1 \left( \frac{e^{2 \tan \phi \rho}}{4 \tan^2 \phi + 1} \right) (2 \tan \phi + \mu) - \mu A_2] \sin \rho \\ & + [A_1 \left( \frac{e^{2 \tan \phi \rho}}{4 \tan^2 \phi + 1} \right) (1 - 2\mu \rho) - A_2] \cos \rho \end{aligned} \quad (6)$$

$$\begin{aligned} \frac{P_{21}}{r\sigma_c} = & [A_1 \left( \frac{e^{\pi \tan \phi}}{4 \tan^2 \phi + 1} \right) (1 - 2\mu \rho) - A_2] \\ & - [A_1 \left( \frac{e^{2 \tan \phi \rho}}{4 \tan^2 \phi + 1} \right) (1 - 2\mu \rho) \sin \rho \\ & - [A_1 \left( \frac{e^{2 \tan \phi \rho}}{4 \tan^2 \phi + 1} \right) (\mu + 2 \tan \phi) - \mu A_2] \cos \rho \end{aligned} \quad (7)$$

$$\text{where } A_1 = \left( \frac{1 + \sin \phi}{2 \sin \phi} \right), \quad A_2 = \left( \frac{1 - \sin \phi}{2 \sin \phi} \right)$$

As shown in the following brittle solution, the components  $P_{11}$  and  $P_{21}$  are used to determine bit weight,  $W_1$ , and bit torque  $T_1$ , due to "cutting stresses." Continuing with the brittle solution directly from the paper:

The mathematical model chosen to represent the physical situation encountered by the drag bit blade is shown schematically in figure (4).

Static equilibrium of the chip in figure (5) requires that



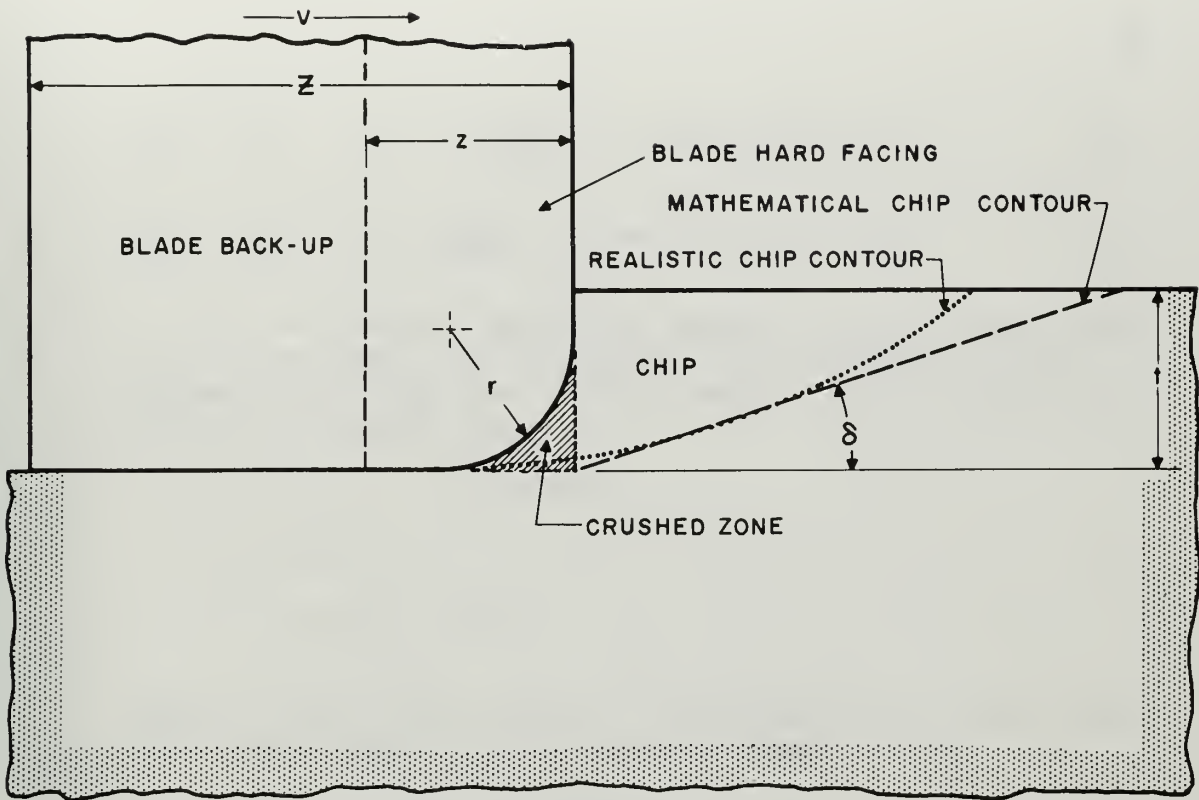


FIG. 4: TWO-DIMENSIONAL REPRESENTATION OF DRAG BIT BLADE OPERATION (DULL BLADE) (After Appl and Rowley)

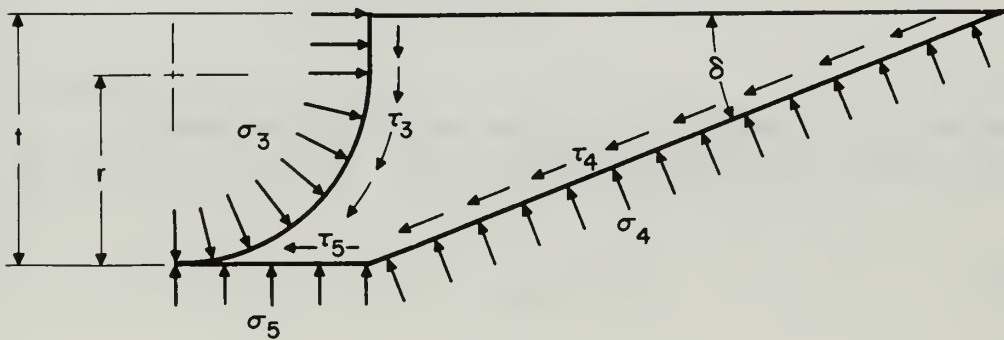


FIG. 5: SCHEMATIC REPRESENTATION OF STRESSES TO FORM CHIP (After Appl and Rowley)





$$\sigma_3 t - \tau_3 r - \tau_5 r - \frac{t}{\sin \delta} \{ \tau_4 \cos \delta + \sigma_4 \sin \delta \} = 0 \quad (8)$$

$$\sigma_3 r - \tau_3 t - \sigma_5 r - \frac{t}{\sin \delta} \{ \sigma_4 \cos \delta - \tau_4 \sin \delta \} = 0 \quad (9)$$

If we assume that rock shears on the plane where  $\tau_4 = c + \sigma_4 \tan \phi$  we can write the equation for the normal stress on the cutting edge,  $\sigma_3$ , by using the following equalities

$$\sigma_5 = \sigma_3 \quad (\text{assumed})$$

$$\tau_3 = \mu \sigma_3$$

$$\tau_5 = \mu_1 \sigma_5 = \mu_1 \sigma_3$$

where  $\mu$  (tool-rock) and  $\mu_1$  (rock-rock) are the effective coefficients of friction. Thus

$$\sigma_3 = \frac{c / \sin^2 \delta}{[1 - \frac{r}{t} (\mu + \mu_1)] [\cot \delta - \tan \phi] - \mu (1 + \tan \phi \cot \delta)} \quad (10)$$

The angle  $\delta$  \* of the shear plane is found by setting the derivative of  $\sigma_3$  with respect to  $\delta$  equal to zero. The result is transcendental, but is solved graphically by plotting assumed values of  $\delta$  against the quantity

$$\frac{1 - \frac{r}{t} (\mu + \mu_1)}{\mu}$$

for various values of  $\phi$ .

We assume that the radial distribution of normal stress is uniform. The vertical and horizontal loads per inch of radial width are respectively:

$$P_1 = (r + \mu t) \sigma_3 + \sigma_1 (z - r) + \sigma_2 (Z - z) \quad (11)$$

---

\*Note: This derivation is contained in Appendix I.



$$P_2 = (t - \mu r)\sigma_3 + \mu\sigma_1(z - r) + \mu\sigma_2(Z - z) \quad (12)$$

The vertical and horizontal forces due to cutting stresses are

$$P_{11} = (r + \mu t)\sigma_3 \quad (13)$$

$$P_{21} = (t - \mu r)\sigma_3 \quad (14)$$

The bit weight and bit torque due to cutting stresses are obtained as follows

$$W_1 = n \int_{L_1}^{L_0} P_{11} dL = \int_{L_1}^{L_0} (r + \mu t)\sigma_3 dL \quad (15)$$

$$T_1 = \frac{n}{12} \int_{L_1}^{L_0} P_{21} L dL = \frac{n}{12} \int_{L_1}^{L_0} (t - \mu r)\sigma_3 L dL \quad (16)$$

Figures (2), (3), (4), and (5), although renumbered to conform to the order of this thesis, are taken from the original paper. The symbolism has also been changed slightly to maintain continuity with other work completed and in progress at The University of Texas.

Gray [9] provides a detailed critique of the analysis proposed by Appl and Rowley and to include it in total here would be needless repetition; however, one of his points pertains directly to the work that follows.

Quoting Gray's remarks:

It is interesting to compare the experimental relationship between  $F_v$  and  $F_h$  with the analytical



relation between bit weight and bit torque for the shear failure case. By dividing equation (15) by (16), the ratio of bit weight to torque is

$$\frac{W_1}{T_1} = \frac{n \int_{L_1}^{L_0} (r + \mu t) \sigma_3 \, dL}{\frac{n}{12} \int_{L_1}^{L_0} (t - \mu r) \sigma_3 \, L dL} \quad (17)$$

$$\frac{W_1}{T_1} = \frac{(r + \mu t) (L_0 - L_1)}{\frac{1}{12} (t - \mu r) \left( \frac{L_0^2 - L_1^2}{2} \right)}$$

$$\frac{W_1}{T_1} = \left( \frac{24}{L_0 + L_1} \right) \left( \frac{r + \mu t}{t - \mu r} \right) \quad (18)$$

The ratio given in equation (18) is independent of the rock properties  $\phi$  and  $\sigma_c$ ; rock properties are involved only to the extent that they influence the friction coefficient  $\mu$ .

A similar approach for the plastic failure solution yields.

$$\frac{W_1}{T_1} = \left( \frac{24}{L_0 + L_1} \right) \left( \frac{\mu + \cos \rho - \mu \sin \rho}{1 - \sin \rho - \mu \cos \rho} \right) \quad (18a)$$

where again, except for  $\mu$ , equation (18a) is independent of rock properties.

As can be seen from the foregoing derivations, Appl and Rowley disregarded the stresses on the flat, back up portion of the bit behind the cutting tip. The purpose



of the experimental portion of this thesis is to evaluate whether this portion of their analysis is valid. Friction contributes one force component to the stresses developed behind the cutting tip.

#### 1.4 Friction

Two of the parameters, considered by Appl and Rowley to have a bearing on the force required to drill rock with a drag bit, are the tool-rock coefficient of friction and rock-rock coefficient of friction. It is considered desirable to try to measure these friction coefficients under conditions similar to those associated with the planing experiments and to determine, if possible, what effect lubrication of the contact area has on the frictional forces.

The exact nature of frictional forces is unknown; however, it is known that friction always acts to oppose the movement of one body over another when their surfaces come in contact. The force which opposes the initial movement of one body over another is called starting, or static, friction; the force which opposes continued movement of a moving body is called sliding, or kinetic, friction. Static friction is greater than kinetic friction. In general, friction is governed by three laws:





(1) Friction is independent of the area of contact between the solids. (2) Friction is proportional to the load normal to the contact surfaces. (3) The coefficient of kinetic friction is less than the coefficient of static friction and is independent of the relative velocity of the rubbing surfaces. Since drilling is carried on under high temperatures and pressures, a closer study is warranted.

Friction is a surface contact phenomenon. Solid surfaces, even highly polished surfaces, are rough and irregular under a microscope. When one solid surface supports another, contact is achieved only at the high points (asperities) of each. As the weight of the top body settles on the bearing surface, load is transferred through these asperities. At first the stress concentrations at these asperities are very high, exceeding the indentation hardness of the softer material, so the softer material flows until sufficient contact between the bodies is achieved to re-establish equilibrium. The end result is a penetration of the surface of the softer material by the asperities of the harder one and perhaps fusion of the materials at the points of real contact. If the load is doubled, the areas of real contact must also be doubled in order to support the load. This area of real contact for flat steel surfaces 21 square centimeters in macroscopic area has been



measured electrically and the following table is taken from Bowden and Tabor [10].

# AREA OF REAL CONTACT BETWEEN FLAT STEEL SURFACES

<u>Load Kg</u>	<u>True Area of Contact</u>	<u>Fraction of Macroscopic Area in Contact</u>
500	0.05	1/400
100	0.01	1/2000
5	0.0005	1/40,000
2	0.0002	1/100,000

Figure (6) indicates the nature of real and apparent contact areas.

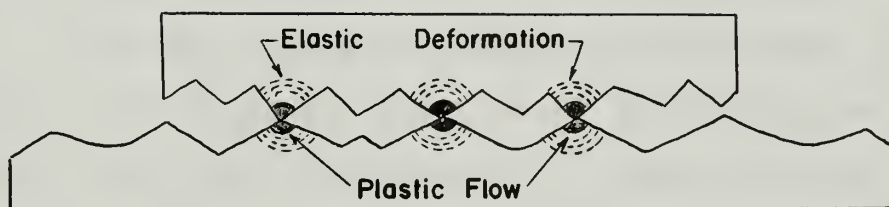


Figure (6) Real vs Apparent Contact Area.

In the regions where intimate contact occurs, strong adhesion takes place and the specimens become, in effect, a continuous solid. As a lateral force is applied the junctions must be sheared, and the force required to



do this is approximately equal to the frictional resistance. The removal of the vertical force, and the separation of the bodies normally without apparent tensile failure is explained by the elastic rebound of the materials as the load is removed, i.e. the rebounding of the materials accomplishes separation of the cold joints. If the material to be sheared has a mean shear strength,  $s$ , and a true contact area,  $A$ , we may write

$$F = As \quad (19)$$

Continuing the analysis:

$$\frac{F}{W} = \frac{As}{AP} = \frac{s}{P} = \frac{\text{Shear strength}}{\text{Yield pressure}} \quad (20)$$

Experiments show that  $s$  is roughly equal to the bulk shear modulus of the softer material of the sliding pair.

Load may affect the measured coefficient of friction. This is particularly so if the sliding materials do not have clean surfaces, or if their surfaces are subject to chemical reactions producing rusts or other oxides. This is explained by returning to the mechanism of asperite contact. Under heavy loads the asperites are driven through the coating and fused to the pure material; thus the shear strength of the pure material influences the frictional forces. If the contact is only subjected to light loading the shear characteristics of the coating



will determine the frictional forces. Figure (7) , copied from Bowden and Tabor, indicates graphically this relationship between friction coefficient and load for copper sliding on copper.

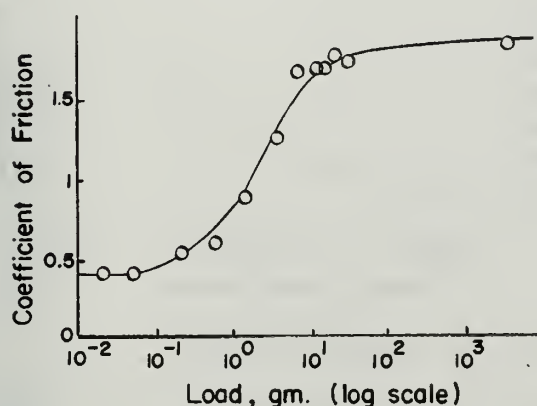


Fig. (7): Graph showing variation of friction with load for copper on copper.

At high loads the oxide film is penetrated and the friction is high. At low loads the friction is essentially that of copper oxide. (After Bowden and Tabor.)

Bowden and Tabor have also shown experimentally that at high sliding speeds the temperature rise at the surface between two sliding surfaces is roughly proportional to  $\sqrt{v}$ , where  $v$  is the sliding velocity. This could mean hot spots in excess of 500 degrees centigrade on the face of the bit. The temperature rise at the interface will be limited by the lower melting point of the two materials in contact, unless an exothermal chemical reaction takes place simultaneously at the point of contact. If melting actually takes place at the points of contact, the molten material may act as a lubricant and reduce the







friction coefficient, at least until seizure. Figure (8), taken from Bowden and Tabor, illustrates this point.

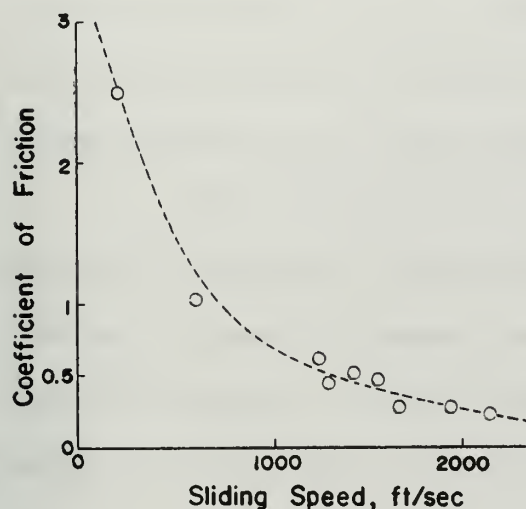


Figure (8): Friction of a steel ball on copper as a function of sliding speed. By way of reference the peripheral speed of a drag bit drilling an 8" hole at 450 rpm is in excess of 900 fpm. (After Bowden and Tabor.)

The mechanism of friction as discussed previously applies to friction between metal surfaces. It is dependent on deformation by asperities, and the formation and subsequent shearing of metallic junctions in the presence of localized "hot spots." It has been experimentally determined that the same mechanism occurs with materials such as rock salt, which is brittle at low stress states, but which flows plastically under high temperatures and pressures. In evaluating experimental data contained elsewhere in this thesis, the author has assumed that the mechanism also applies to Leuders limestone.

Tungsten carbide tips are prepared by sintering fine powders of tungsten and carbide together with a cobalt binder. At high temperatures the cobalt has been observed



to be expressed from metal cutting tools and smeared over the carbide particles, providing lubrication between the sliding surfaces. This leads one to expect a relatively low coefficient of friction between tungsten carbide and other materials at high temperatures.

The function of a boundary lubricant is to interpose a film between the sliding surfaces that will reduce the true contact between the asperities, but that is itself easily sheared. At high temperatures the attraction between the lubricant film and either surface is lost, the asperities penetrate the film easily and the lubricant approaches uselessness. Mathematically we can express boundary lubrication effects in an equation similar to the one derived for friction:

$$F = A(\alpha s + (1-\alpha)s_1) \quad (21)$$

where  $\alpha$  = fraction of the area over which metallic junctions are formed.

$s$  = shear strength of the material to be sheared.

$A$  = true contact area.

$s_1$  = shear strength of the lubricant.

The main function of lubrication in the rock planing process is to cool the bit, and to remove cuttings in actual drilling operations. To the extent that the



lubricant reduces contact between the asperities of the bit and the rock surfaces, the lubricant is detrimental to drilling efficiency.

Drilling is carried on under sufficient pressure to alter the surface characteristics of the rock. The problem of isolating frictional forces from cutting stresses is a difficult one because under pressure the metal actually indents the rock surface and on movement, planing results. For this reason a special friction measuring head was fabricated, and is further described in the following chapter.

### 1.5 Purpose

The purpose of this project is to provide basic information needed to improve the Appl and Rowley mathematical model of the stresses developed on a drag bit during the planing operation. Gray and Lawler [11] raised the question of the effect of frictional drag forces on bit stresses on the basis of early experimental work. More recently Gray [9], Maurer [12] and others have questioned whether the Appl and Rowley model could be improved by the addition of a friction term defining the forces on the flat back-up portion of the bit blade. It is intended that the experimental work reported by this thesis shed some light on the role of friction in developing stresses on a drag



bit blade. More specifically, this thesis is limited to studying:

(1) The effect of flat horizontal and vertical contact areas adjacent to the cutting tip for six different tip configurations.

(2) The effect of tool-rock and rock-rock friction on the stresses developed in a drag bit. Laboratory measurements are taken, and rock-to-rock and tool-to-rock coefficients of friction are computed for Leuders limestone and W-31 tungsten carbide.

(3) The effect of lubrication on friction factors.

General conclusions are drawn from the data recorded herein.





## CHAPTER II

### EXPERIMENTAL WORK

#### 2.1 Apparatus

The basic apparatus used in this investigation has been described in detail elsewhere [9]. Figure (9) shows a pictorial diagram of the cutting head and its associated electronic measuring components. Figure (10) is a diagram of the cutting head assembly, and Figure (11) shows a wiring diagram for the strain gages and their location on the dynamometer ring. The strain gage circuits are described by Gray [9] as follows:

Eight type SR-4 strain gages were mounted on the dynamometer to provide two complete strain gage bridge circuits, one for vertical and one for horizontal force components. The four gages comprising each bridge were wired as shown in figure (11) so that the strains appearing at the vertical channel due to a horizontal force were balanced out, as were signals from the horizontal gages due to a vertical force. This system was very sensitive; just the slightest touch on the cutting tool gave sensible force response.

The cited reference contains a detailed analysis of the limitations of this equipment including a discussion of



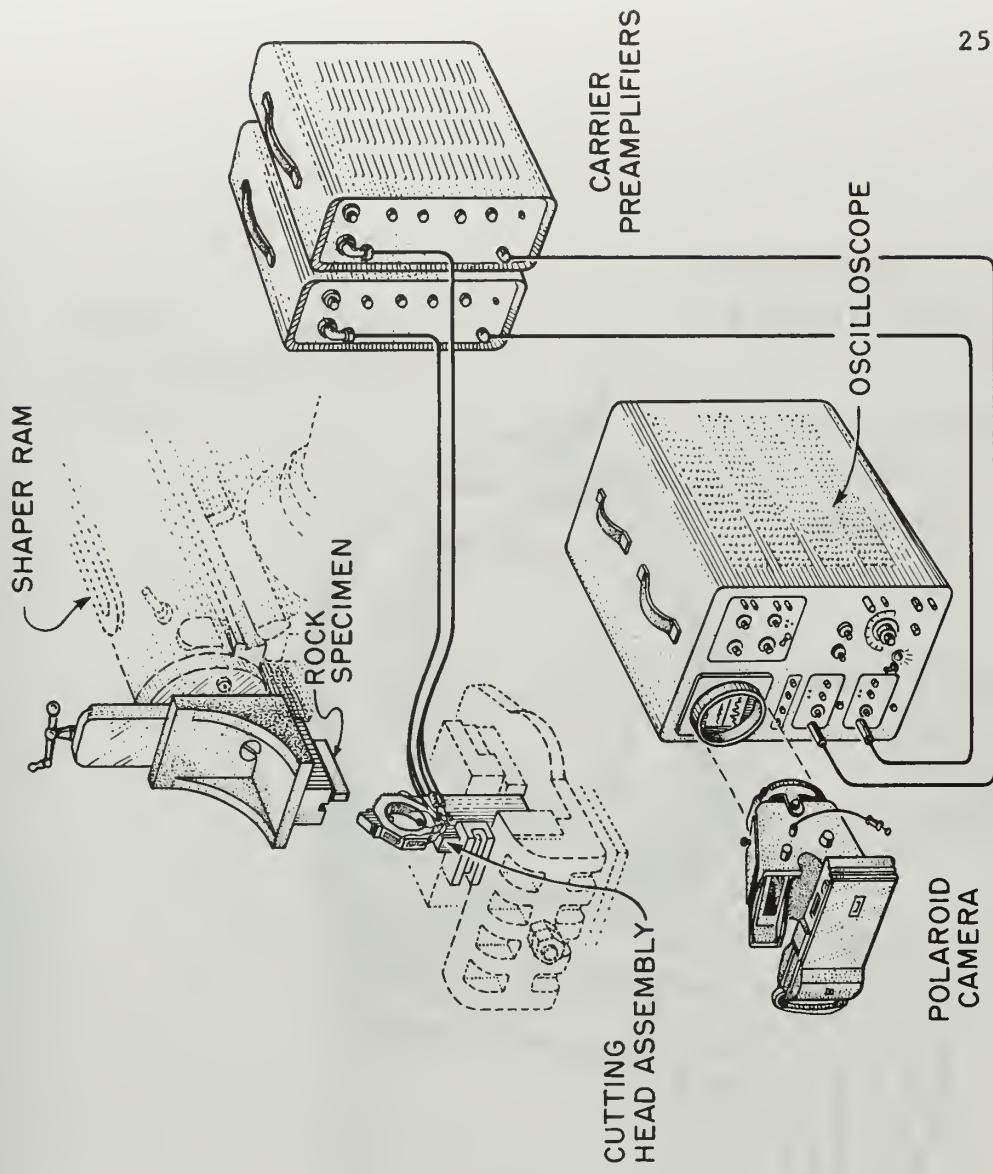


FIG. 9: SCHEMATIC DIAGRAM OF ROCK CUTTING APPARATUS



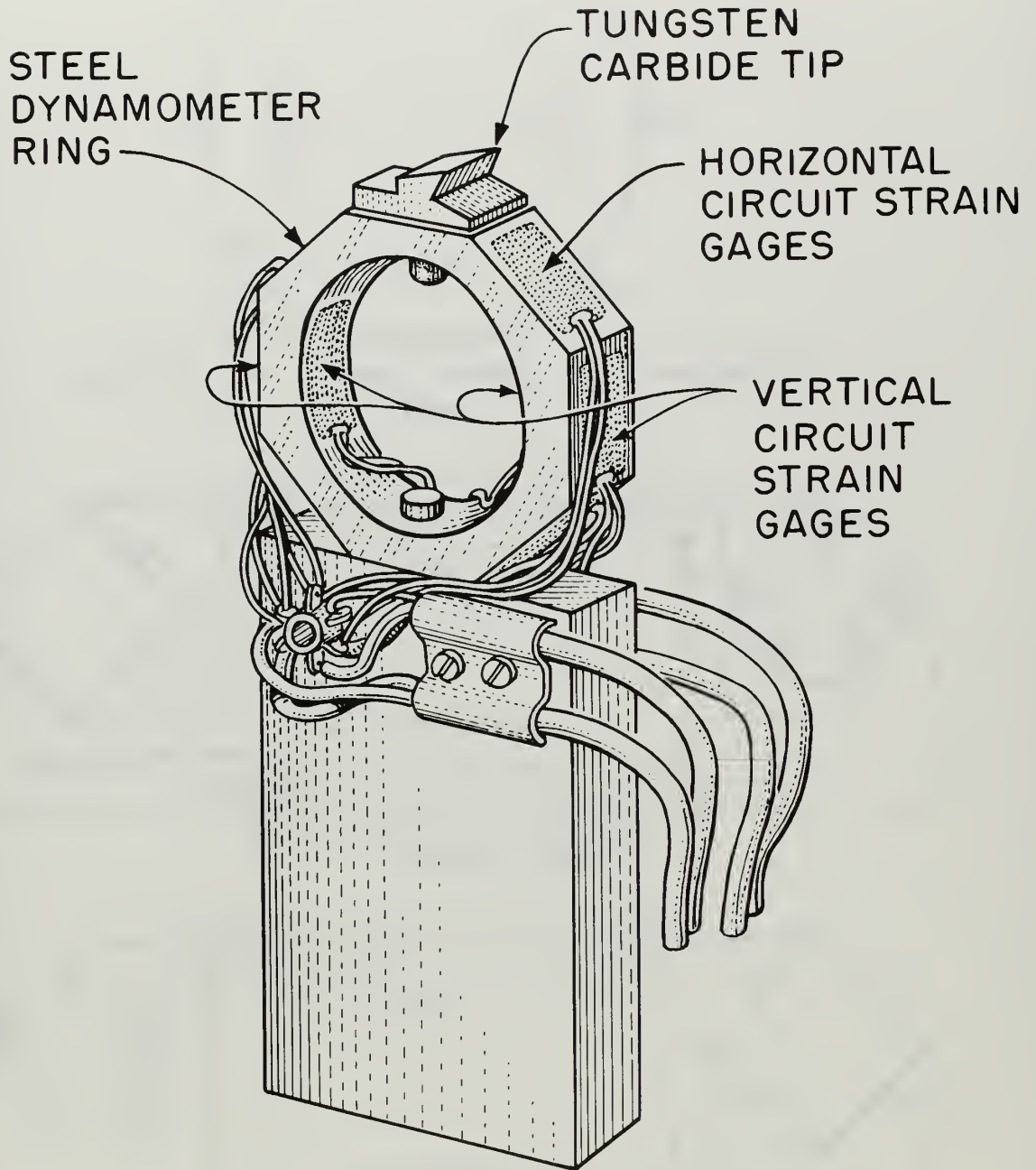
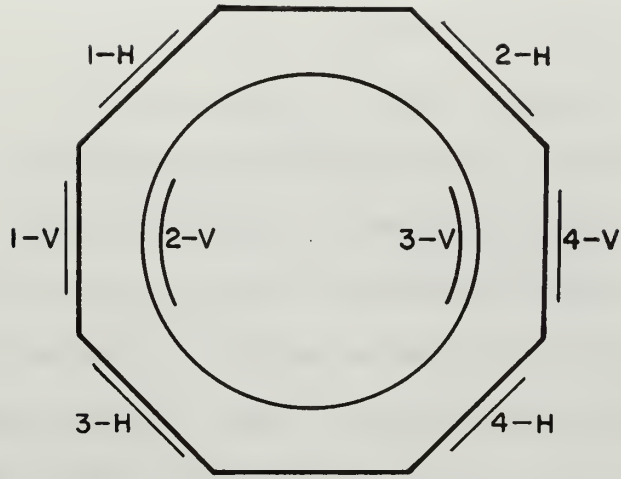


FIG. 10: CUTTING HEAD ASSEMBLY (After Gray)





LOCATION OF STRAIN GAUGES ON DYNAMOMETER RING

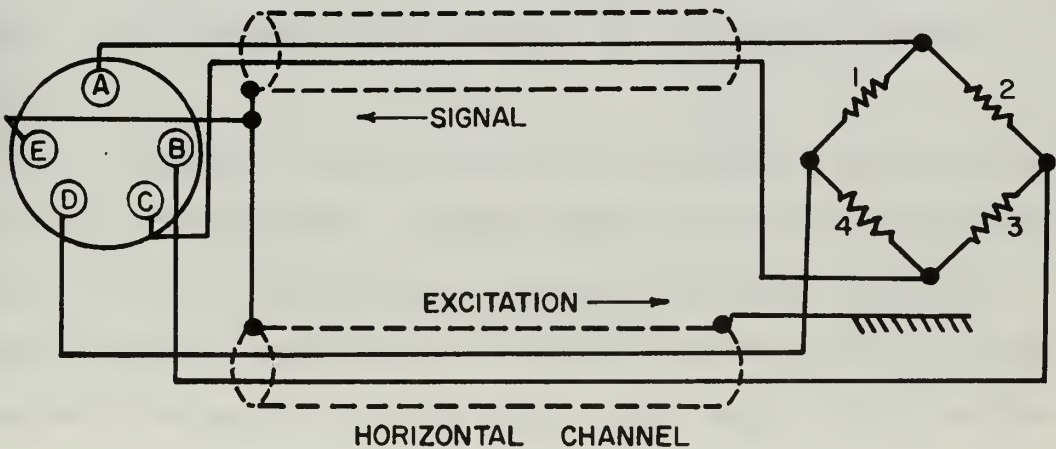
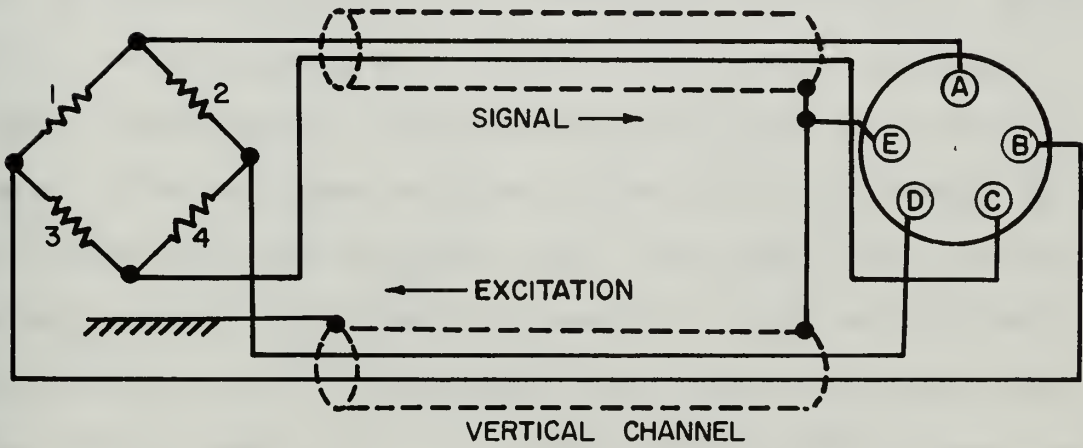


FIG. II. LOCATION OF STRAIN GAGES ON DYNAMOMETER RING AND WIRING DIAGRAM





the fidelity of strain gage signals and the vibrational aspects of force measurement in this manner.

It was originally planned to use the cutting head with a flat friction blank of tungsten carbide to measure tool-rock friction, but with increasing vertical loads the cutting head tended to rotate offering the edge of the blank (a sharp cutting edge) to the rock instead of the flat friction surface intended. Also, the cutting head provided no practical means of securing a rock sample for use in determining rock-rock friction coefficients. Therefore a friction head was constructed as shown in Figure (12). The friction head is more rigid than the cutting head. With the sides affixed it mounts a rock sample up to 1 inch wide and 4 inches long. When the sides are removed it mounts the same bits used with the cutting head. The friction head is obviously more torque resistant than the cutting head, but it is also less sensitive, requiring higher oscilloscope sensitivities to display a readable trace.

Figure (13) shows the strain gage circuits used with the friction head. Eight type SR-4 strain gages were mounted on each dynamometer ring to provide a complete bridge circuit each for the vertical and horizontal force components detected at each ring. The legs of the bridge



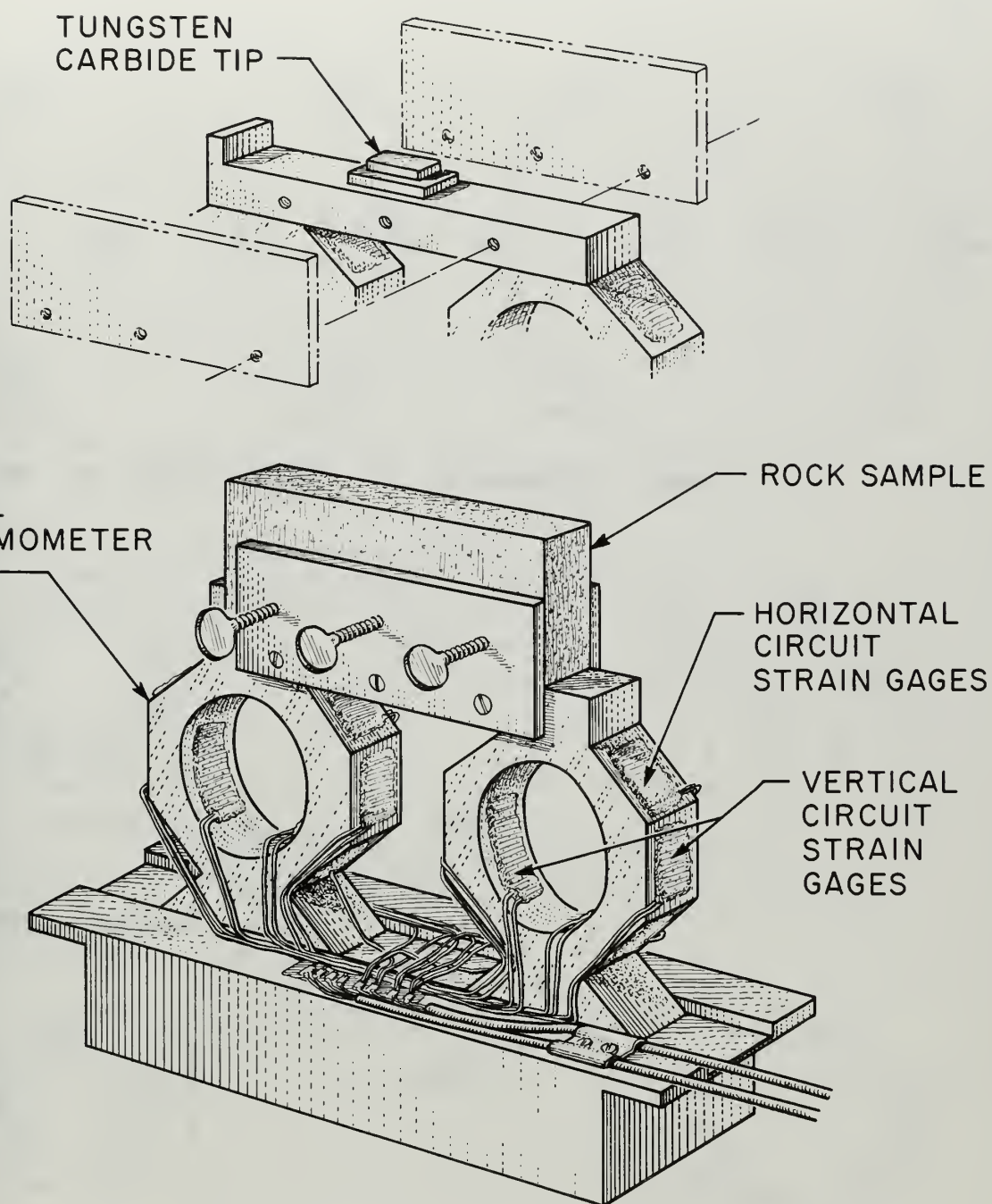
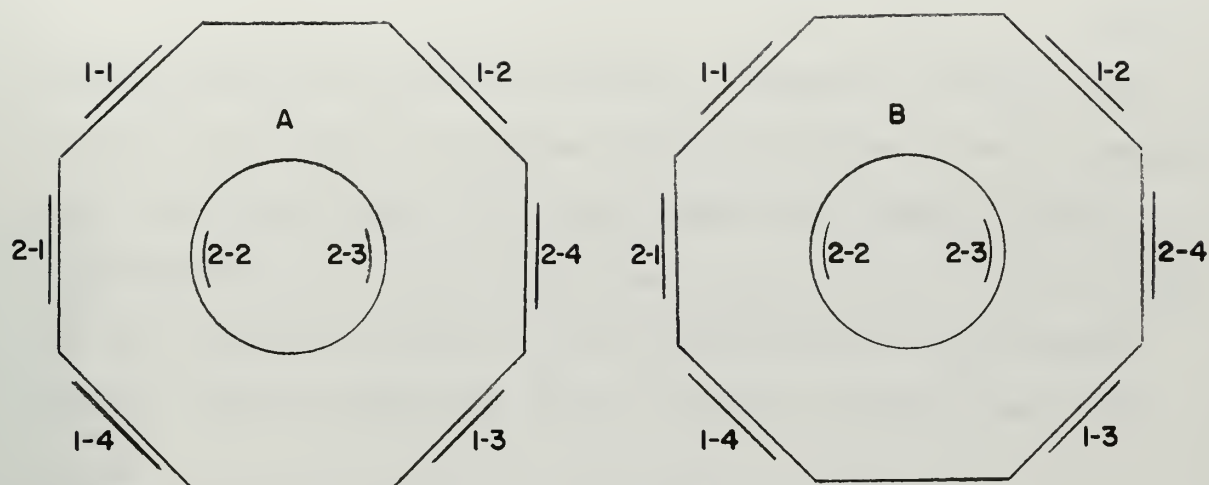
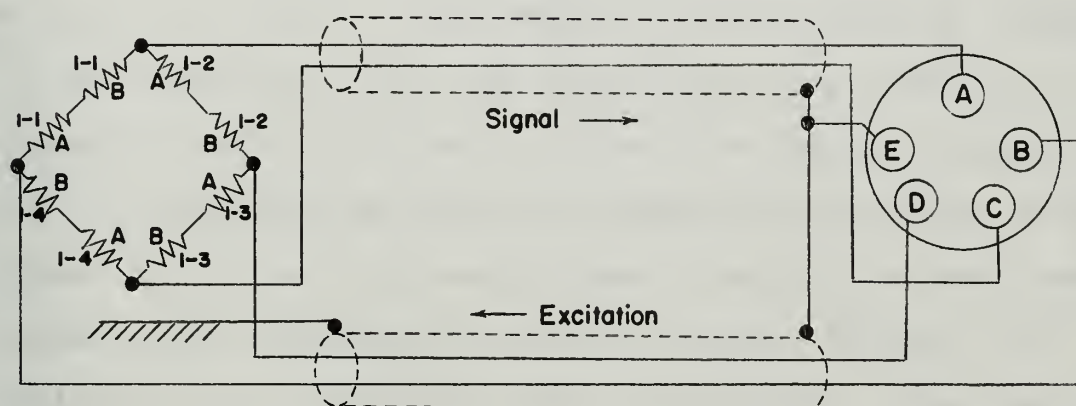


FIG. 12. FRICTION HEAD ASSEMBLY.

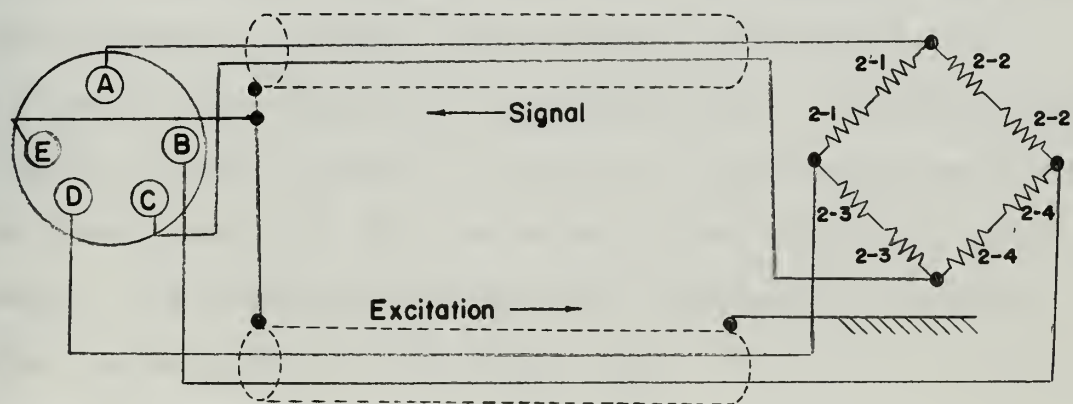




LOCATION OF STRAIN GUAGES ON DYNAMOMETER RINGS.



HORIZONTAL CHANNEL



VERTICAL CHANNEL

FIG. 13 LOCATION OF STRAIN GUAGES ON FRICTION HEAD AND WIRING DIAGRAM.





circuits were then wired in series as shown in Figure (13) so that the signals from the "stretch" gages on each dynamometer and the signals from the compression gages on each dynamometer were additive in the bridge circuit. The wiring of the bridge provided for the cancellation of horizontal strain signals appearing at the vertical channel and vice versa.

A conventional Steptoe Shaper was modified so that a 3-1/2" by 2" by 1" rock sample could be securely clamped to the underside of the ram in the position normally occupied by the cutting tool. Either the cutting head or the friction head was securely clamped to the frame of the shaper in a vise. The strain gage circuits on either head assembly were connected through two Sanborn Carrier Pre-amplifiers to a Tectronics 535A oscilloscope. The oscilloscope had a dual preamplifier with an integral 100 kilocycle chopper, and thus could display horizontal and vertical force components simultaneously. A Hewlett-Packard polaroid camera clamped to the face of the scope recorded the force traces as the ram moved across either of the heads. The scope and camera were triggered to coincide with the movement of the shaper ram.



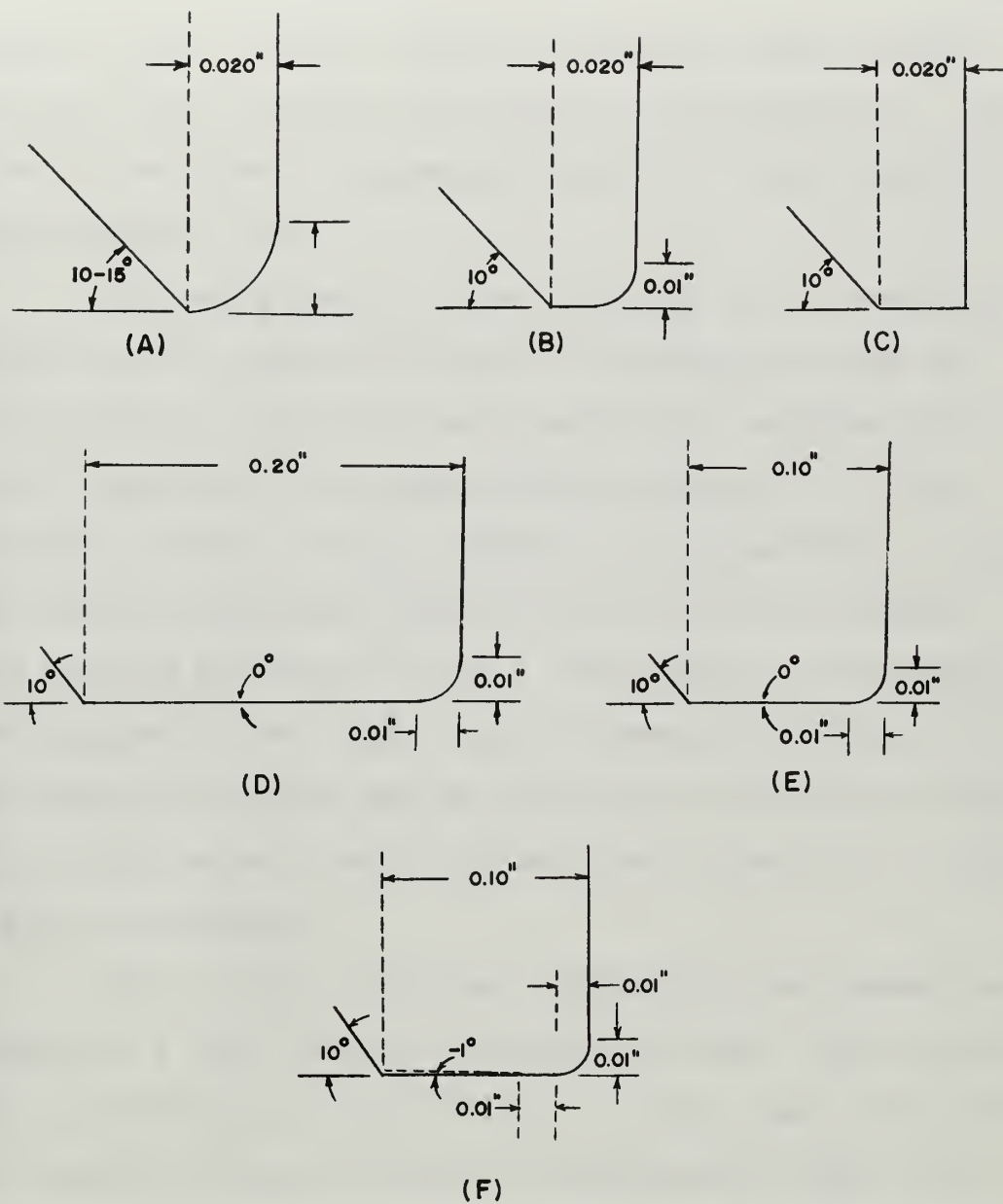


## 2.2 Experimental Procedure

Rock samples were cut from quarried bricks of Leuders limestone to approximately 1" x 3" x 4" dimensions. All of the cutting trial specimens except the wet-dry specimen were from the same brick. The sample width was approximately twice the bit width. Successive passes were made with a single rock specimen over one bit geometry until at least two readings were obtained for each of the following depths of cut: .005", .010", .015", .020", .030", and .040". The cutting velocity was in each case 15 feet per minute. Oscilloscope traces of both horizontal and vertical force components were recorded using the polaroid camera. The cuttings were collected after each pass and are on file at the Department of Petroleum Engineering, The University of Texas. The contact area was measured after each pass on those bits with flat horizontal areas behind the cutting tips (B, C, D, E, and F). This procedure was repeated with each of the bit geometries shown in Figure (14).

The effect of side contact between rock and bit was measured by taking successive force readings at constant depths of cut with the same bit, but without planing the edges level between passes. A series of this type was run using two different depths of cut, .010" and .020",





MATERIAL : TUNGSTEN CARBIDE.

BLADE WIDTH = 0.516 INCH.

FIG. 14 TIP GEOMETRIES.



and the "B" bit. Forces plotted from these data indicate that side contact between rock and bit are negligible. The plot of forces versus successive heights of side contact is shown as Figure (15).

Following the dry runs with each bit, a new rock specimen was cut, first with the "D" bit dry for each of the six depths of cut previously mentioned, and then with the bit lubricated with common SAE 30 machine oil. The lubrication of the rock-bit contact was accomplished by the simple means of placing a drop of oil on the bit surface before passing the rock over it. The physical arrangement of the apparatus precluded contact between the rock and oil before cutting so there was no possibility that absorption of oil by the pores altered the physical properties of the rock prior to planing.

Tool-to-rock friction coefficients were measured by attaching a flat blank of tungsten carbide, 0.25 square inches in macroscopic area, to the friction head, with the sides removed, midway between the dynamometer rings. The rock surface was planed smooth and the ram positioned over the blank so that the leading edge of the rock sample covered the friction blank. The depth of cut setting on the ram was then adjusted so that a vertical force was registered on the oscilloscope. The shaper was started



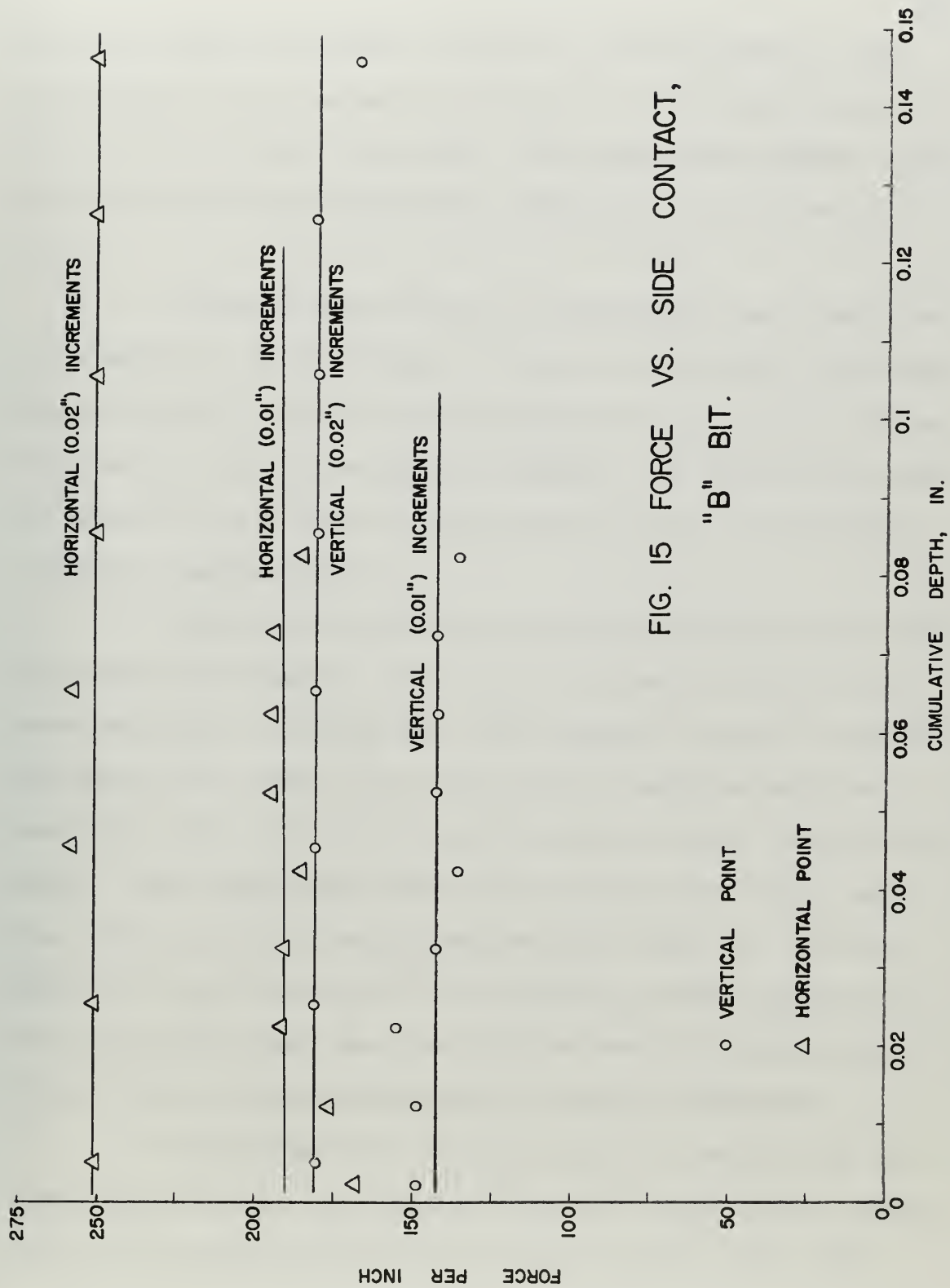


FIG. 15 FORCE VS. SIDE CONTACT,  
"B" BIT.





and the scope and camera triggered simultaneously. Runs were made in this manner starting with vertical forces of 5, 25, 50, 75, and 100 pounds. The runs were repeated with the friction blank lubricated, again with SAE 30 machine oil.

Rock-to-rock friction coefficients were measured by clamping a rock specimen in the friction head, and again adjusting the vertical forces applied to 5, 25, 50, 75, and 100 pounds before starting the shaper. No attempt was made to measure the effect of lubrication on the rock-to-rock friction coefficients.

All of the tool-rock friction runs were made with the same rock sample. All of the rock-rock friction runs were made with the same two rock samples; however, neither the tool-rock sample nor the rock-rock samples had been used for runs prior to the initial run in their respective sets. This means that after the initial run in each set the friction factor being measured was that of a surface which had been subjected to increasing surface pressures. It is believed that the rock encountered by a drag bit in a bore hole has been subjected to similar treatment.

Horizontal and vertical forces developed in the cutting tests were calculated from the oscilloscope traces using the calibration data described by Gray [9]. The



most common maximum vertical and horizontal force deflections were read and recorded as  $D_v$  and  $D_h$ . The force components were computed by multiplying the deflection values by the calibration factors recorded in Appendix II.

The static friction peak is readily recognizable at the start of motion on the horizontal force traces of the tool-rock friction runs (trials numbered 1 through 9 in Appendix IV). The vertical force deflection for computing the coefficient of static friction was read at a point directly above the static peak on the horizontal trace. The deflections for computing the coefficients of dynamic friction were read as close to the static peak as possible, but in all cases at a point where the vertical deflection was approximately equal to that read before motion was imposed on the system. In a few cases, as the higher vertical forces were imposed, a small horizontal force component was observed before motion started. In these cases a base line was recorded (prior to loading) and the horizontal deflection used to compute the friction factor was measured from the recorded base line. In many cases the vertical force levels were observed to increase or decrease after movement was established. The increased forces were due to the build-up of rock particles on the metal friction surface as the rock moved across it. Local decreases were recorded as the friction surface was dragged clean again.



Deflection readings were taken from the traces at a point close to the start of motion for the rock-rock friction runs. A static friction peak was not recognizable with these runs. Although there were minor fluctuations in the force levels as the samples moved across each other, the general trend in all of the runs was for the vertical forces to decrease. This was because the contact surfaces of the samples were not precisely parallel. The samples were tilted so that the spacing was always closer at the beginning of the run than it was at the end of the run. This should not adversely affect the friction factors computed, however, since friction coefficients are not a function of macroscopic contact area. The approximate macroscopic surface contact area, measured from the scarred lower rock surface was 1 square inch. For discussion purposes the vertical force imposed in pounds is numerically equal to the surface pressure in pounds per square inch.

### 2.3 Discussion of Cutting Trial Results

Data were taken from the laboratory planing experiments in the form of force versus time traces recorded from the oscilloscope by the polaroid camera. These traces are displayed in Appendix III. Notice the force fluctuations displayed by the traces. These fluctuations were much more





pronounced with the "A", "B", and "C" bits, the ones with small flats. The "D", "E", and "F" bits having larger flats did not exhibit this large fluctuation. With the first group of bits this fluctuation was commonly on the order of 40 to 60 pounds. With the second group the fluctuation was limited to 20 pounds or less in most cases. Lubrication did not seem to affect the force fluctuation. The lack of fluctuation for the wide flat bits indicates that this facet of tip geometry damps the impact mechanism. The peak horizontal and vertical force traces were higher for this group than for the group with small flats, which may be a qualitative indication of the importance of impact on the planing operation. In all cases, the damping of force fluctuations by the bit flat was more pronounced on the vertical trace than it was on the horizontal trace. It is interesting to note that the flats seemed to cause a greater increase in vertical force than they did in horizontal force. This observation was also reported by Fairhurst and Lacabanne [6].

Another general observation is that a very highly compacted rock powder was observed on the flats after each dry trial. The surface pressures on the rock under the bit flats were on the order of 2000 psi or greater. Chenevert [13] has determined that Leuders limestone





exhibits plastic failure characteristics under compressive loads of 2000 psi. The compressed rock powder was not detected on the perpendicular bit face or on the curved surface of the tip.

The curves in Figures (16) and (17) compare the horizontal and vertical force per inch of bit width for each bit at each depth of cut. The vertical forces build to a maximum at some critical depth of cut and thereafter remain constant. The shape of the "A" bit curve indicates that this critical depth of cut may be tied to the tip radius. The vertical forces increased with increase in flat width for all depths of cut for the given tip radius (.010 inch). It is believed that this phenomenon is due in part to the flat damping out the impact action of the bit along the vertical axis. The horizontal force traces did not exhibit as marked a critical tip radius phenomenon as did the vertical forces. Although the rate of rise in horizontal force with increasing depth of cut declined for the deeper cuts, it did not appear that a constant maximum force level would be achieved as for the vertical traces. This may be explained by realizing that as the cuts increase in depth there is more mass of rock for the bit to move; since the mass is small in comparison with the forces in the system its effect will be small, but not necessarily negligible.



A, B, C, D, E, & F BITS, LEUDER & LIMESTONE.

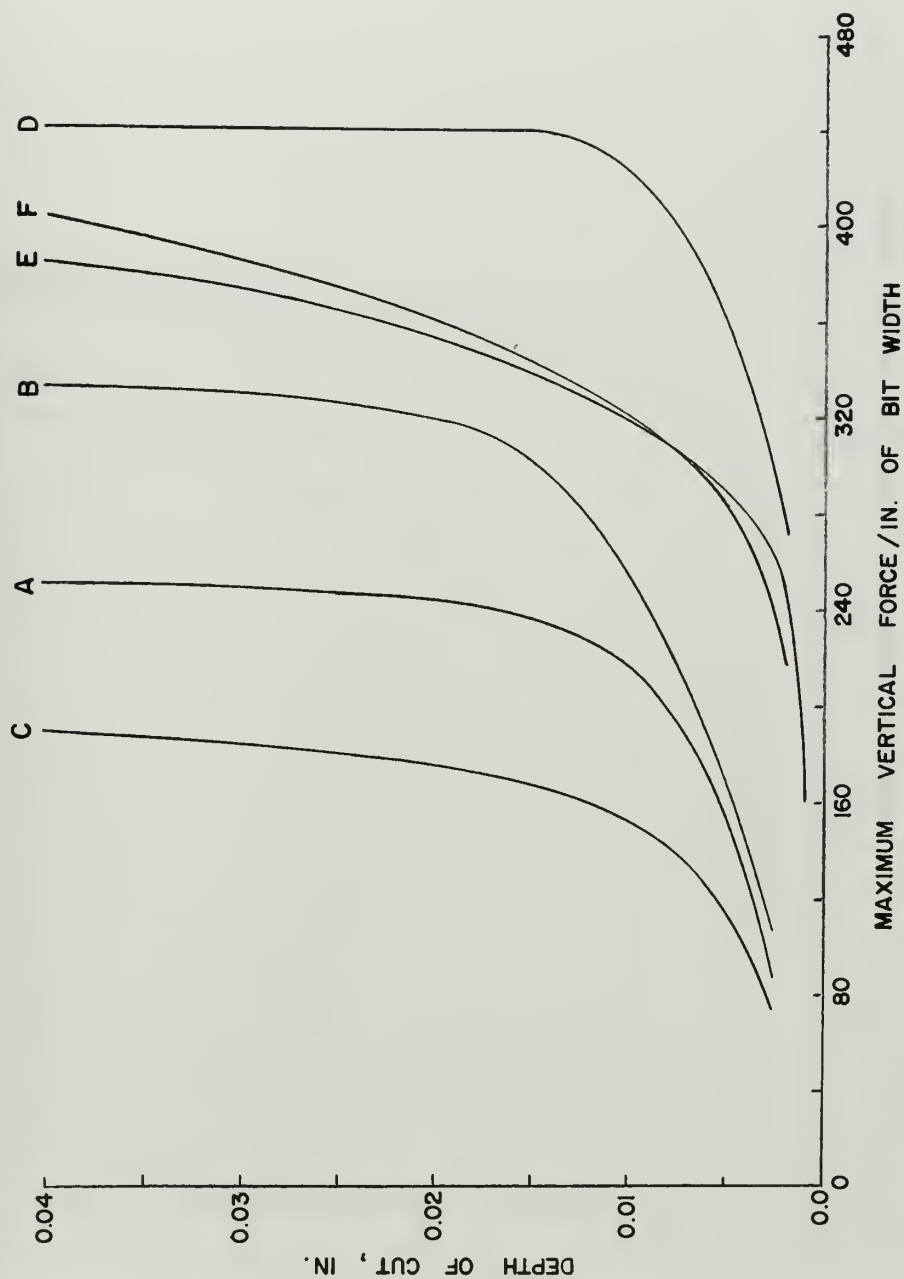


FIG. 16 COMPARISON OF MAXIMUM VERTICAL FORCE/INCH OF BIT WIDTH VS. DEPTH OF CUT FOR ALL BIT GEOMETRIES.



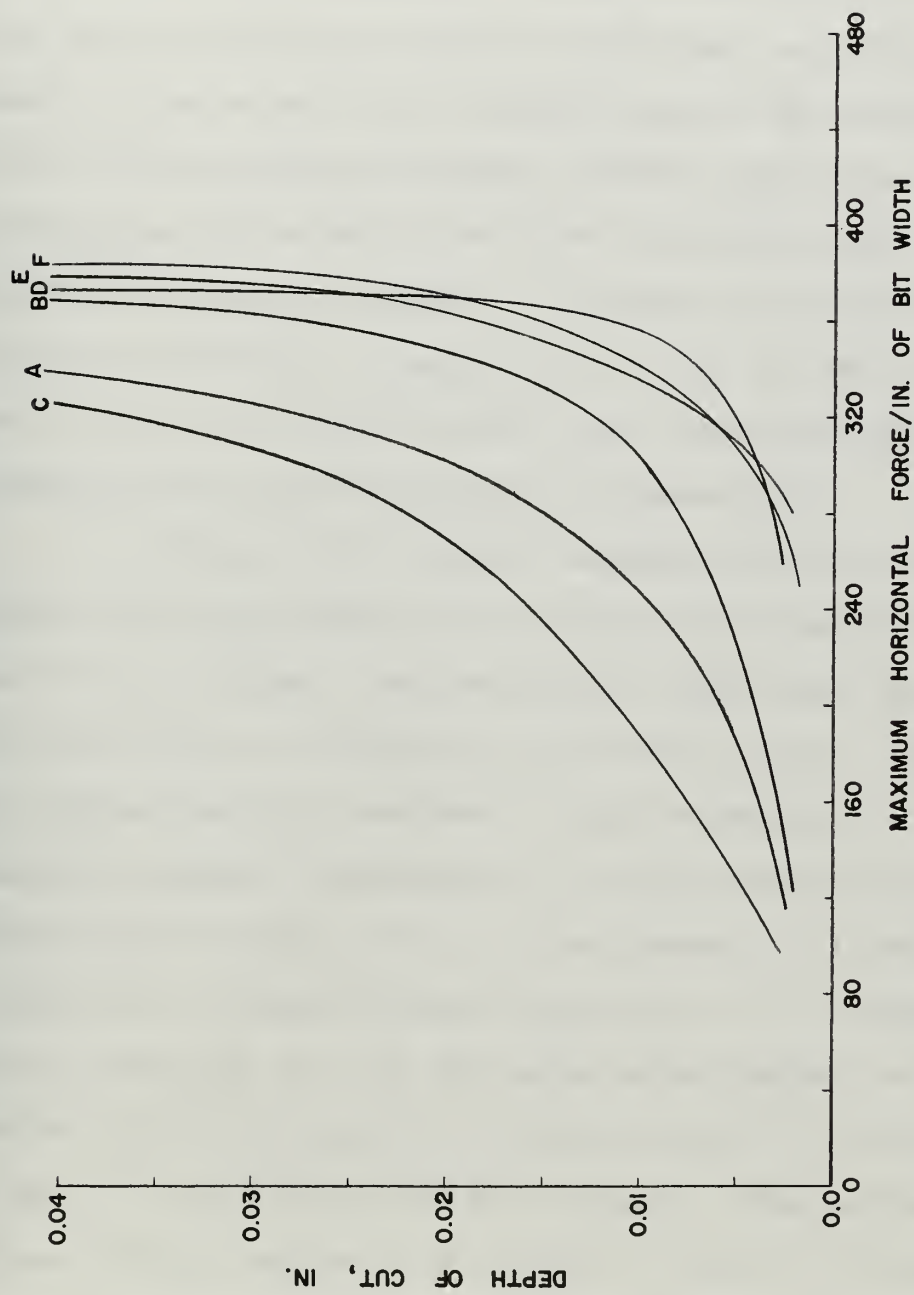


FIG. 17 COMPARISON OF MAXIMUM HORIZONTAL FORCE/INCH OF BIT WIDTH VS. DEPTH OF CUT FOR ALL BIT GEOMETRIES.



Increasing the flat widths did not have as marked an effect on the horizontal forces as was first expected. This may be explained first by recalling that friction depends on the normal force rather than on the macroscopic contact area between surfaces; second, horizontal impact damping was not as efficient with increasing flat width as the vertical impact damping. If impact does influence rock failure by planing, as many [5, 6, 7, 8, 9] have indicated that it does, one would expect force requirements to increase as the impact mechanism is damped out.

Figure (18) displays maximum vertical and horizontal forces per inch of bit width versus depth of cut for the "A" bit trials. The horizontal forces were greater than the vertical forces for all depths of cut. The vertical forces reached a maximum at approximately  $t = r$  and remained constant thereafter. The horizontal forces increased most rapidly for  $t < r$  but seemed to increase at a constant, although reduced, rate for  $t > r$ . Measured vertical forces for the "A" bit were approximately 40 pounds heavier for each depth of cut than for the "C" bit (similar to the "A" bit but with no tip radius). The horizontal forces for all values of  $t$  for the "A" and "C" bits were almost identical. The shapes of the vertical force curves for the two bits are similar.





SAMPLE I-1, A-BIT, LEUDERS LIMESTONE.

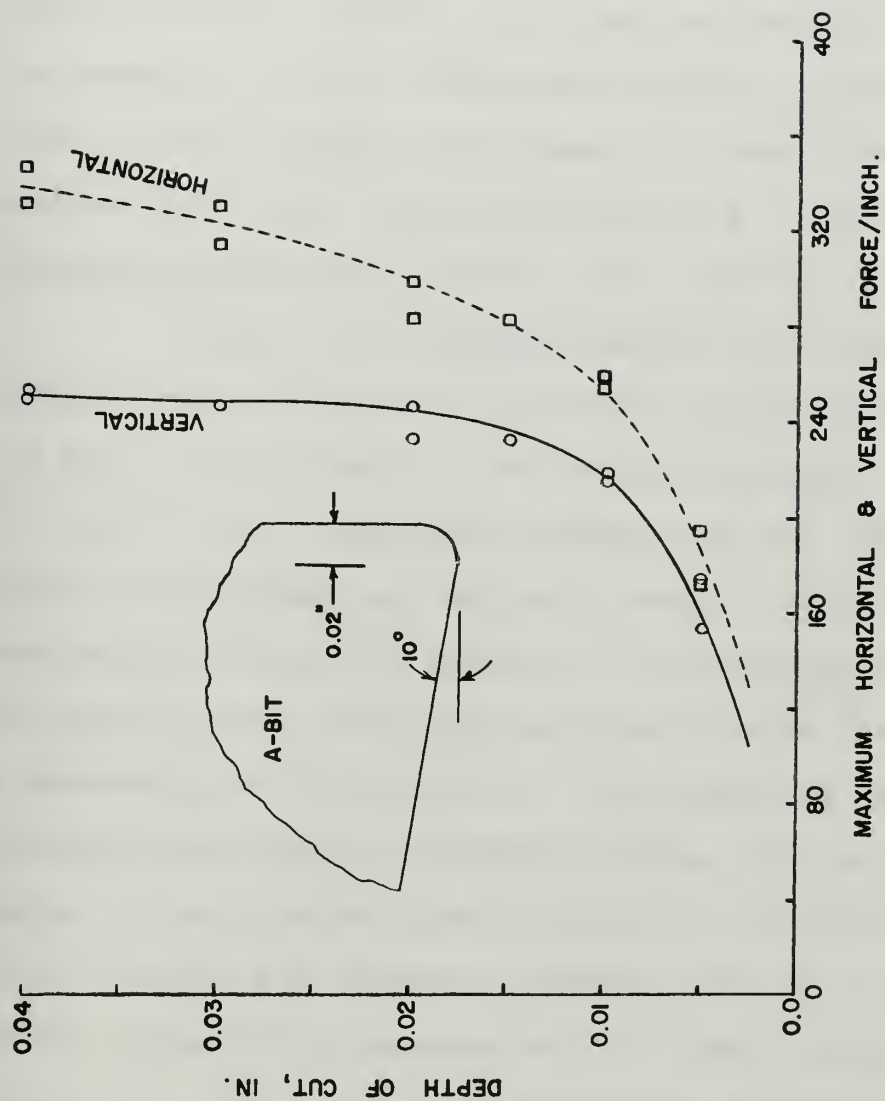


FIG. 18 MAXIMUM VERTICAL & HORIZONTAL FORCE / INCH OF BIT WIDTH VS. DEPTH OF CUT, "A" BIT.



Figure (19) displays maximum vertical and horizontal forces per inch of bit width versus depth of cut for the "B" bit trials. Again the horizontal forces were greater for all depths of cut than the vertical forces. The shapes of the two curves are similar. Forces again built up most rapidly for values of  $t$  less than  $r$ . The maximum horizontal forces measured at  $t = .040$ " were approximately equal for the "B", "E", and "D" bits.

Figure (20) displays maximum vertical and horizontal forces per inch of bit width versus depth of cut for the "C" bit trials. The horizontal forces recorded for the "C" bit trials were greater for all depths of cut than the corresponding vertical forces. There was no similarity between the shapes of the horizontal and vertical force curves. The vertical force curve increased at a decreasing rate to about  $t = .015$  inch and then was vertical indicating a constant maximum vertical force for depths of cut greater than .015 inch. The horizontal force curve increased at almost a constant rate to  $t = .020$  inch, broke sharply and increased at a constant but lower rate thereafter. The break in the curve is assumed to be tied to the maximum rock contact with the vertical face of the bit. The maximum horizontal force at  $t = .040$  inch was 40 pounds less for the "C" bit than it was for the "B" bit,



SAMPLE I-2, B-BIT, LEUDER'S LIMESTONE.

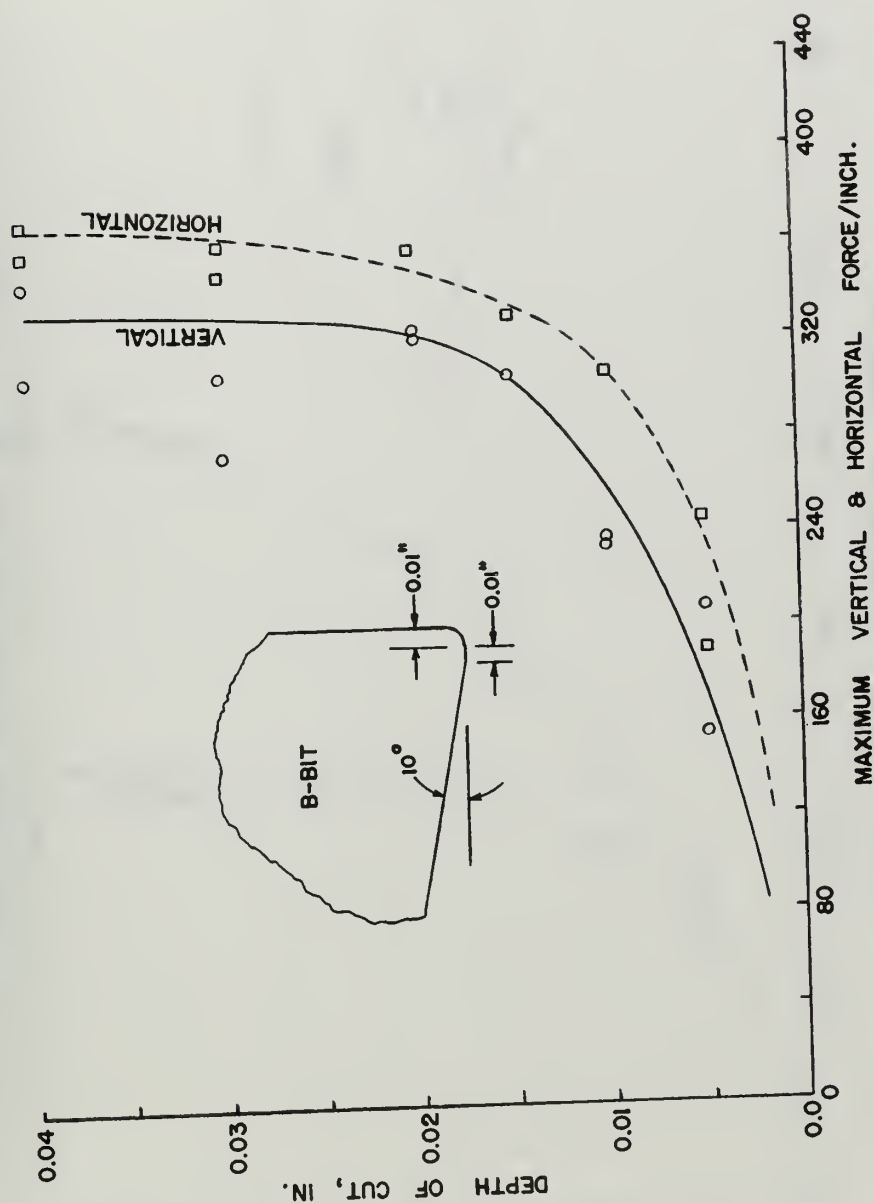


FIG. 19 MAXIMUM VERTICAL AND HORIZONTAL FORCE / INCH OF BIT WIDTH VS. DEPTH OF CUT, "B" BIT.



SAMPLE I-3, C-BIT, LEUDERS LIMESTONE.

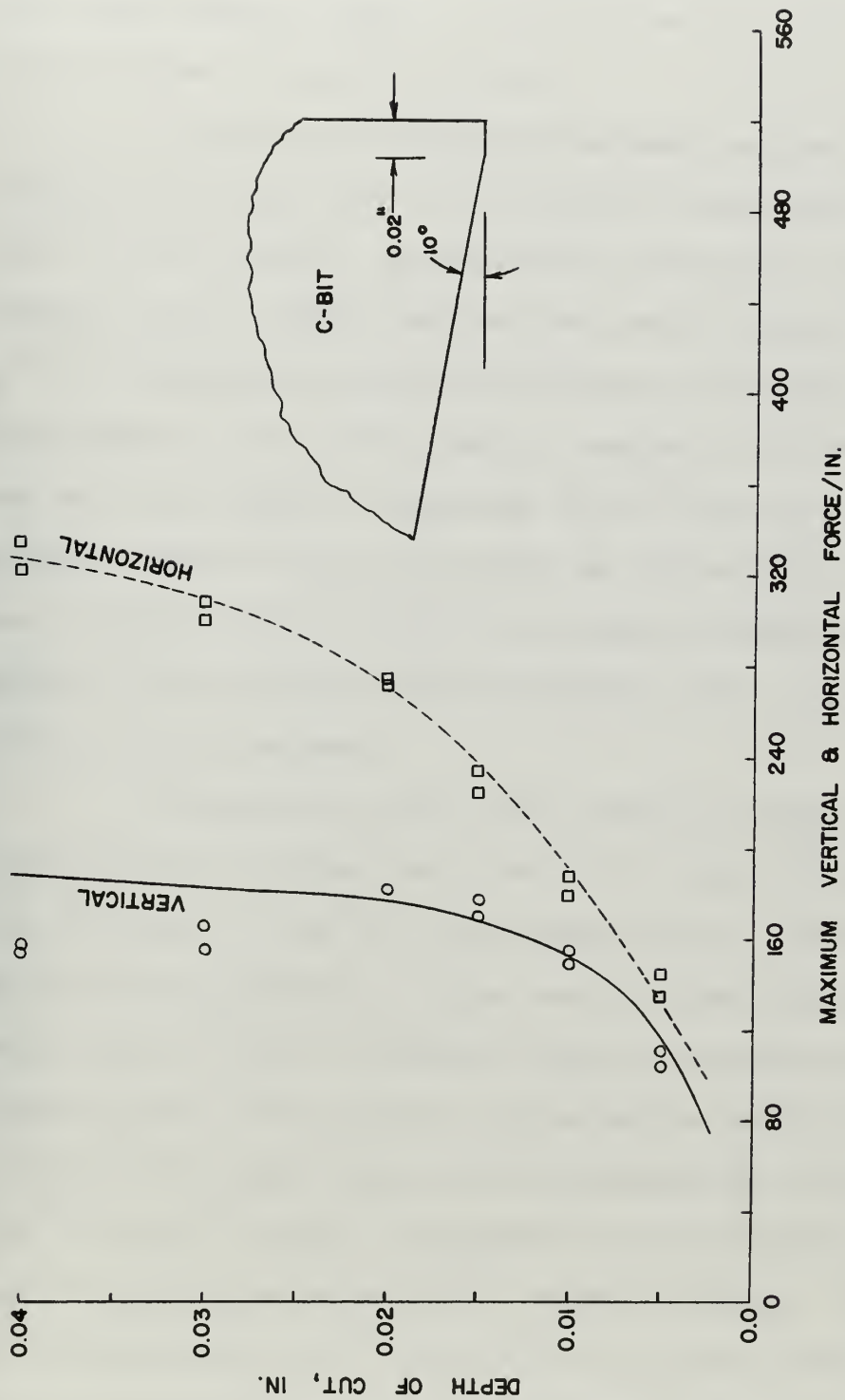


FIG. 20 MAXIMUM VERTICAL & HORIZONTAL FORCE/INCH OF BIT WIDTH VS. DEPTH OF CUT, "C" BIT.





but approximately equal to the horizontal force measured for the same  $t$  with the "A" bit.

Figure (21) displays maximum vertical and horizontal forces per inch of bit width versus depth of cut for the "D" bit trials. The vertical forces for this tip were greater in all cases than the horizontal forces. The shapes of the horizontal and vertical force curves are similar. The range of forces for the six depths of cut was 80 pounds, one half the range of measured forces for the "B" bit. The highest vertical force recorded in the cutting series trials was recorded with this bit (in excess of 440 pounds). In general the vertical forces increased with increasing flat width to this maximum.

Figures (22) and (23) display maximum vertical and horizontal forces per inch of bit width versus depth of cut for the "E" and "F" bits respectively. The only difference in the geometries of the two bits was that the "F" bit had a small, minus 1 degree, negative clearance angle rather than a flat surface following the cutting tip. The "E" bit had a flat width midway between the flat widths of the "B" and "D" bits. In general the horizontal forces were slightly greater than the vertical forces. The shapes of the horizontal and vertical force curves were similar. The vertical force levels were midway between those recorded



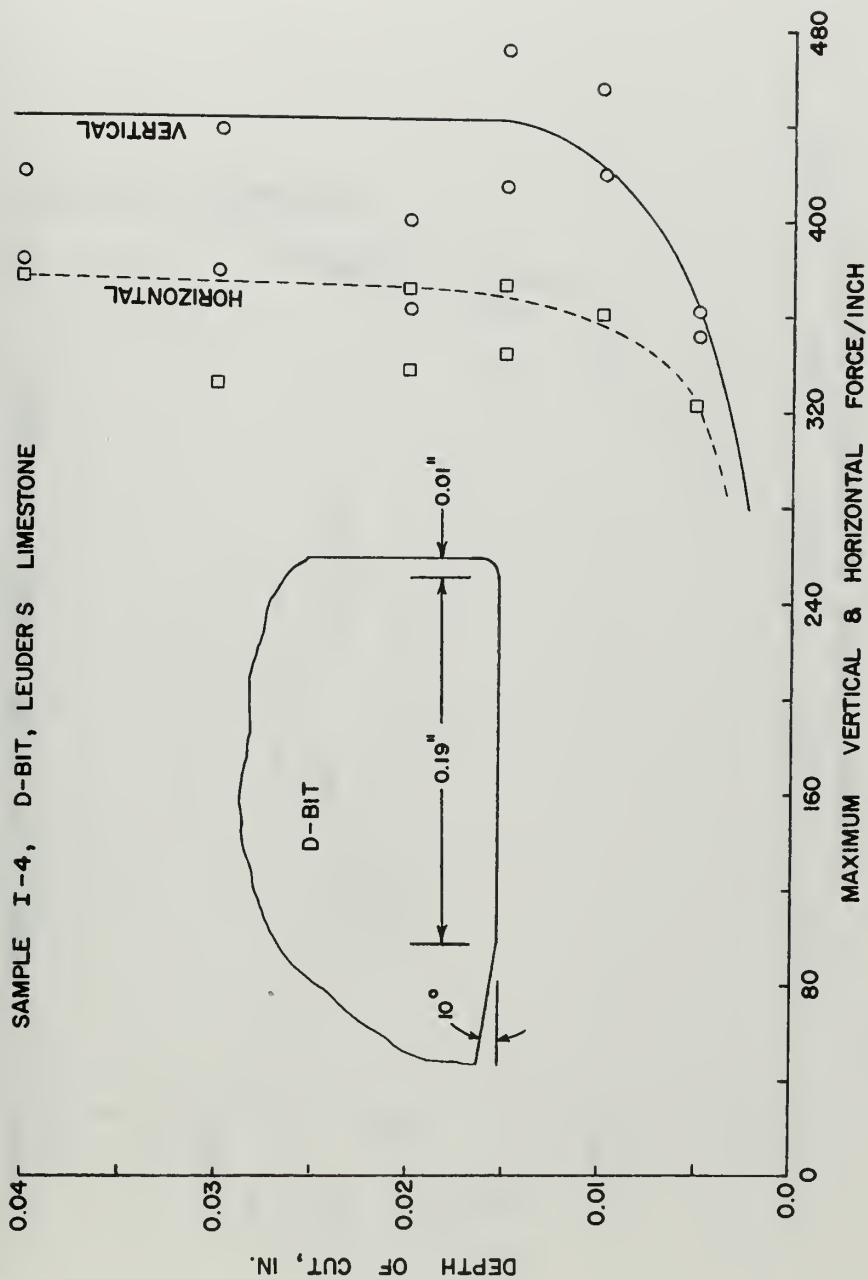


FIG. 21 MAXIMUM VERTICAL & HORIZONTAL FORCE/INCH OF BIT WIDTH VS. DEPTH OF CUT, "D" BIT.



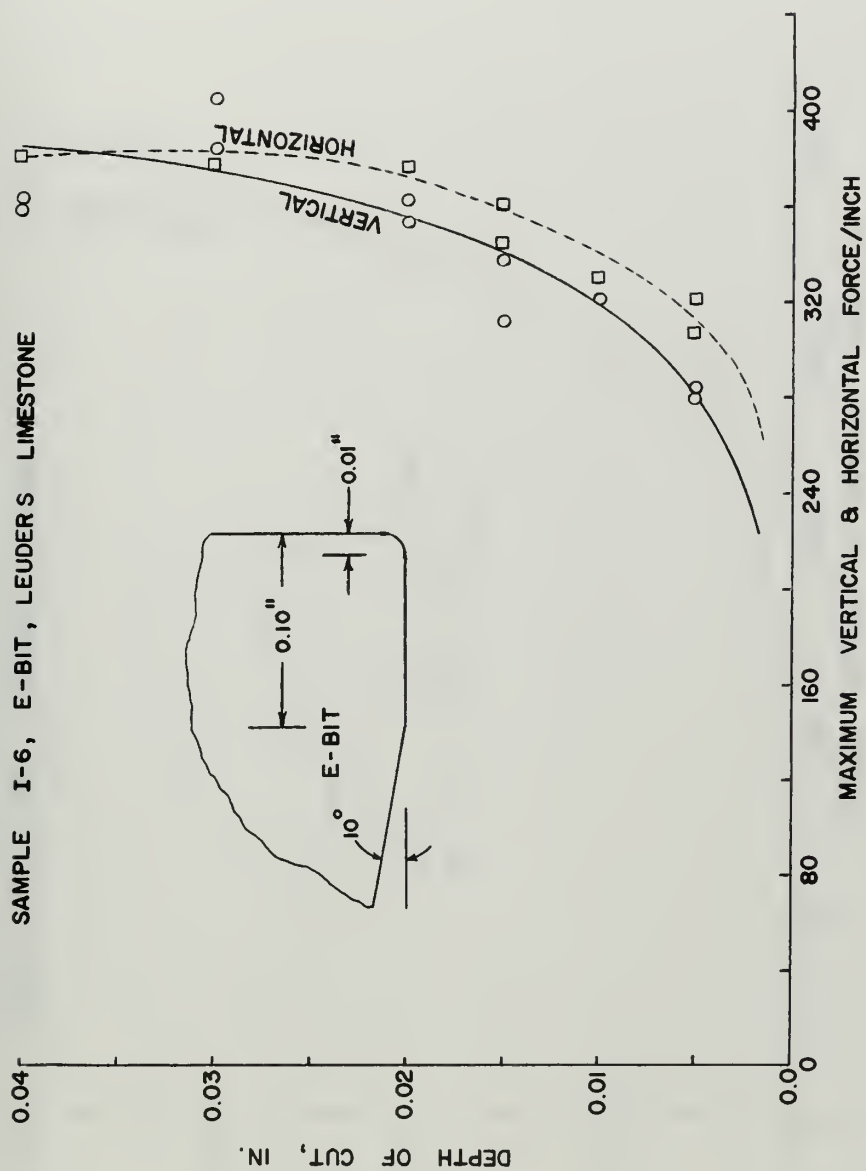


FIG. 22 MAXIMUM VERTICAL & HORIZONTAL FORCE/INCH  
OF BIT WIDTH VS. DEPTH OF CUT, "E" BIT.



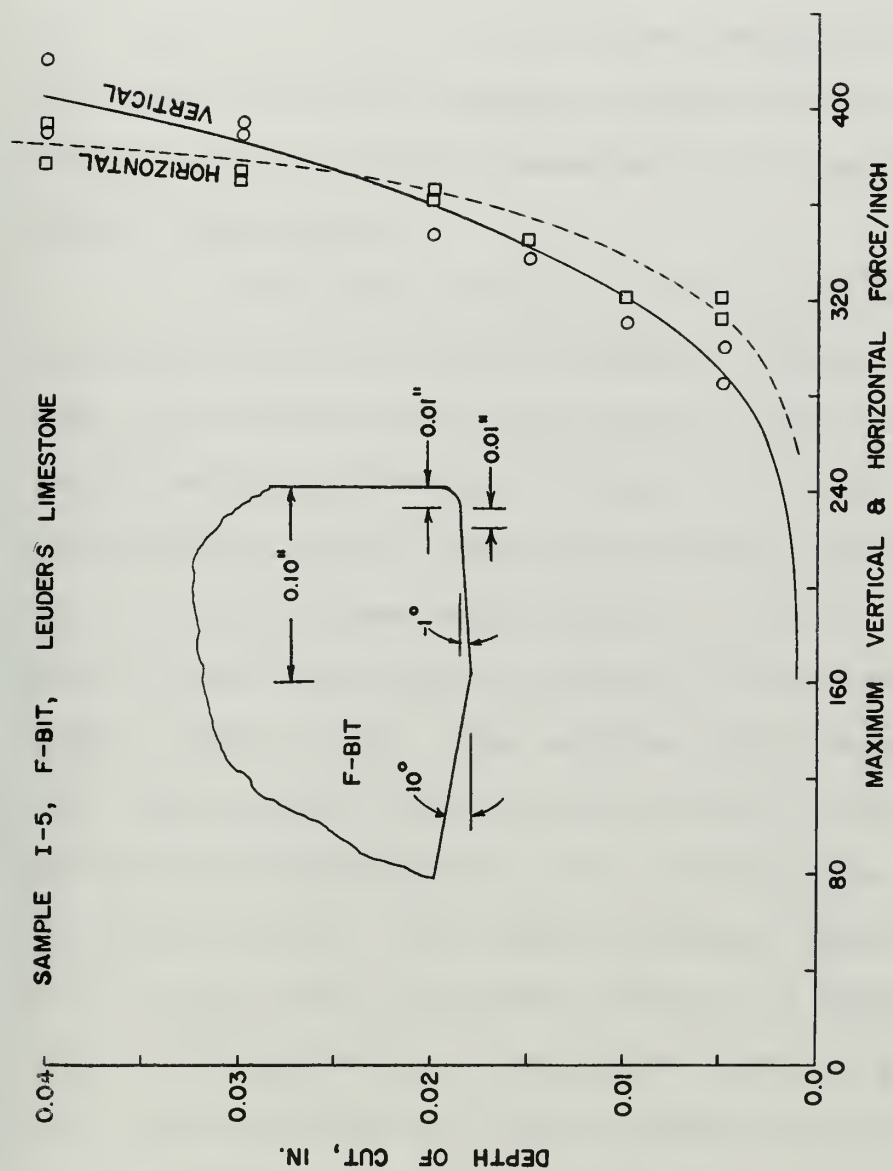


FIG. 23. MAXIMUM VERTICAL & HORIZONTAL FORCE/INCH OF BIT WIDTH VS. DEPTH OF CUT, "F" BIT.





for the "B" and "D" bits. The horizontal force curves for the "D", "E", and "F" bits are almost identical, as can be seen in Figure (17). The "F" bit curves were similar in all respects to the "E" bit curves leading one to suspect that small negative clearance angles will not greatly affect the force levels generated by a drag bit, all other things being equal.

The trials for the "D" bit, performed alternately lubricated and dry, were run using a different rock sample than the previous dry trials with the same bit. This accounts partially for the difference in force levels recorded for the dry trials of the third set and the dry trials of the first and second sets with the "D" bit. The horizontal force curves were almost identical for the wet and dry trials, Figure (24). The vertical curve shapes, Figure (25), were similar but the force levels recorded for the dry runs were approximately 100 pounds higher than for the lubricated trials. The Appl and Rowley equations for forces on a bit tip based on elastic failure ( $t$  greater than  $r$ ), quoted in this thesis as equations numbered (11) and (12), imply that reducing the tool-to-rock friction will have a greater effect on the vertical force than on the horizontal force in some cases. In the equation for vertical force, (11), there is but one term containing the tool-rock friction



SAMPLE L-5, D-BIT, LEUDERS LIMESTONE

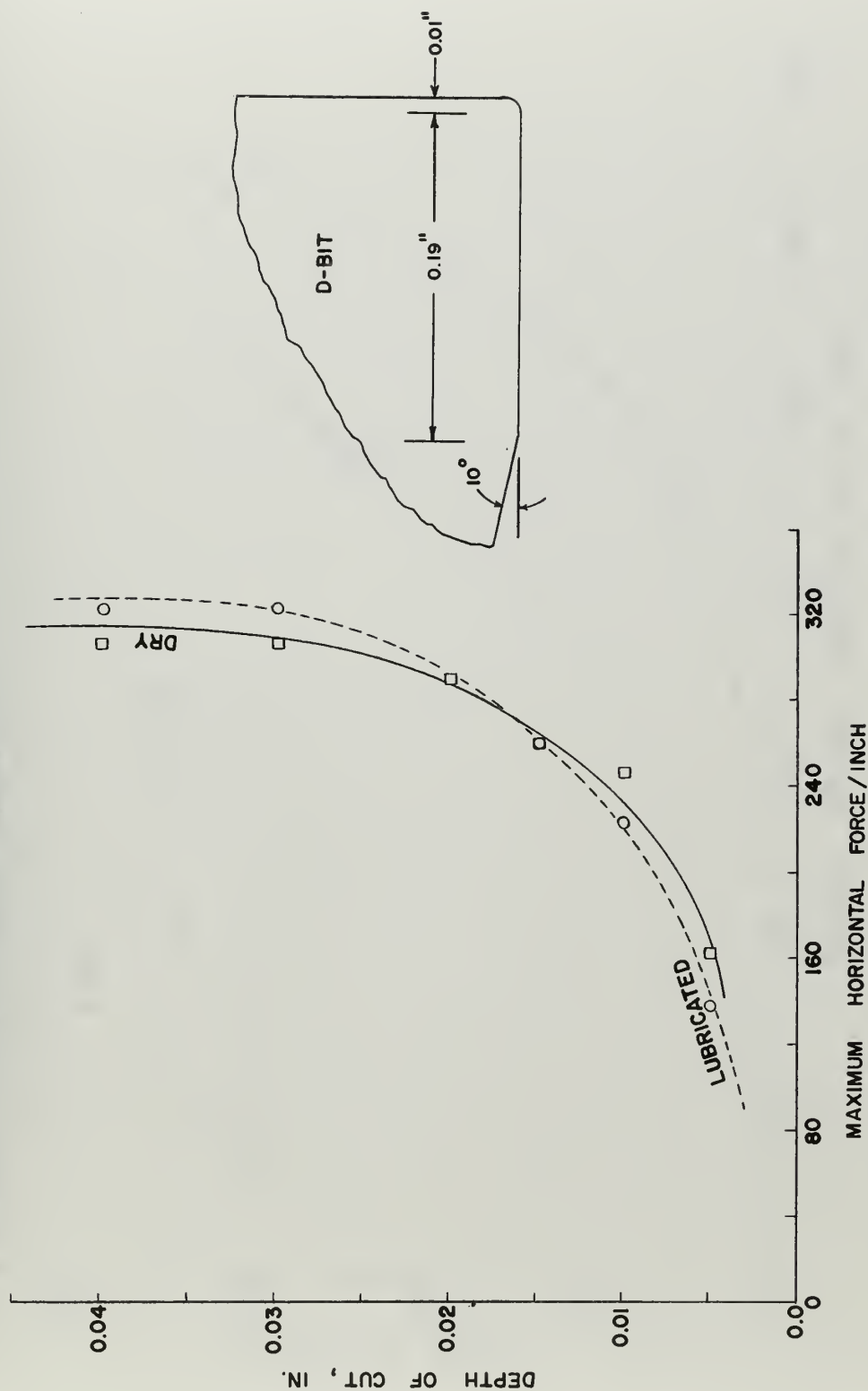


FIG.24. MAXIMUM HORIZONTAL FORCE/INCH OF BIT WIDTH VS. DEPTH OF CUT FOR LUBRICATED-DRY TRIALS WITH "D" BIT.



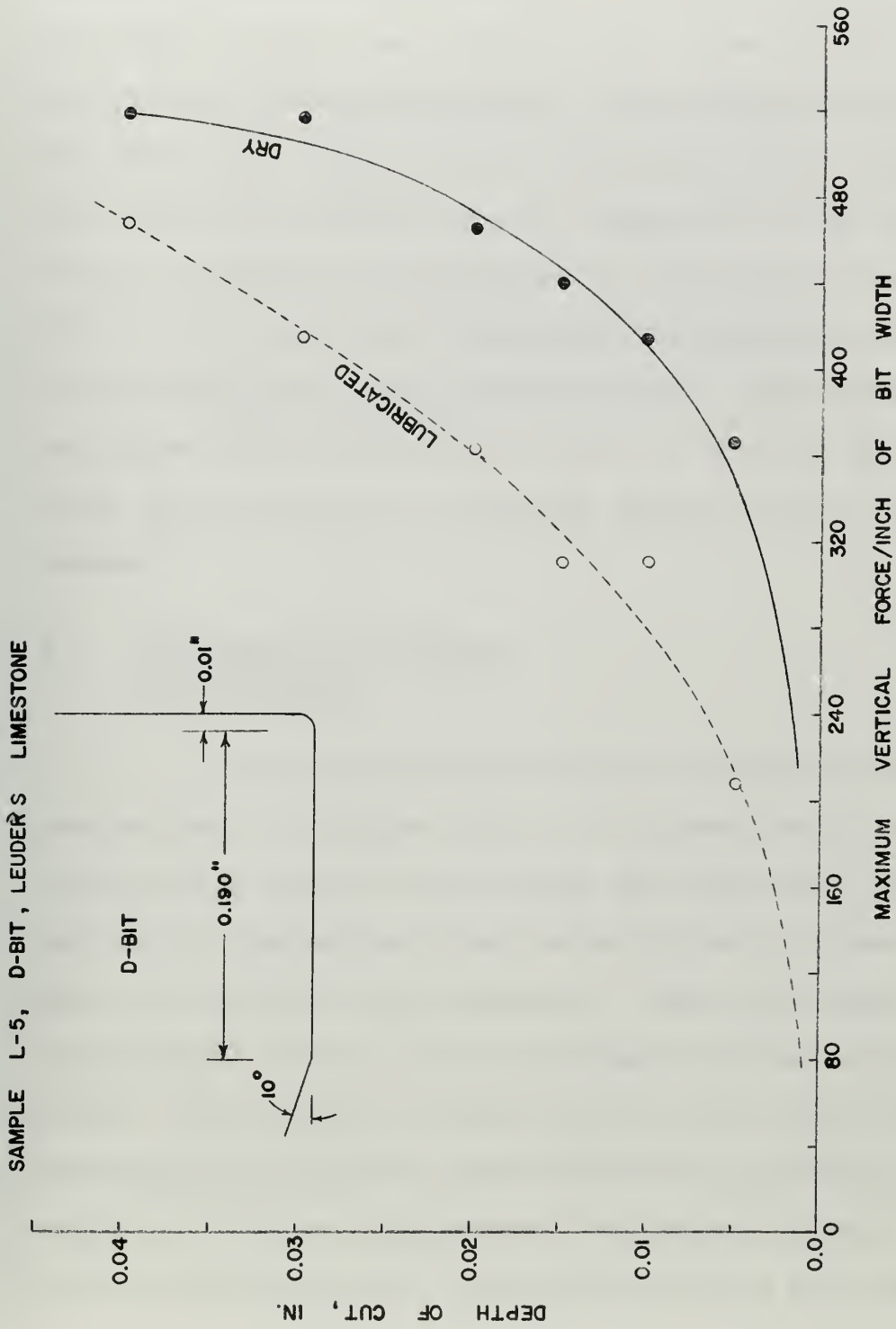


FIG. 25 MAXIMUM VERTICAL FORCE/INCH OF BIT WIDTH VS. DEPTH OF CUT FOR LUBRICATED-DRY TRIALS WITH "D" BIT.



friction coefficient; reduction of the friction factor in that term reduces the vertical force provided the stress distribution remains constant. The expression for horizontal force (12) uses the tool-rock friction coefficient in each term. In the first term, reduction of the friction factor increases the horizontal force, but the same reduction in friction factor decreases the horizontal force contributed by the second and third terms. The Fairhurst and Lacabanne force distribution fails to predict this observation, particularly if a friction factor greater than one is assumed.

#### 2.4 Discussion of Friction Trial Results

Figure (26) shows a typical record of the force traces from a friction trial. The upper trace is the vertical trace, and the lower trace the horizontal trace. This particular run was recorded using the cutting head, and the tool-rock contact was lubricated. The static peak is easily recognizable at the start of movement on the horizontal trace. The initial vertical force on the contact was approximately 130 pounds. The decrease in vertical force recorded as the ram moved across the friction blank is believed due to the surfaces not being parallel for the entire run.





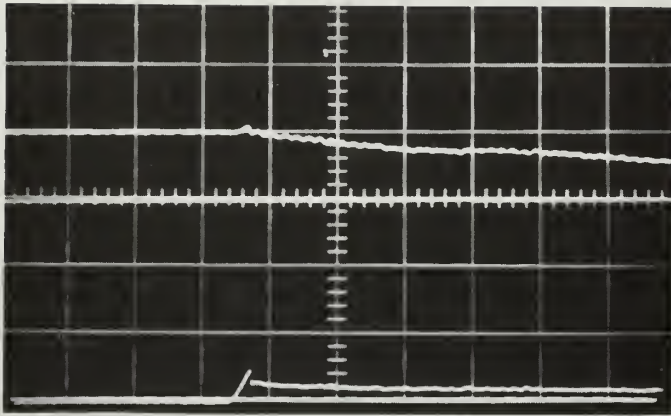


Figure (26): Typical Friction Trial Force Traces.

Figure (27) illustrates the tool-rock friction coefficients for 31 W tungsten carbide and Leuders limestone. Figure (28) illustrates the rock-to-rock friction coefficients. The slight increasing trend of the rock to rock friction coefficients as the vertical force increased leads one to believe that frictional coefficients may be considerably higher as the vertical forces are increased to the plastic failure level. Also, as rock flour is picked up on the bit flat surface it may be expected that rock-to-rock friction will determine the level of frictional forces on a drag bit rather than the less severe tool-to-rock friction coefficient. With lubrication



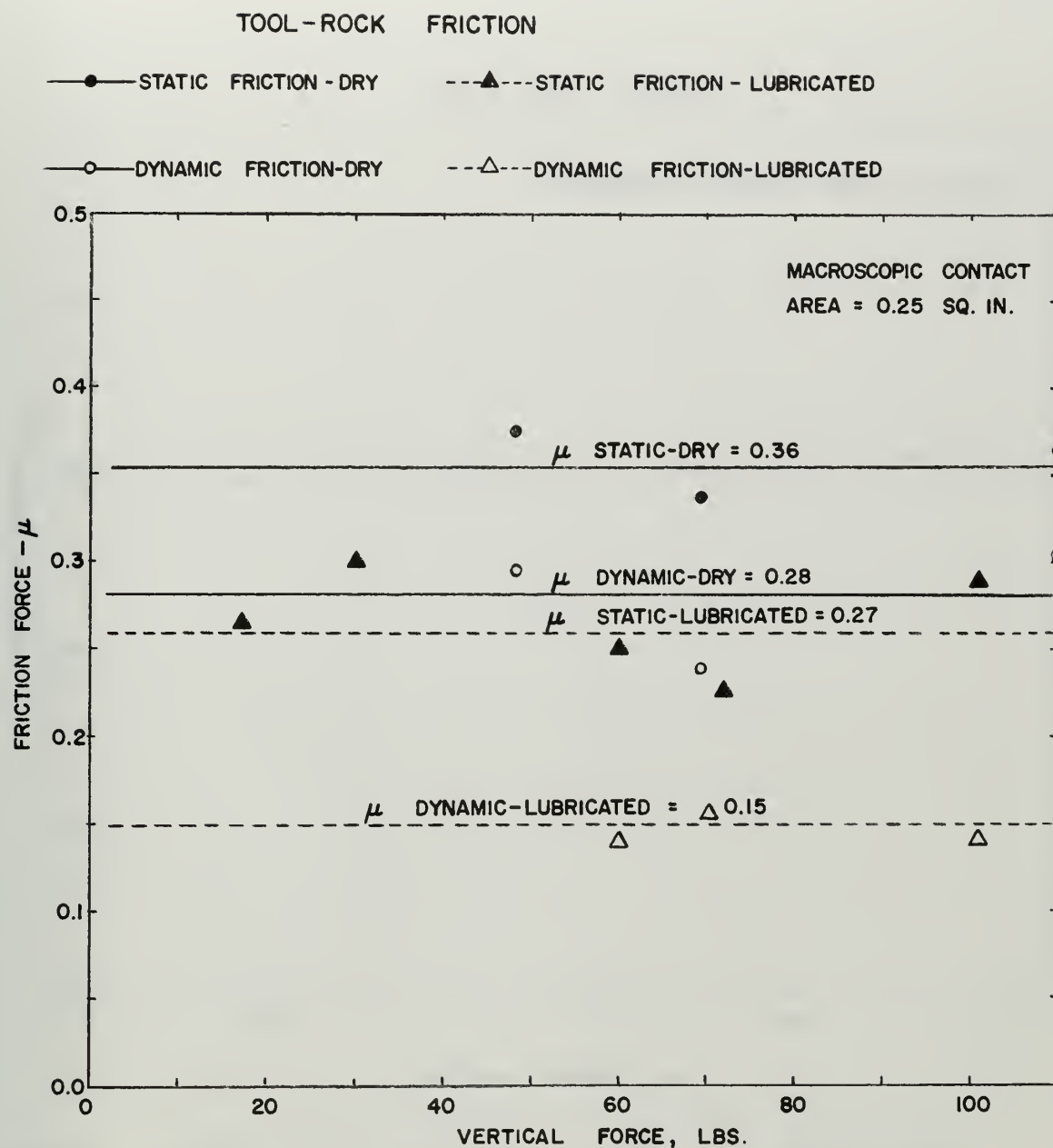


FIG. 27. EFFECT OF VERTICAL LOAD ON TOOL-ROCK  
FRICTION FACTOR,  $\mu$ .



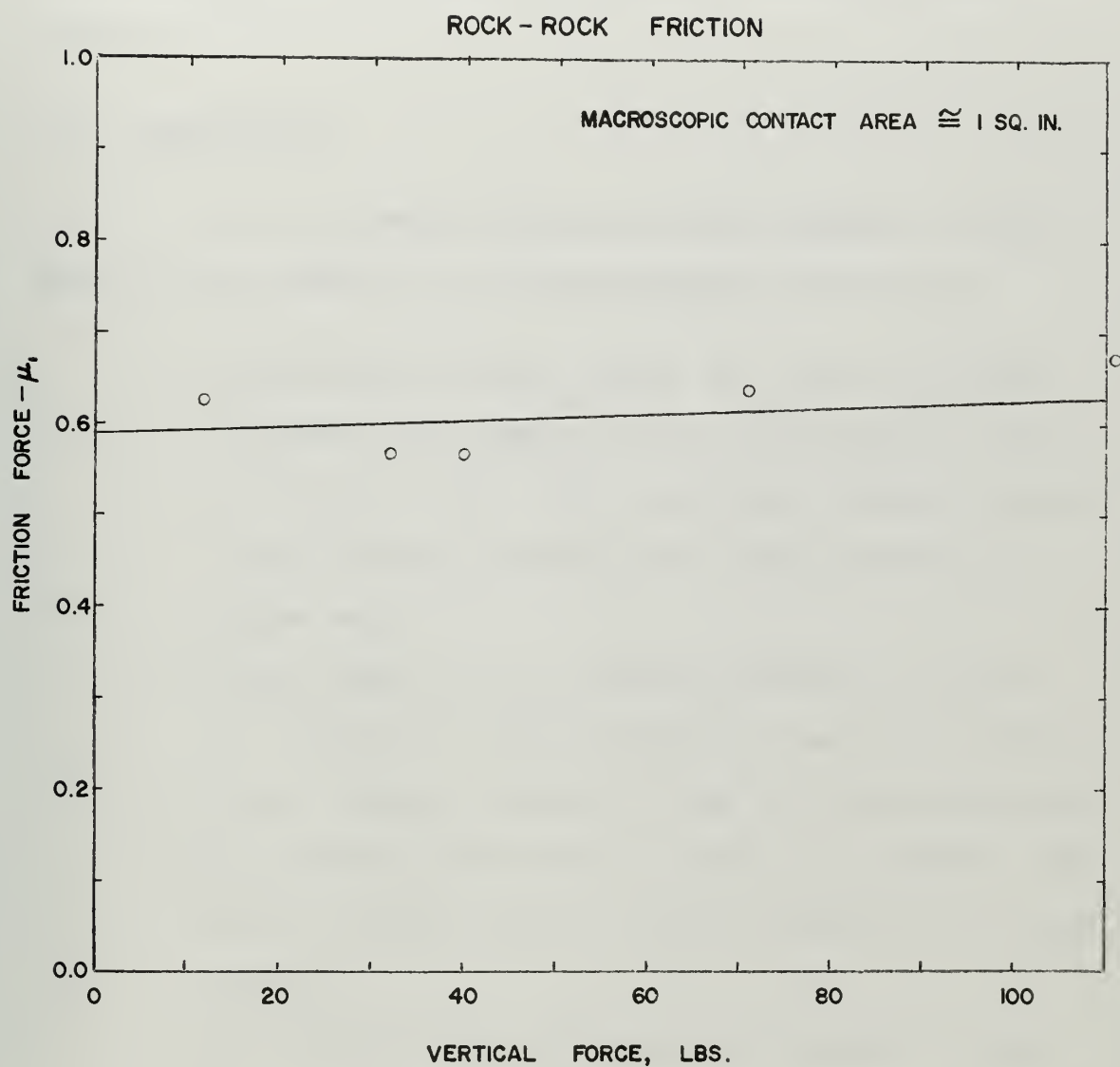


FIG.28. EFFECT OF VERTICAL LOAD ON ROCK-ROCK

FRICTION COEFFICIENT,  $\mu_1$ . ( $\mu_1 \cong 0.6$  for LEUDERS Ls.)

NOTE : Static-Dynamic Friction Factors were Indistinguishable.



the tendency of rock flour to collect on the bit was reduced.

## 2.5 Conclusions

The following conclusions were reached on the basis of the results of the experimental trial data:

1. Increasing the flat width on a drag bit blade decreases the impact forces transmitted to the rock by the bit. As a corollary, impact forces significantly decrease the forces required to plane rock.
2. There seems to be a critical depth of cut for the vertical force in excess of which the force level remains constant. The "A" bit trials and the previous work done by Gray [9] indicate that this critical depth of cut is related to the tip radius.
3. Horizontal force increases with depth of cut; however, the rate of increase is greater for depths of cut less than  $r$  than for depths of cut greater than  $r$ .
4. The small negative clearance angle on the "F" bit had little or no effect on the force levels generated.





5. Friction has a more pronounced effect on the vertical forces developed on a drag bit during planing than on the horizontal forces. By adjusting the width of bit flat, horizontal and vertical forces can be made to assume a variety of ratios.
6. Lubrication of the bit effectively reduces vertical forces on the drag bit during the planing operation. The Appl and Rowley equations for horizontal and vertical forces on a drag bit based on the elastic failure case provide for this eventuality, whereas the Fairhurst and Lacabanne proposal does not.



## CHAPTER III

### IMPACT, HOLE GEOMETRY, AND RECOMMENDATIONS FOR FUTURE STUDY

#### 3.1 Impact

Several investigators [5, 6, 7, 8, 9] have recognized the probable importance of impacting to the rock planing operation. Gray [9] made the following observation:

As the force level on the cutting head assembly increases, the tendency for the head to vibrate laterally also increases. Thus the tool may be impacting the rock with sufficient intensity to influence the magnitude of the apparent force at failure. The result is that at deeper cuts, the recorded force is less than would be the case if there were no impact. . . . [This] implies that the strength of the rock sample is less under impact than under a static load of the same magnitude.

Allsman [14] and Ruff [15] have described a reflected wave theory which may have some application to the planing problem. Their work was done with respect to blasting rock and it must be recognized that the blasting of large quantities of rock is not analogous to rock failure in laboratory-size specimens because, while blasting must not only break the rock but lift it too, the mass of the laboratory specimens is usually not a major factor in resisting breakage. But



for the moment, neglecting this difference, let us compare the failure of rock by blasting and the failure of rock by planing.

In the blasting operation, a hole or series of holes is drilled and loaded with a certain quantity of explosive; hole volume not containing explosive is sealed with stemming of a non-combustible material. Detonation produces high temperatures and pressures and a shock front is formed. This shock front is initially transferred to the surrounding media as a high speed compression wave or impact. The wave travels away from the source of detonation until it reaches an atmospheric boundary where it is reflected back into the host material as a tensile wave; this tensile wave will eventually return the pressure at the source of detonation to normal. Allsman [14] further explains the phenomena:

The reflection of the shock pulse in tension may produce spalling at the free face, by the same mechanism as the well described scabbing in steel plates. As the shock front travels through the rock, its movement of the last layers of rock particles is resisted only by the ineffective mass of air. Thus the forward springing rock particles create a tensile stress at this surface. . . .

Figure (29) illustrates the scabbing of a steel plate.



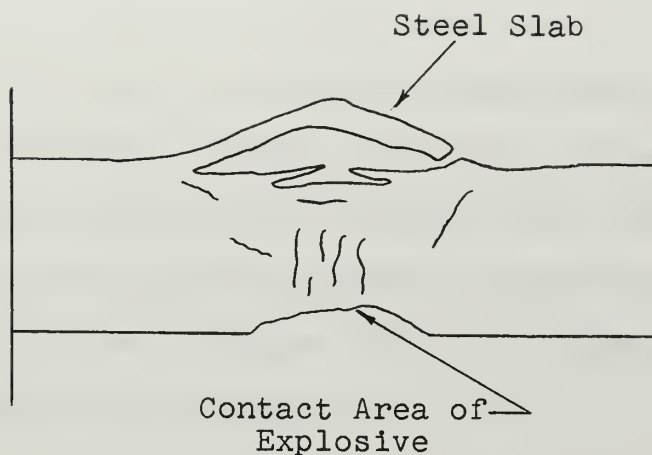


Figure (29): Vertical section of slabbing caused by reflected tension waves in 3" steel plate.  
(After Ruff[15])

Ruff [15] states that any strong impact force, such as a hammer blow on the end of a rod, can produce a compression pulse. This pulse imparted to a rock surface will be reflected back from free faces as a tension wave. Experimental measurements made by Ruff and others indicate that the magnitude of the reflected wave with respect to a particular location can be smaller than, equal to, or larger than the compression wave at the same location.

Applying the reflected wave theory to the phenomena reported by Goodrich and Gray, we note considerable correlation. First, the oscilloscope traces photographed by Gray show force fluctuations up to 80 pounds, indicating that the tooth impacts the rock during planing. Applying Ruff's findings we may assume that tensile forces of this





magnitude are possible in the rock ahead of the bit. Since rock will fail more readily by tension than by compression, it may be that the source of the large chips reported by both Gray and Goodrich is a tensile wave front ahead of the bit instead of a critical angular relationship between bit and rock surfaces. Figure (30) is an idealized picture of how this might take place.

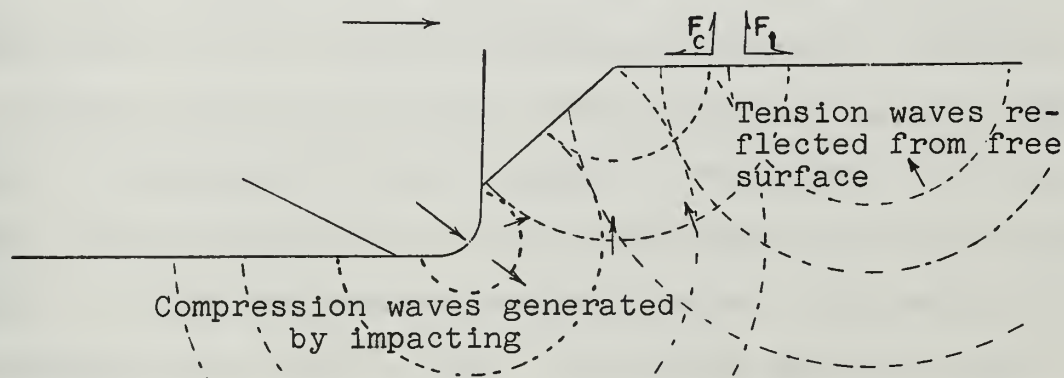


Figure (30): Participation of reflected waves in the planing operation. Note that the vertical components of the tensile and compressive waves are additive at the free surface.

### 3.2 Bore Hole Geometry

Failure may be thought of as a mechanism for re-establishing equilibrium in a system acted upon by unbalanced forces. Two things cannot occupy the same space at the same time. When a bit is pressed against a rock surface with great force something must give. If the surface



is ductile under the local high temperatures and pressures, it will flow to the sides to make room for the bit until sufficient contact is established between the bit and the rock to reduce the surface pressure below the failure strength. If the rock material is not ductile and the cohesive forces are small, equilibrium may be re-established by repacking the grains in a fashion that will reduce porosity locally and thus provide space for the bit to penetrate, or the rock will fracture; but again, fracture is another way for the rock to make room for the bit. When rock is fractured its bulk density is decreased, its porosity is increased, and it requires more space per unit weight than it did in the undisturbed bulk state. Robinson [16] recognized this fact in 1958. In seeking space for fracture the rock will expand in the path of least resistance, toward a free face. The ease with which a brittle material fractures is thus influenced by the proximity of a free face to move toward.

When a force is applied normal to a brittle surface it may be resolved into stress components acting on particles within the material in either direction up to but not including 90 degrees from the axis of the force. The general relationship between the drill string and the bore hole is such that the principal force applied to the rock



(bit weight) is applied perpendicular to the single free face and in a direction opposite to that which the rock must move to fracture. This force is thus very inefficient in terms of breaking the rock. The weight of the mud column offers additional resistance to vertical movement of rock chips seeking room to fracture. A relatively small horizontal force may be applied to the free face by means of the torque transmitted to the bit face through the drill stem, but unless the material being drilled is soft or there is an irregular surface at the bottom of the hole for the blade to attack, the mechanism is not very effective.

Practically, the solution to improving drag bit performance lies in devising some means of efficiently creating more than one free face at the bottom of the bore hole. One solution to this problem might be to design a bit which will alternate drag and indexing action. A study of this phenomena is being conducted concurrently by Young [17]. Another solution already proposed by Christensen Diamond Products is to design a bit which advances the hole as a series of tiered benches. Figure (31) is a cross section of the hole produced by such a bit; note the additional free faces created.





Figure (31): Stepped hole produced by Christensen bit.

### 3.3 Recommendations for Future Study

Gray [9] outlined an extensive research program in his "Recommendations for Future Study." One of his recommendations was to construct a more rigid cutting head and duplicate some of the cutting trials previously run. The friction head described herein seems ideally suited for such tests as it can mount the same bits as the single ring head. Comparison tests with the two heads would provide an indication of just how much impact loading affects the planing process.

Additional friction measurements are needed to determine the effect of increased surface pressure on tool-to-rock and rock-to-rock friction. These tests could be performed at atmospheric pressure. It would be interesting to see if the friction factors change as the surface pressures approach the plastic range or if it is possible, in this range, to isolate the cutting forces from the friction forces.







Further work with rock to rock friction coefficients may also shed some light on the nature of the angle of internal friction,  $\phi$ . From a  $\tau - \sigma$  diagram, the angle of internal friction is defined as the angle of intersection between a tangent to the failure envelope and the normal stress axis. Using the Mohr-Coulomb theory, the failure envelope is a straight line as shown in Figure (32). In this special case, both  $\theta$  and  $\phi$  are constant. In general, however, the failure envelope of a material becomes curved as the stress state is elevated, the relationship between  $\phi$  and  $\theta$ , the angle of failure, being

$$\theta = \frac{1}{2} (\pi/2 - \phi)$$

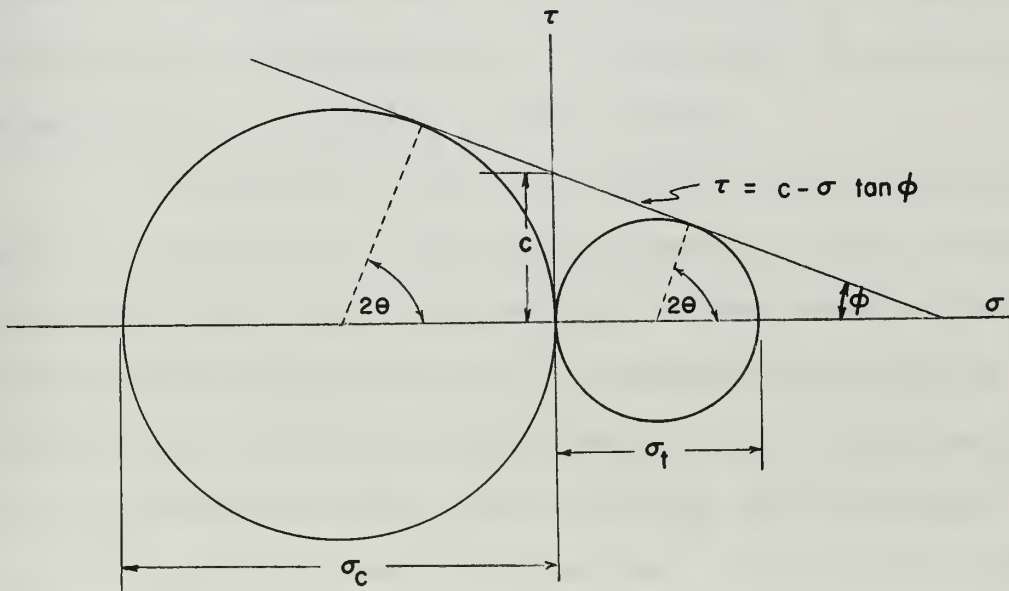


Figure (32): Linear failure envelope for  $\sigma_c \neq \sigma_t$ .



At atmospheric pressure the failure envelope for many rocks is linear but departs from linearity with increased confining pressures. If the rock to rock friction coefficient is equivalent to the angle of internal friction, i.e., if  $\mu_1 = \tan \varphi$ , the friction head described herein may be the most direct way of obtaining that quantity. Figure (28) indicates that  $\mu_1 \cong 0.58$  for Leuders limestone; hence  $\varphi$  should be about  $30^\circ$ . This agrees quite well with triaxial data of Chenevert [13], who reports values of  $\theta = 27^\circ$  and  $\varphi = 32^\circ$  for Leuders lime. Specifically, it is recommended that (1) atmospheric pressure friction trials be made on rocks for which the failure envelope is known, and (2) if correspondence between  $\mu_1$  and  $\varphi$  can be determined at unconfined stress states, the friction head should be modified for high pressure operation to investigate the postulated relationship at elevated stress states.

Finally in some future tests it may be worthwhile to reverse the strain measurements so that the force being applied to the rock specimen is measured rather than the forces on the cutting bit. Perhaps this could be simply done by placing a rock sample in the friction head and traversing the ram, with a cutting tool attached, over the rock sample in the normal manner. If this will not



work some thought might be given to mounting strain gages directly on a rock specimen.



## BIBLIOGRAPHY

1. Simon R.: "Theory of Rock Drilling," Battelle Memorial Institute.
2. Hartman, H. L.: "Basic Studies of Percussion Drilling," Mining Engineering, Trans. AIME TP 4785A, 11, No. 1, Jan., 1956.
3. Appl, Fredric C., and Rowely, David S.: "Drilling Stresses on Drag Bit Cutting Edges," presented at Fifth Rock Mechanics Symposium, School of Mines and Metallurgy, U. of Minnesota (May 3-5, 1962).
4. Maurer, W. C.: "The 'Perfect Cleaning' Theory of Rotary Drilling," Transactions AIME (1962), Vol. 225, p. 1270.
5. Goodrich, R. H.: "High Pressure Rotary Drilling Machines," Bulletin 94, Missouri School of Mines (1956).
6. Fairhurst, C., and Lacabanne, W. D.: "Hard Rock Drilling Techniques," Mine and Quarry Engineering (April-May, 1957).
7. Gray, K. E., Armstrong, F., and Gatlin, C.: "Two-Dimensional Study of Rock Breakage in Drag-Bit Drilling at Atmospheric Pressure," Trans. AIME (1962), Vol. 225, p. 93.
8. Gray, K. E., and Gatlin, C.: "The Effect of Tip Dulling on Tool Forces in Drag Bit Drilling," Bureau of Engineering Research, The University of Texas, January, 1962.
9. Gray, K. E.: "Fixed-Blade Planing of Rocks in the Brittle Stress State," Ph.D. dissertation, The University of Texas, August, 1962.
10. Bowden, F. P., and Tabor, D.: Friction and Lubrication, John Wiley and Sons, Inc., New York, 1957.





11. Gray, K. E., and Lawler, T. J.: "High-Speed Photography--Rock Cutting," Hy-Speed Data Laboratory Report No. 1, The University of Texas, College of Engineering (Sept., 1960-Jan., 1961).
12. Maurer, W. C.: Personal communication.
13. Chenevert, M.: "The Deformation-Failure Mechanism of Anisotropic Sedimentary Rocks at Elevated Stress States," Ph.D. dissertation, The University of Texas (in progress).
14. Allsman, Paul L.: "Analysis of Explosive Action in Breaking Rock," AIME Transactions, Vol. 217, 1960.
15. Ruff, Arthur W.: "Blasting Theories and Seismic Waves. Part I.: Résumé of Recent Blasting Theories," AIME Transactions, Vol. 220, 1961.
16. Robinson, L. H., Jr.: "The Effect of Pore and Confining Pressures on the Failure Process in Sedimentary Rocks," presented at Third Rock Mechanics Symposium, Colorado School of Mines (April 20-22, 1959).
17. Young, Farrile S.: Master's thesis, The University of Texas (in progress).
18. Gray, K. E.: Lectures in Rock Mechanics II, The University of Texas (Spring, 1963).



## NOMENCLATURE

A, B, C, D, E, and F refer to bit geometries illustrated in Figure (14)

A	true contact area
$D_h$	horizontal force deflection on oscilloscope trace, cm
$D_v$	vertical force deflection on oscilloscope trace, cm
F	force, pounds
$F_h$	horizontal force components on cutting tool, pounds
$F_v$	vertical force component on cutting tool, pounds
L	indicates trial was lubricated
$L_1$	radius of center cut out of drag bit blade, inches
$L_0$	radius of bit or radius of drilled hole, inches
$P_1$	weight per inch of radial blade width, pounds/inch
$P_2$	horizontal force per inch of radial blade width/inch
$P_{11}$	portion of weight per inch needed for cutting, pounds/inch
$P_{21}$	portion of horizontal force per inch needed for cutting, pounds/inch
P	yield pressure
$P(\gamma)$	pressure on rounded chisel penetrating a rigid-plastic material, psi



$s$	mean shear strength
$s_1$	mean shear strength of lubricant
$V$	oscilloscope gain, volts/cm
$W$	weight of body
$W_1$	portion of bit load needed for cutting
$Z$	width of drag bit blade, inches
$c$	cohesive strength, psi
$n$	number of blades on a drag bit
$r$	radius of rounded cutting tool, inches
$t$	depth of cut, inches
$\alpha$	fraction of surface area over which metallic junctions are formed
$\delta$	shear angle used by Appl and Rowley
$\eta$	angle with horizontal made by force resultant $F_r$
$\mu$	tool-rock coefficient of friction
$\mu_1$	rock-rock coefficient of friction
$\sigma$	normal stress, psi
$\sigma_c$	compressive strength, psi
$\sigma_3$	minimum normal stress, psi
$\tau$	shear stress
$\phi$	angle of internal friction
$\rho$	radial coordinate used in plastic failure theory
$\theta$	failure angle



## APPENDICES





## APPENDIX I

Appl and Rowley [3] derived the following expression for the normal stress on a drag bit cutting edge during the planing process, a brittle shear failure mechanism being assumed.

$$\sigma_3 = \frac{c/\sin^2 \delta}{\left[1 - \frac{r}{t} (\mu + \mu_1)\right] (\cot \delta - \tan \varphi) - \mu (\tan \varphi \cot \delta + 1)} \quad (10)$$

where  $\sigma_3$  = normal stress on the drilling blade  
 $c$  = cohesive strength of the rock  
 $\delta$  = shear angle  
 $r$  = radius of the bit tip  
 $t$  = depth of cut; assumed to be equal to the vertical contact between bit and rock  
 $\mu$  = tool-rock coefficient of friction  
 $\mu_1$  = rock-rock coefficient of friction  
 $\varphi$  = angle of internal friction

In order to find the shear angle they set the derivative of expression (10) equal to zero and simplified the resulting equation to

$$\left[ \frac{1 - \frac{r}{t} (\mu + \mu_1)}{\mu} \right] = - \left[ \frac{\tan \delta + \tan \varphi}{(\tan \varphi \tan \delta - 1) + \frac{(1 + \tan^2 \varphi) \tan \delta}{\sin 2\delta + \tan \varphi \cos 2\delta}} \right] \quad (22)$$



The solution of this equation was obtained graphically by plotting the left hand member against the shear angle,  $\delta$ , for several values of  $\varphi$ .

Crisp and Gray [18], each working independently, derived a simplified form of the same expression from which the shear angle,  $\delta$ , can be calculated directly. The result is Equation (23). Figure (33) is a plot of the equation showing that it is identical to that derived by Appl and Rowley, but that asymptotes exist for each value of the angle of internal friction,  $\varphi$ . Note that  $\delta$  is very sensitive to values of  $1 - \frac{r}{t}(\mu + \mu_1)$  for small values of  $\delta$ . It is, therefore, suggested that a replot of the stress versus penetration rate graphs contained in the original Appl and Rowley paper might reflect a more accurate picture of the authors' theory if calculated rather than graphic values of  $\delta$  were used.

The derivation of Equation (23) is as follows.

$$\sigma_3 = \frac{c/\sin^2 \delta}{[1 - \frac{r}{t}(\mu + \mu_1)](\text{ctn} \delta - \tan \varphi) - \mu(\tan \varphi \text{ctn} \delta + 1)} \quad (10)$$

Differentiating (10) with respect to  $\delta$ , let



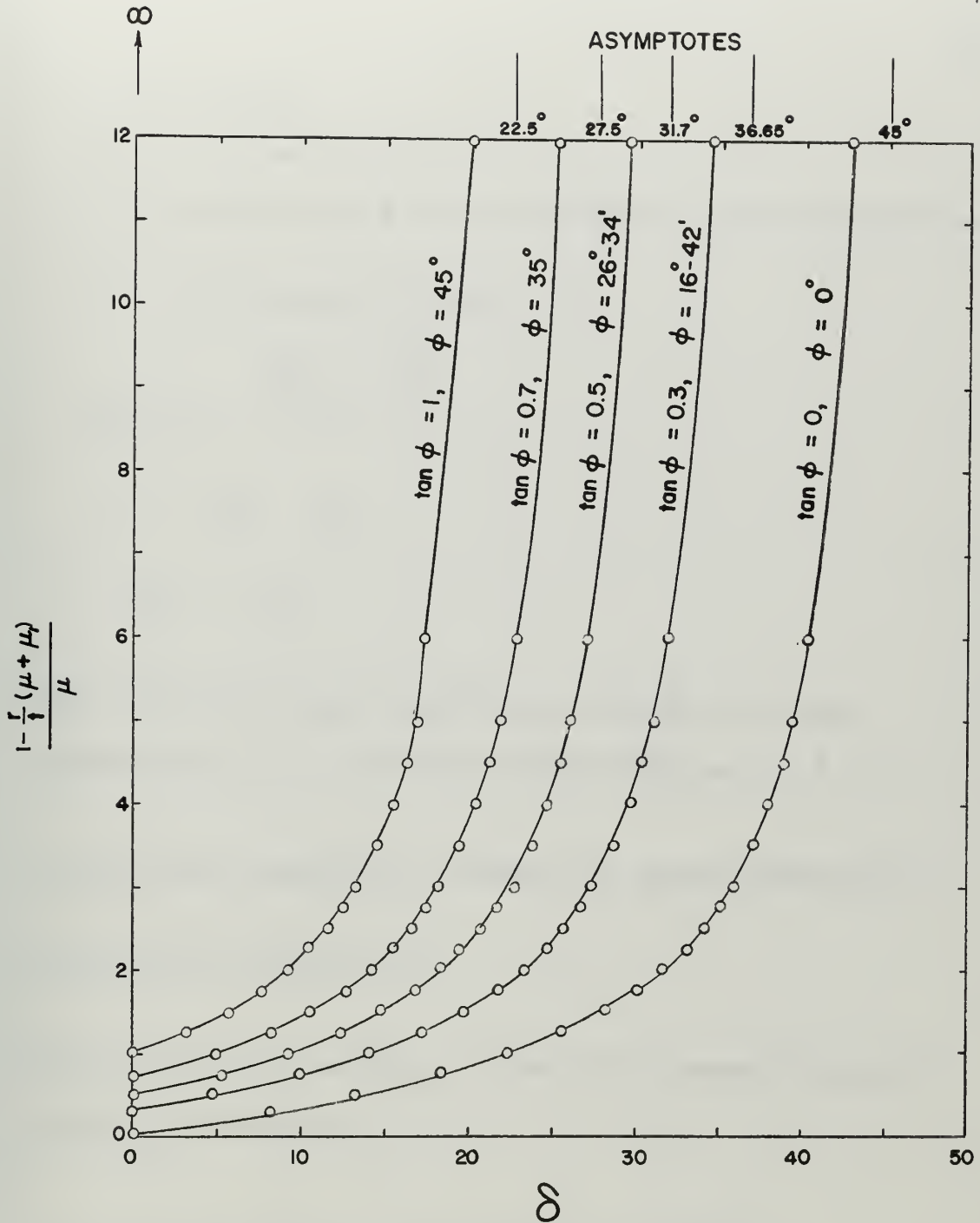


FIG. 33. THE APPL & ROWLEY GRAPHICAL SOLUTION FOR SHEAR ANGLE,  $\delta$ , WITH THE PROPOSED SIMPLIFICATION.

NOTE:  $\tan(2\delta + \phi) = \frac{1 - \frac{r}{1}(\mu + \mu_1)}{\mu}$ .



$$u = c \csc^2 \delta$$

$$du = -2c \csc^2 \delta \cot \delta$$

$$v = \cot \delta - \tan \varphi - \frac{r}{t} (\mu + \mu_1) \cot \delta + \frac{r}{t} (\mu + \mu_1) \tan \varphi - \mu \tan \varphi \cot \delta - \mu$$

$$dv = \csc^2 \delta [\mu \tan \varphi + \frac{r}{t} (\mu + \mu_1) - 1]$$

$$\frac{d}{dx} \left( \frac{u}{v} \right) = \frac{v \frac{du}{dx} - u \frac{dv}{dx}}{v^2}$$

$$0 = v \frac{du}{dx} - u \frac{dv}{dx}$$

$$v \frac{du}{dx} = u \frac{dv}{dx}$$

$$(-1c \csc^2 \delta \cot \delta) [\cot \delta - \tan \varphi - \frac{r}{t} (\mu + \mu_1) \cot \delta + \frac{r}{t} (\mu + \mu_1) \tan \varphi - \mu \tan \varphi \cot \delta - \mu] = c \csc^2 \delta \{ \csc^2 \delta [\mu \tan \varphi + \frac{r}{t} (\mu + \mu_1) - 1] \}.$$

$$\begin{aligned} & -2 \cot \delta [\cot \delta - \tan \varphi - \frac{r}{t} (\mu + \mu_1) \cot \delta + \frac{r}{t} (\mu + \mu_1) \tan \varphi - \mu \tan \varphi \cot \delta - \mu] \\ & = \csc^2 \delta [\mu \tan \varphi + \frac{r}{t} (\mu + \mu_1) - 1]. \end{aligned}$$

$$\begin{aligned} & -2 \cot^2 \delta - 2 \tan \varphi \cot \delta + \frac{2r}{t} (\mu + \mu_1) \tan \varphi \cot \delta + 2 \mu \tan \varphi \cot \delta + 2 \mu \cot \delta \\ & = \csc^2 \delta [\mu \tan \varphi + \frac{r}{t} (\mu + \mu_1) - 1]. \end{aligned}$$

$$\begin{aligned} & 2 \tan \varphi \sin \delta \cos \delta + \frac{2r}{t} (\mu + \mu_1) \tan \varphi \sin \delta \cos \delta + 2 \mu \cos \delta \sin \delta \\ & = [\mu \tan \varphi + \frac{r}{t} (\mu + \mu_1) - 1] [1 - 2 \cos^2 \delta]. \end{aligned}$$

$$2 \sin \delta \cos \delta = \sin 2\delta$$





$$1 - 2\cos^2\delta = -\cos 2\delta$$

$$\sin 2\delta \left[ \tan\varphi - \frac{r}{t}(\mu + \mu_1) \tan\varphi + \mu \right] = \left[ \mu \tan\varphi + \frac{r}{t}(\mu + \mu_1) - 1 \right] [-\cos 2\delta].$$

$$-\tan 2\delta = \frac{\mu \tan\varphi + \frac{r}{t}(\mu + \mu_1) - 1}{\tan\varphi \left[ 1 - \frac{r}{t}(\mu + \mu_1) \right] + \mu}$$

$$\tan 2\delta = \frac{1 - \mu \tan\varphi - \frac{r}{t}(\mu + \mu_1)}{\tan\varphi \left[ 1 - \frac{r}{t}(\mu + \mu_1) \right] + \mu} \quad (23)$$

Equation (23) may be solved for  $\frac{1 - \frac{r}{t}(\mu + \mu_1)}{\mu}$  in the following manner.

$$\tan 2\delta \left\{ \tan\varphi \left[ 1 - \frac{r}{t}(\mu + \mu_1) \right] + \mu \right\} + \mu \tan\varphi = 1 - \frac{r}{t}(\mu + \mu_1).$$

$$\tan 2\delta \tan\varphi + \mu \tan 2\delta + \mu \tan\varphi = 1 - \frac{r}{t}(\mu + \mu_1) (1 - \tan 2\delta \tan\varphi).$$

$$\tan 2\delta \tan\varphi + \mu \tan 2\delta + \mu \tan\varphi - 1 = \frac{r}{t}(\mu + \mu_1) (1 - \tan 2\delta \tan\varphi).$$

$$\frac{\tan 2\delta \tan\varphi - 1}{1 - \tan 2\delta \tan\varphi} + \frac{\mu \tan 2\delta + \mu \tan\varphi}{1 - \tan 2\delta \tan\varphi} = -\frac{r}{t}(\mu + \mu_1).$$

$$\frac{\mu \tan 2\delta + \mu \tan\varphi}{1 - \tan 2\delta \tan\varphi} = 1 - \frac{r}{t}(\mu + \mu_1).$$

$$\frac{\tan 2\delta + \tan\varphi}{1 - \tan 2\delta \tan\varphi} = \frac{1 - \frac{r}{t}(\mu + \mu_1)}{\mu}.$$

$$\tan(2\delta + \varphi) = \frac{1 - \frac{r}{t}(\mu + \mu_1)}{\mu} \quad (24)$$



APPENDIX II  
CALIBRATION OF THE FRICTION HEAD

The friction head assembly, Figure (12), was calibrated using a proving ring for the horizontal channel and a series of calibration weights for the vertical channel. The calibration of each channel was done separately and the force versus deflection curves are shown as Figure (34). Horizontal and vertical forces were obtained from the friction trials by multiplying the measured deflections by the following constants:

Oscilloscope Gain

1 volt/cm

Force-Chart Deflection Relationship

$$F_v = 100.00 D_v ; F_h = 75.00 D_h$$



VERTICAL & HORIZONTAL GAIN = 1 V/CM.

$$F_V = 100.00 D_V$$

$$F_H = 75.00 D_H$$

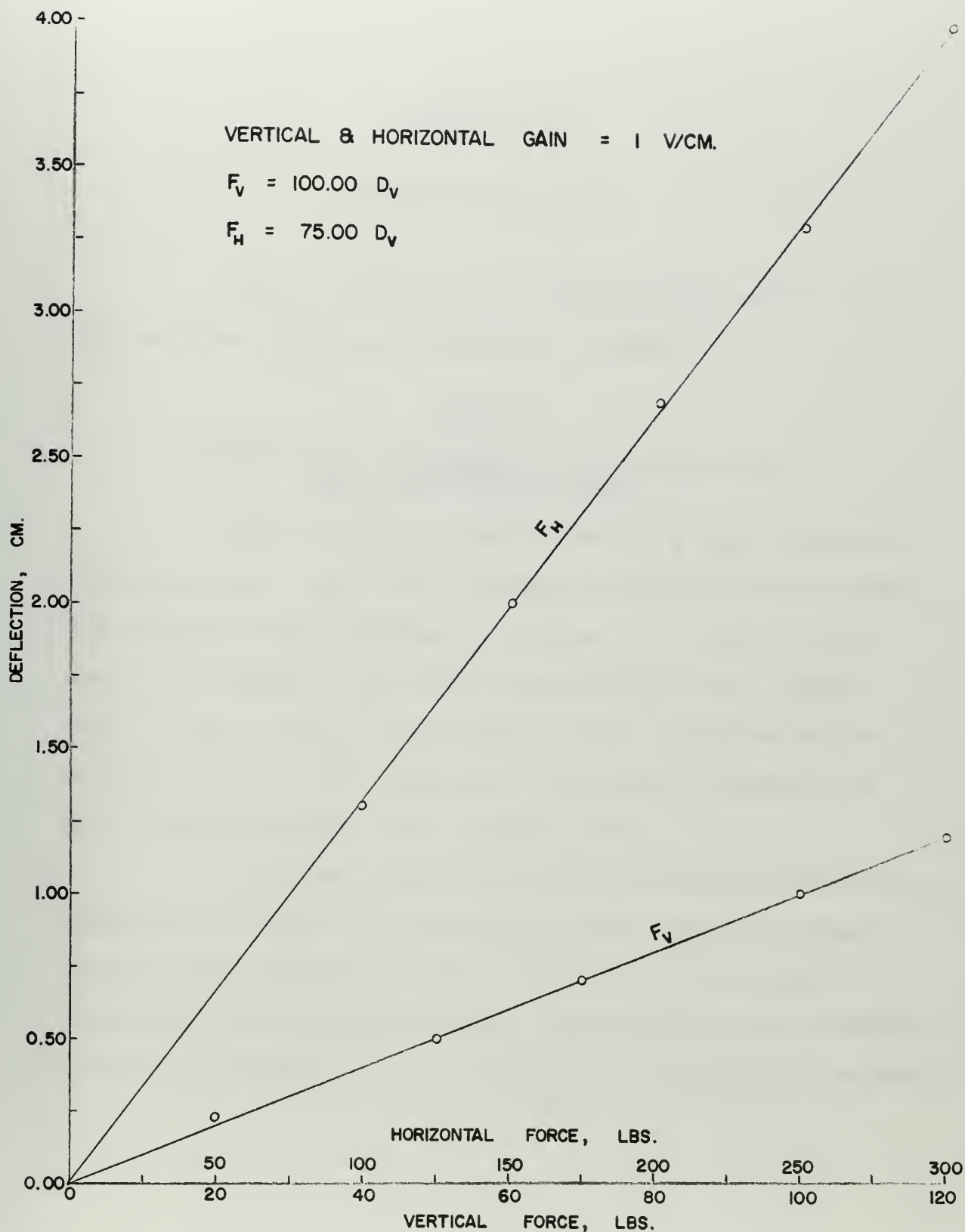


FIG. 34. CALIBRATION CHART FOR FRICTION HEAD, 1 Volt/cm.



## APPENDIX III

### CUTTING TRIAL DATA

Table I contains basic force data computed from the oscilloscope traces displayed in Table II.

TABLE I

#### MAXIMUM FORCE COMPONENTS AND OPERATING DATA FOR THE CUTTING TRIALS

Table I contains basic operating data from the cutting trials. The trial designation indicates, in order, tip geometry corresponding to Figure (14), depth of cut, and trial number. The trial designation A-30(1) means the "A" tip, a 0.030 inch depth of cut, the first of two or more trials. The lubricated trials are designated by an "L" following the trial depth of cut.

Forces were computed from the oscilloscope traces displayed in Table II by reading a most common maximum, in centimeters, designated by  $D_v$  and  $D_h$  for vertical and horizontal traces respectively. This reading was converted to force in pounds by multiplying by the following constants:





Oscilloscope GainForce-Chart Deflection Relationships

5 volts/cm

$$F_v = 66.80 D_v \quad ; \quad F_h = 39.50 D_h$$

10 volts/cm

$$F_v = 133.60 D_v \quad ; \quad F_h = 79.00 D_h$$

20 volts/cm

$$F_v = 267.20 D_v$$



OSCILLOSCOPE SETTINGS    MAXIMUM CHART DEFLECTION, CM    MAXIMUM FORCE COMPONENTS ON CUTTING TOOL, LBS

TRIAL	Sweep Speed, sec/cm	Gain, Ver	V/cm Hor	D <sub>v</sub>	D <sub>h</sub>	Measured		Per Unit Width		Tann
						F <sub>v</sub>	F <sub>h</sub>	F <sub>v</sub> /w	F <sub>h</sub> /w	
A-5(1)	.2	5	5	1.35	2.50	90.18	98.75	174.77	195.82	.91322
A-5(2)	.2	5	5	1.19	2.20	79.49	86.90	154.05	172.32	.91473
A-10(1)	.2	5	5	1.68	3.24	112.22	127.98	217.48	253.78	.87686
A-10(2)	.2	5	5	1.70	3.32	113.56	131.14	220.08	260.05	.86594
A-15(1)	.2	5	10	1.20	1.15	80.16	90.85	155.35	180.16	.88233
A-15(2)	.2	5	10	1.80	1.80	120.24	142.20	233.03	281.98	.84557
A-20(1)	.2	5	10	1.80	1.90	120.24	150.10	233.03	297.65	.80107
A-20(2)	.2	5	10	1.90	1.80	126.92	142.20	245.97	281.98	.89255
A-30(1)	.2	5	10	1.90	2.00	126.92	158.00	245.97	313.31	.80329
A-30(2)	.2	5	10	1.90	2.10	126.92	165.90	245.97	328.98	.76504
A-40(1)	.2	5	10	1.92	2.10	128.26	165.90	248.57	328.98	.77312
A-40(2)	.2	5	10	1.96	2.20	130.93	173.80	253.74	344.65	.75334



OSCILLOSCOPE SETTINGS

MAXIMUM CHART DEFLECTION, CM

MAXIMUM FORCE COMPONENTS ON CUTTING TOOL, LBS

CONTACT SURFACE AREA, sq in.

SWEEP SPEED, sec/cm

GAIN, Ver Hor

MEASURED  $F_v$

PER UNIT WIDTH  $F_v/w$

TANG  $F_v/F_h$

B-5(1)	.005	.2	5	5	1.19	2.40	79.49	94.80	154.05	187.99	.83850
B-5(2)	.005	.2	5	5	1.60	3.10	106.88	122.45	207.13	242.82	.87285
B-10(1)	.005	.2	5	5	1.80	3.90	120.24	154.05	233.03	305.48	.78053
B-10(2)	.005	.2	5	5	1.84	3.90	122.91	154.05	238.20	305.48	.79786
B-15(1)	.005	.2	10	10	1.18	2.10	157.65	165.90	305.53	328.98	.95027
B-15(2)	.005	.2	10	10	1.18	2.10	157.65	165.90	305.53	328.98	.95027
B-20(1)	.005	.2	10	10	1.24	2.28	165.66	180.12	321.05	357.18	.91972
B-20(2)	.005	.2	10	10	1.26	2.28	168.34	180.12	326.24	357.18	.93460
B-30(1)	.005	.2	10	10	1.34	2.30	179.02	181.70	346.94	360.31	.98525
B-30(2)	.005	.2	10	10	1.18	2.20	157.65	173.80	305.53	344.65	.90708
B-40(1)	.005	.2	10	10	1.18	2.36	157.65	186.44	305.53	369.71	.84558
B-40(2)	.005	.2	10	10	1.18	2.28	157.65	180.12	305.53	357.18	.87525



OSCILLOSCOPE SETTINGS				MAXIMUM CHART DEFLECTION, CM		MAXIMUM FORCE COMPONENTS ON CUTTING TOOL, LBS			
TRIAL	Contact Surface Area, sq in.	Sweep Speed, sec/cm	Gain, Ver	V/cm Hor	D <sub>v</sub>	D <sub>h</sub>	F <sub>v</sub> Measured	F <sub>h</sub>	Tann Per Unit Width F <sub>v</sub> /w F <sub>h</sub> /w F <sub>v</sub> /F <sub>h</sub>
C-5(1)	.010	.2	5	5	1.04	1.84	69.47	72.68	134.63 144.12 .95583
C-5(2)	.010	.2	5	5	.80	1.42	53.44	56.09	103.57 111.23 .95275
C-10(1)	.010	.2	5	5	1.20	2.40	80.16	94.80	155.35 187.99 .84557
C-10(2)	.010	.2	5	5	1.16	2.30	77.49	90.85	150.18 180.16 .85294
C-15(1)	.010	.2	5	5	1.32	2.86	88.18	112.97	170.89 224.02 .78056
C-15(2)	.010	.2	5	5	1.37	3.00	91.52	118.50	177.37 234.99 .77232
C-20(1)	.010	.2	10	10	.70	1.76	93.52	139.04	181.24 275.72 .67261
C-20(2)	.010	.2	10	10	.70	1.74	93.52	137.46	181.24 272.58 .68034
C-30(1)	.010	.2	10	10	.64	1.96	85.50	154.84	165.70 307.05 .55218
C-30(2)	.010	.2	10	10	.60	1.92	80.16	151.68	155.35 300.78 .52848
C-40(1)	.010	.2	10	10	.61	2.14	81.50	169.06	157.95 335.25 .48208
C-40(2)	.010	.2	10	10	.60	2.06	80.16	162.74	155.35 322.71 .49256





OSCILLOSCOPE SETTINGS				MAXIMUM CHART DEFLECTION, CM		MAXIMUM FORCE COMPONENTS ON CUTTING TOOL, LBS					
TRIAL	Contact Surface Area, sq in.	Sweep Speed, sec/cm	Gain, V/cm		D <sub>v</sub>	D <sub>h</sub>	Measured		Per Unit Width Tann		
			Ver	Hor			F <sub>v</sub>	F <sub>h</sub>		F <sub>v</sub> /w	F <sub>h</sub> /w
D-5(1)	.057	.2	10	10	1.40	2.05	187.04	161.95	362.48	321.15	1.15492
D-5(2)	.098	.2	10	10	1.36	2.05	181.70	161.95	352.13	321.15	1.12195
D-10(1)	.056	.2	10	10	1.76	2.30	235.14	181.70	455.70	360.31	1.29411
D-10(2)	.098	.2	10	10	1.62	2.30	216.43	181.70	419.44	360.31	1.19113
D-15(1)	.034	.2	10	10	1.82	2.20	243.15	173.80	471.22	344.65	1.39902
D-15(2)	.098	.2	10	10	1.60	2.38	213.76	188.02	414.27	372.84	1.13690
D-20(1)	.098	.2	10	10	1.54	2.36	205.74	186.44	398.72	369.71	1.10352
D-20(2)	.071	.2	10	10	1.40	2.15	187.04	169.85	362.48	336.81	1.10121
D-30(1)	.071	.2	10	10	1.46	2.10	195.06	165.90	378.03	328.98	1.17577
D-30(2)	.081	.2	10	10	1.69	2.12	225.78	167.48	437.56	332.11	1.34810
D-40(1)	.098	.2	10	10	1.62	2.40	216.43	189.60	419.44	375.98	1.14151
D-40(2)	.098	.2	10	10	1.48	2.40	197.73	189.60	383.20	375.98	1.04288



TRIAL	OSCILLOSCOPE SETTINGS				MAXIMUM CHART DEFLECTION, CM		MAXIMUM FORCE COMPONENTS ON CUTTING TOOL, LBS				
	Contact Surface Area, sq in.	Sweep Speed, sec/cm	Gain, Ver	V/cm Hor	D <sub>v</sub>	D <sub>h</sub>	Measured		Per Unit Width F <sub>v</sub> /w	F <sub>h</sub> /w	Tann F <sub>v</sub> /F <sub>h</sub>
							F <sub>v</sub>	F <sub>h</sub>			
E-5(1)	.052	.2	10	10	1.08	1.96	144.29	154.84	279.63	307.05	.93187
E-5(2)	.052	.2	10	10	1.10	2.05	146.96	161.95	284.81	321.15	.90744
E-10(1)	.052	.2	10	10	1.24	2.10	165.66	165.90	321.05	328.98	.99855
E-10(2)	.052	.2	10	10	1.30	2.10	173.68	165.90	336.59	328.98	1.04690
E-15(1)	.052	.2	10	10	1.30	2.30	173.68	181.70	336.59	360.31	.95586
E-15(2)	.052	.2	10	10	1.20	2.20	160.32	173.80	310.70	344.65	.92244
E-20(1)	.052	.2	10	10	1.40	2.40	187.04	189.60	362.48	375.98	.98650
E-20(2)	.052	.2	10	10	1.36	2.30	181.70	181.70	352.13	376.18	1.00000
E-30(1)	.052	.2	10	10	1.56	2.40	208.42	189.60	403.92	375.98	1.09926
E-30(2)	.052	.2	10	10	1.48	2.40	197.73	189.60	383.20	375.98	1.04288
E-40(1)	.052	.2	10	10	1.38	2.42	184.37	191.18	357.31	379.11	.96438
E-40(2)	.052	.2	10	10	1.40	2.42	187.04	191.18	362.48	379.11	.97835



OSCILLOSCOPE SETTINGS				MAXIMUM CHART DEFLECTION, CM		MAXIMUM FORCE COMPONENTS ON CUTTING TOOL, LBS					
TRIAL	Contact Surface Area, sq in.	Sweep Speed, sec/cm	Gain, V/cm		D <sub>v</sub>	D <sub>h</sub>	Measured		F <sub>v</sub> /w	F <sub>h</sub> /w	Tann F <sub>v</sub> /F <sub>h</sub>
			Ver	Hor			F <sub>v</sub>	F <sub>h</sub>			
F-5(1)	.052	.2	10	10	1.16	2.05	154.97	161.95	300.33	321.15	.95690
F-5(2)	.052	.2	10	10	1.10	2.00	146.96	158.00	284.81	313.31	.93013
F-10(1)	.052	.2	10	10	1.20	2.05	160.32	161.95	310.70	321.15	.98994
F-10(2)	.052	.2	10	10	1.20	2.05	160.32	161.95	310.70	321.15	.98994
F-15(1)	.052	.2	10	10	1.30	2.20	173.68	173.80	336.59	344.65	.99931
F-15(2)	.052	.2	10	10	1.30	2.20	173.68	173.80	336.59	344.65	.99931
F-20(1)	.052	.2	10	10	1.40	2.30	187.04	181.70	362.48	360.31	1.02939
F-20(2)	.052	.2	10	10	1.34	2.34	179.02	184.86	346.94	366.58	.96841
F-30(1)	.052	.2	10	10	1.50	2.38	200.40	188.02	388.38	372.84	1.06584
F-30(2)	.052	.2	10	10	1.52	2.36	203.07	186.44	393.55	369.71	1.08920
F-40(1)	.052	.2	10	10	1.62	2.52	216.43	199.08	419.44	394.78	1.08715
F-40(2)	.052	.2	10	10	1.50	2.40	200.40	189.60	388.38	375.98	1.05696



TRIAL	OSCILLOSCOPE SETTINGS			MAXIMUM CHART DEFLECTION, CM		MAXIMUM FORCE COMPONENTS ON CUTTING TOOL, LBS				
	Sweep Speed, sec/cm	Gain, Ver	V/cm Hor	D <sub>v</sub>	D <sub>h</sub>	Measured		Per Unit F <sub>v</sub> /w	Width F <sub>h</sub> /w	Tan η F <sub>v</sub> /F <sub>h</sub>
						F <sub>v</sub>	F <sub>h</sub>			
<u>Lubricated Run</u>										
D-5(L)	.2	20	10	0.40	.90	106.88	71.10	207.14	137.79	1.375
D-10(L)	.2	20	10	0.60	1.45	160.32	114.55	310.70	222.00	1.405
D-15(L)	.2	20	10	0.60	1.70	160.32	134.30	310.70	260.27	1.195
D-20(L)	.2	20	10	0.70	1.95	187.04	154.05	362.48	298.55	1.215
D-30(L)	.2	20	10	0.80	2.10	213.76	165.90	414.26	321.51	1.286
D-40(L)	.2	20	10	0.90	2.10	240.48	165.90	466.06	321.51	1.450
<u>Dry Run</u>										
D-5(3)	.2	10	5	1.30	2.10	173.68	82.95	336.60	160.76	2.092
D-10(3)	.2	20	10	.80	1.60	213.76	126.40	414.26	244.96	1.689
D-15(3)	.2	20	10	.85	1.70	227.12	134.30	440.16	260.27	1.620
D-20(3)	.2	20	10	.90	1.90	240.48	150.10	465.00	290.87	1.593
D-30(3)	.2	20	10	1.00	2.00	267.20	158.00	517.84	306.20	1.690
D-40(3)	.2	20	10	1.00	2.00	267.20	158.00	517.84	306.20	1.690



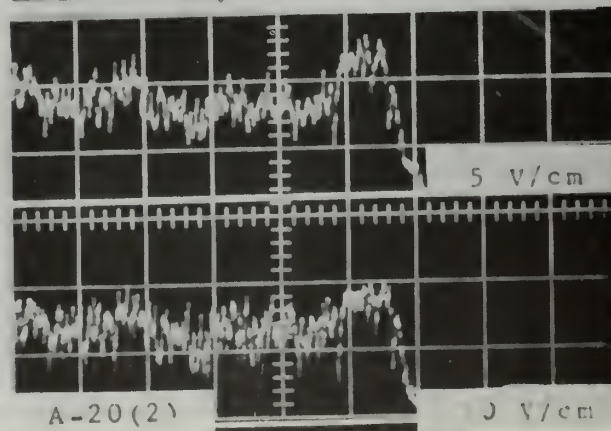
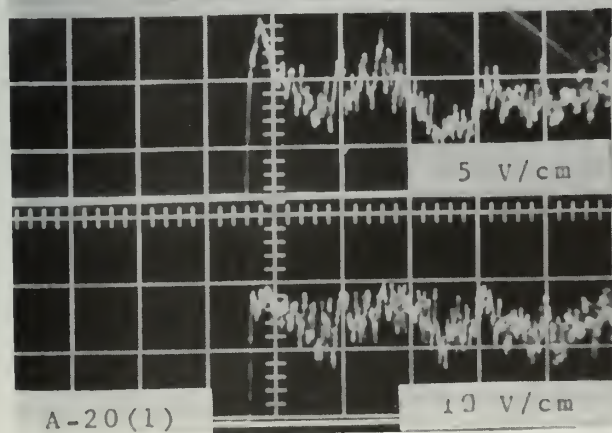
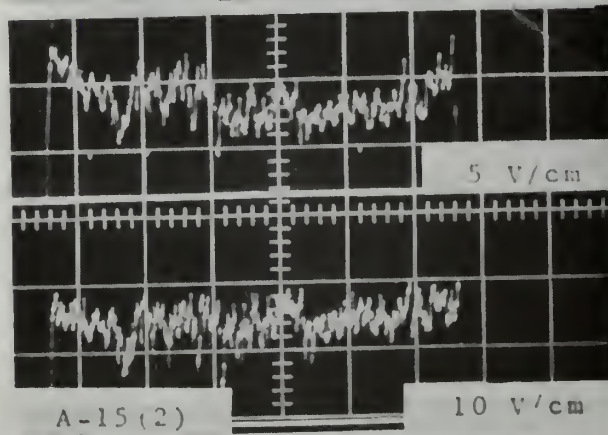
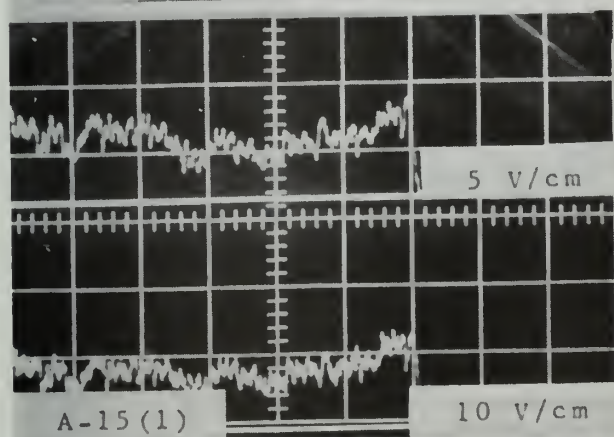
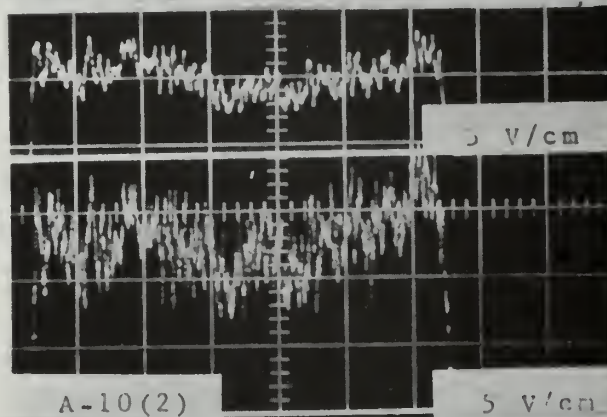
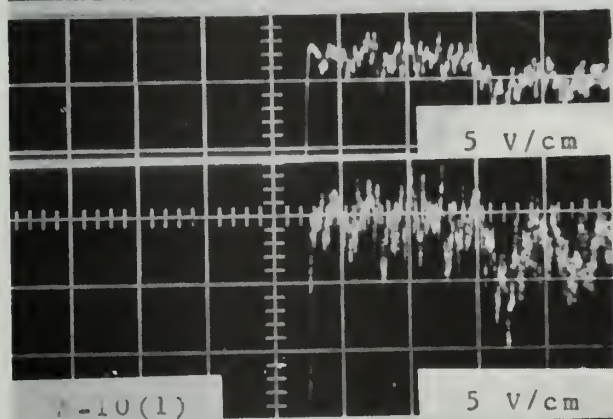
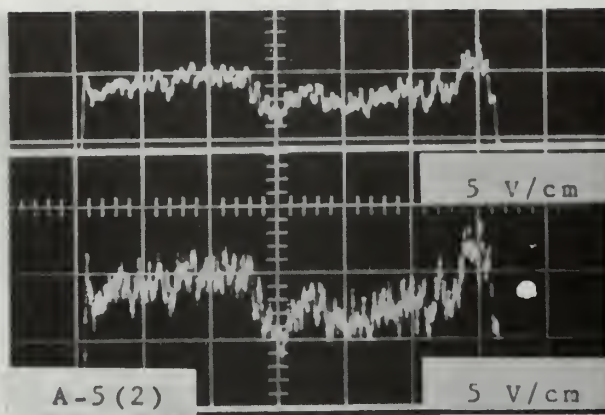
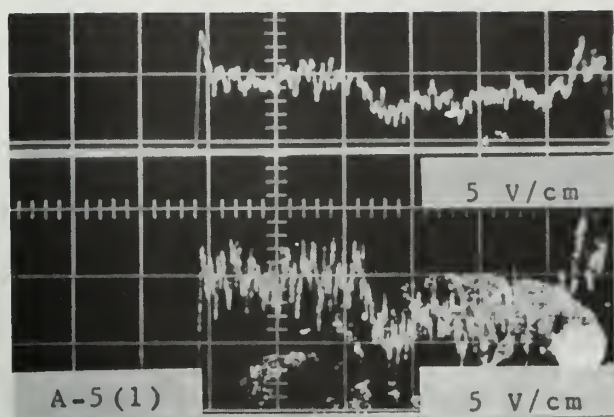


## TABLE II

## OSCILLOSCOPE TRACES FOR THE CUTTING TRIALS

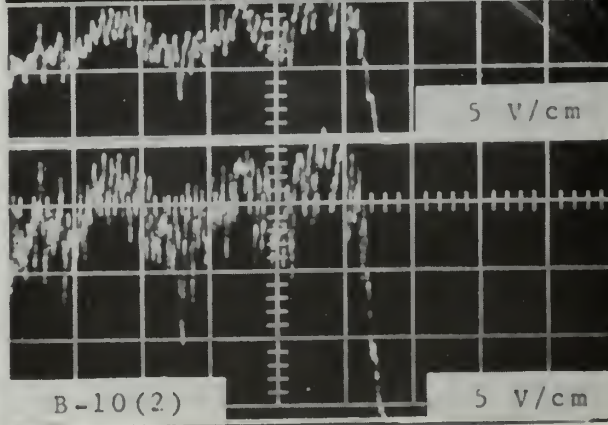
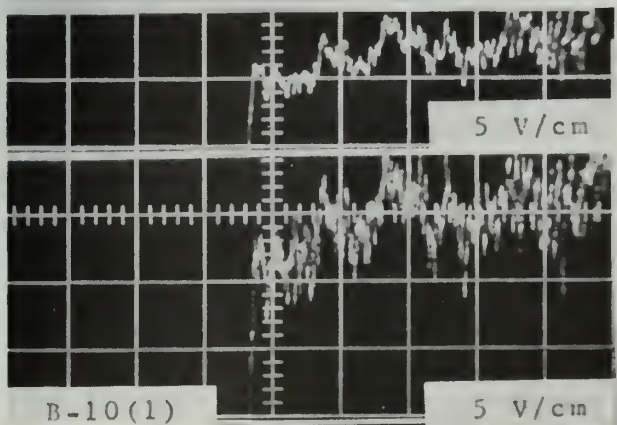
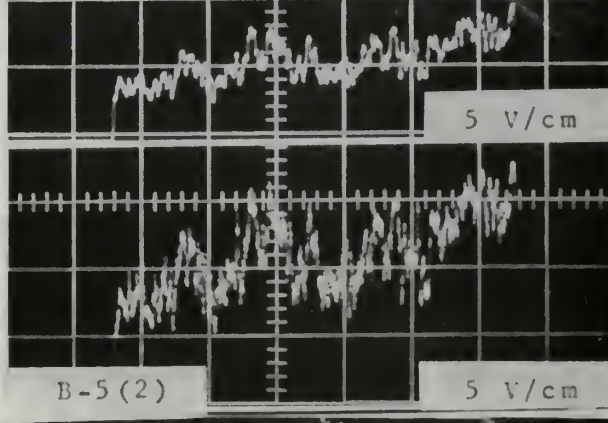
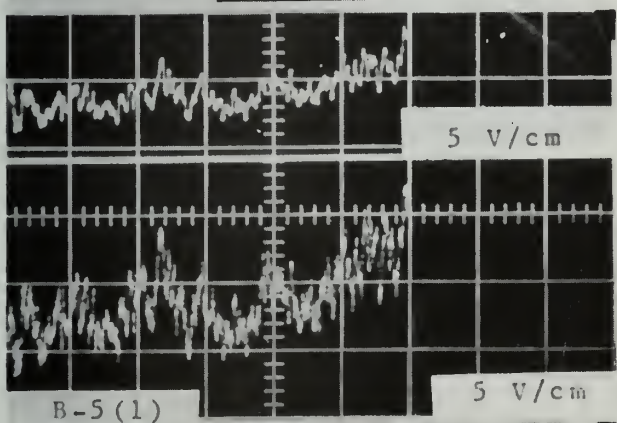
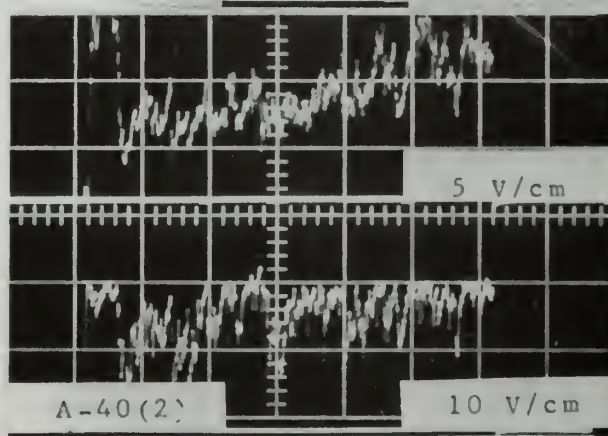
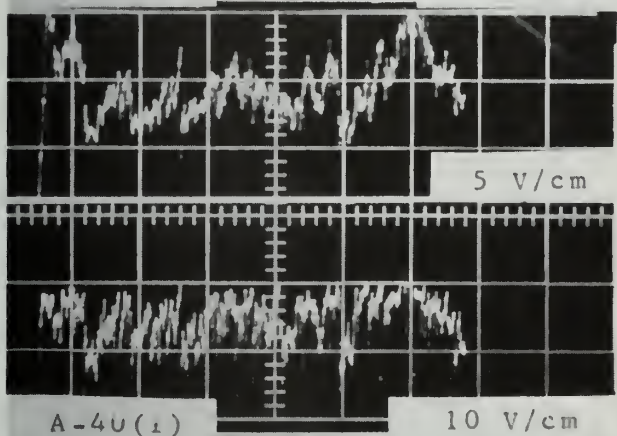
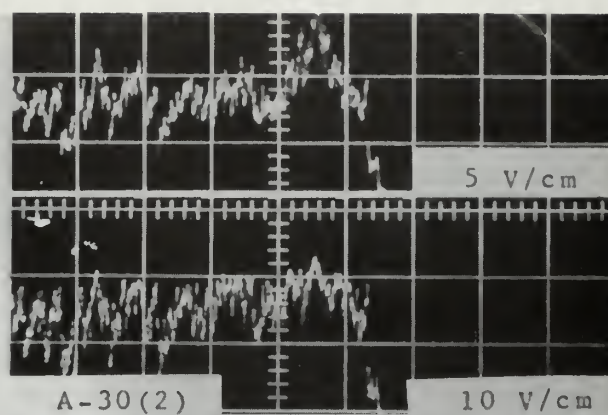
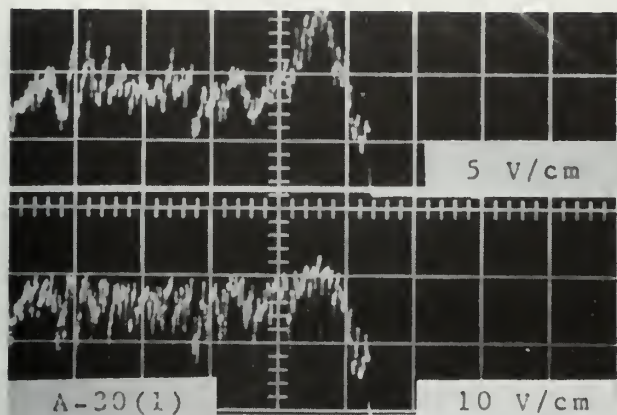
Table II contains the photographs of the oscilloscope traces from which the data in Table I was reduced. In all cases the uppermost trace is vertical force and the lower trace is horizontal force.





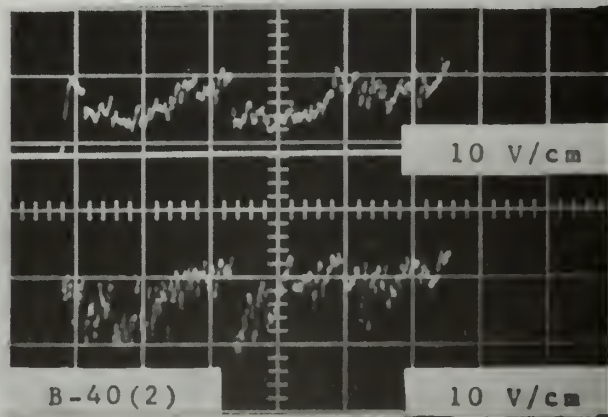
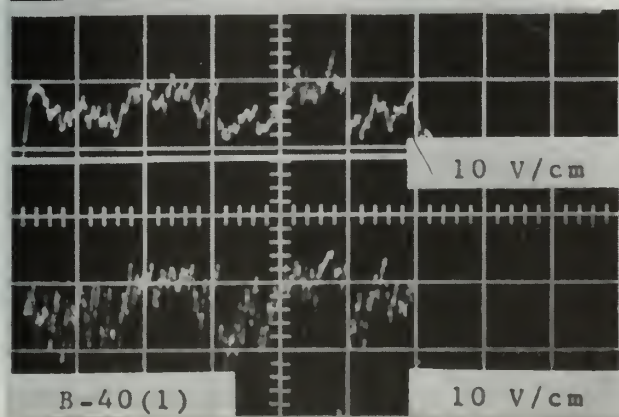
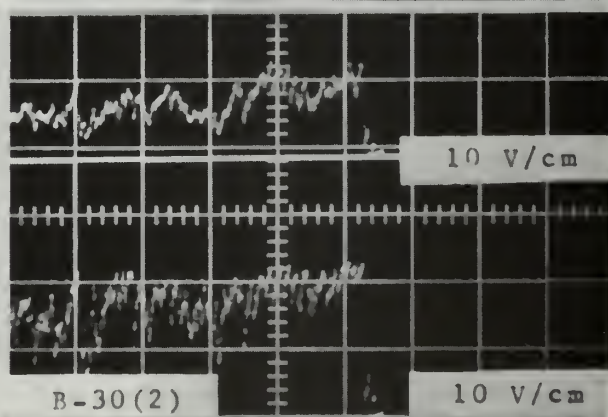
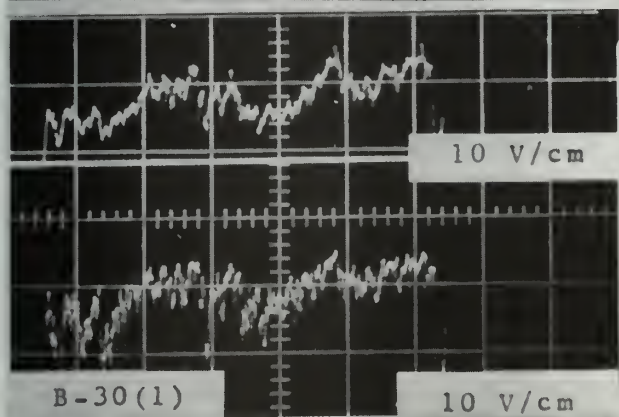
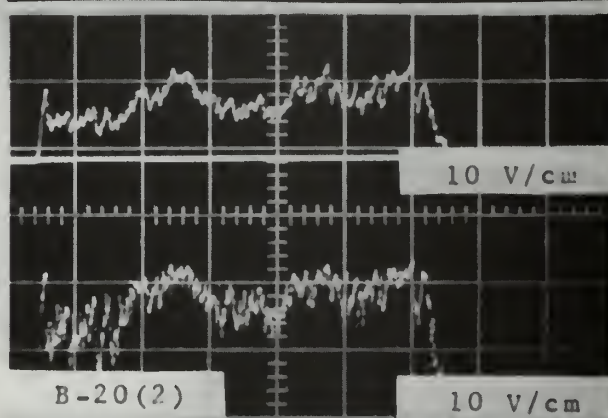
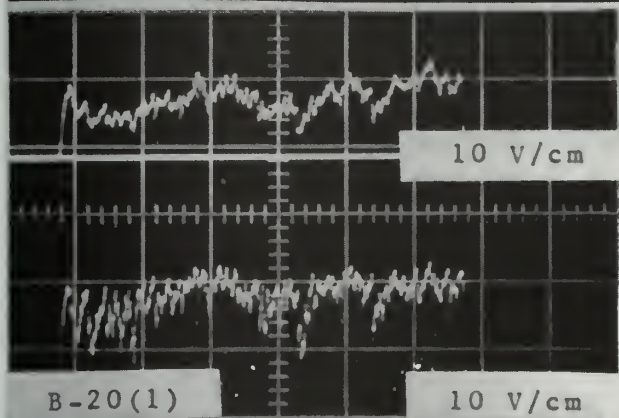
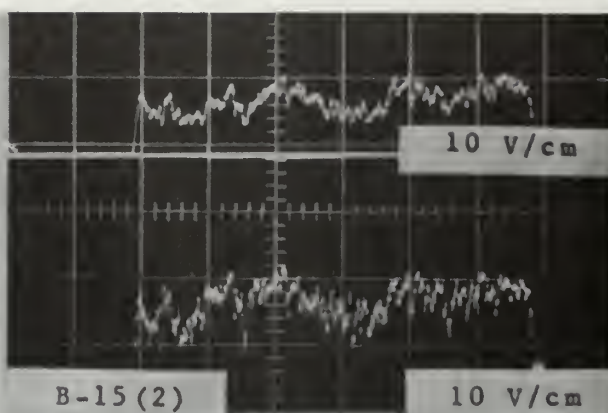
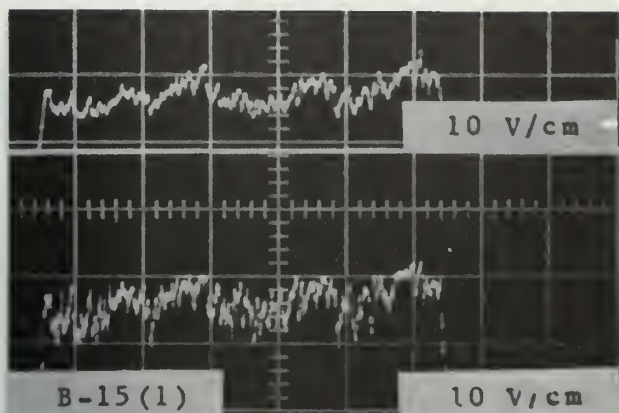






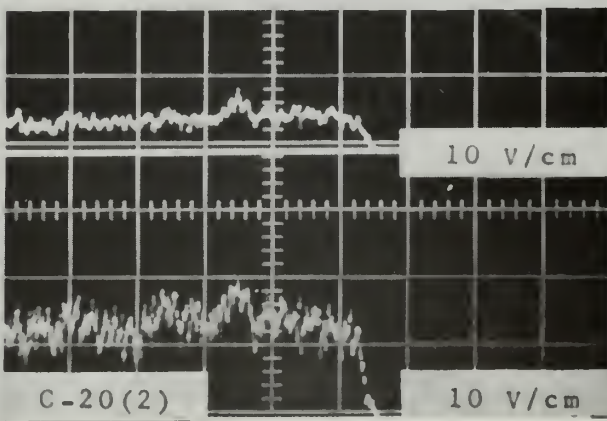
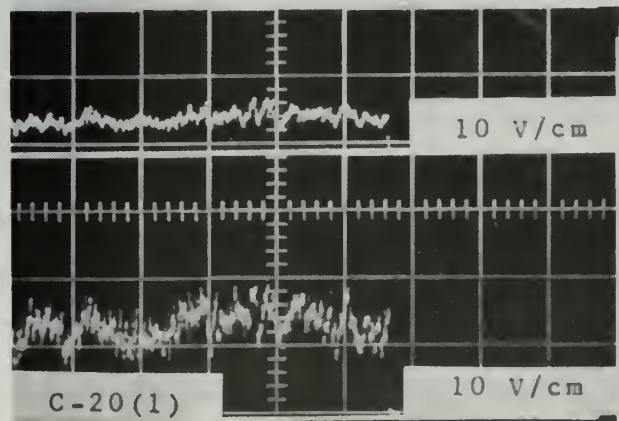
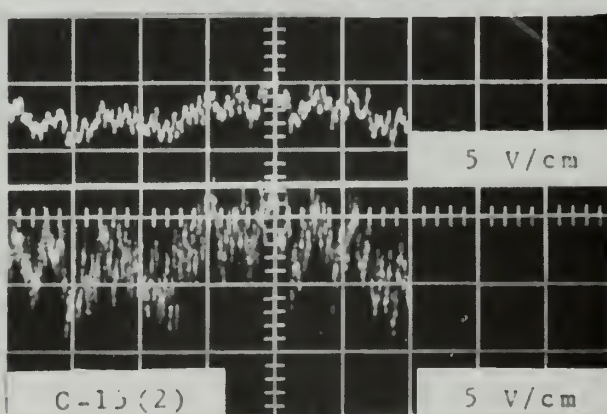
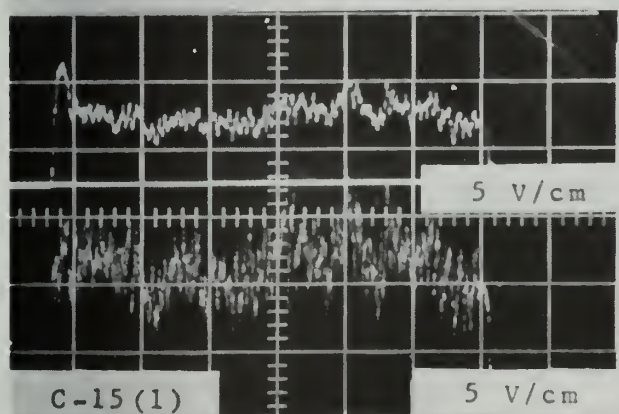
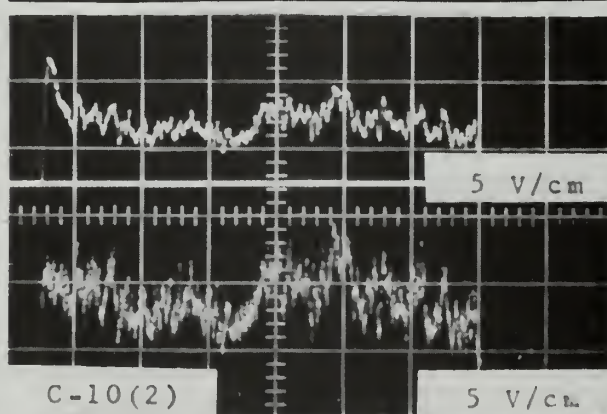
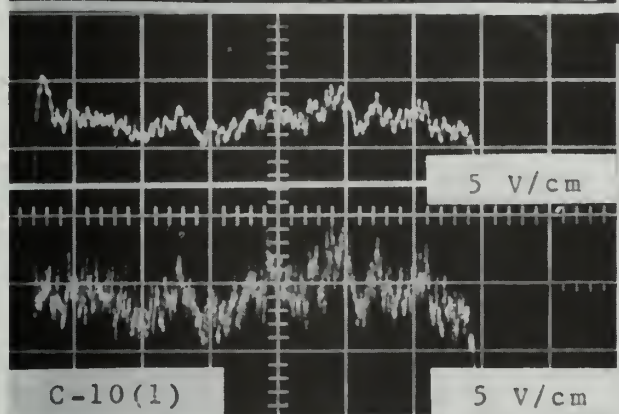
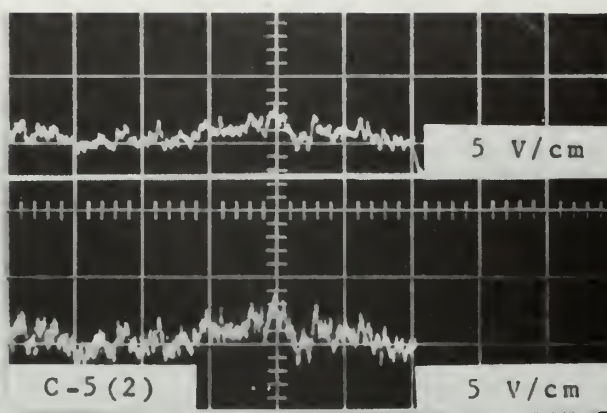
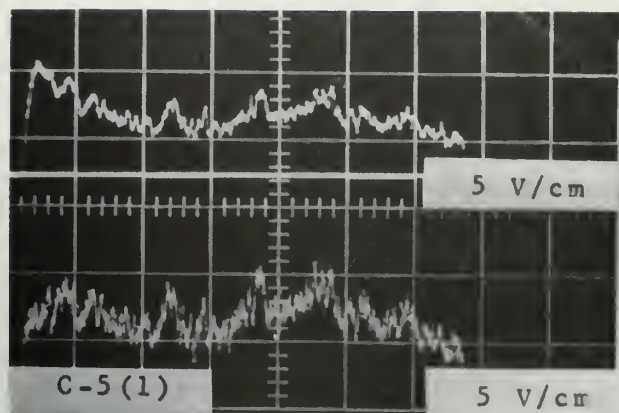






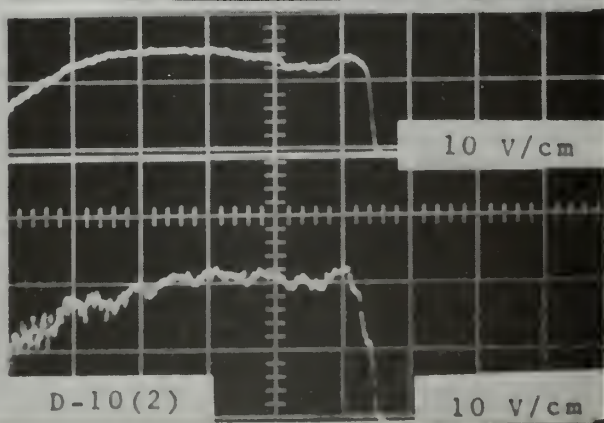
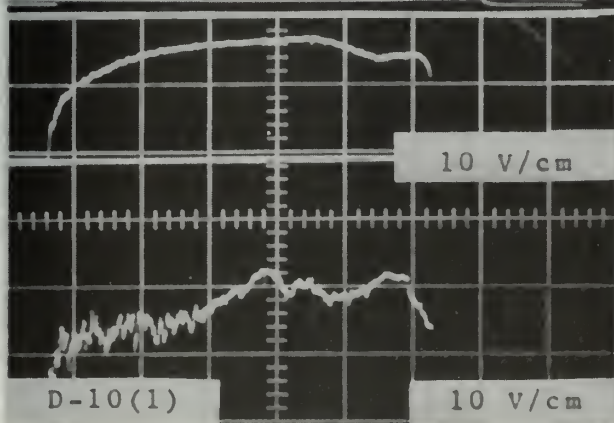
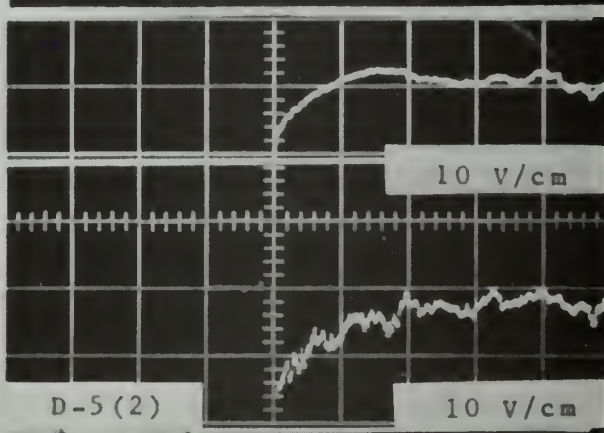
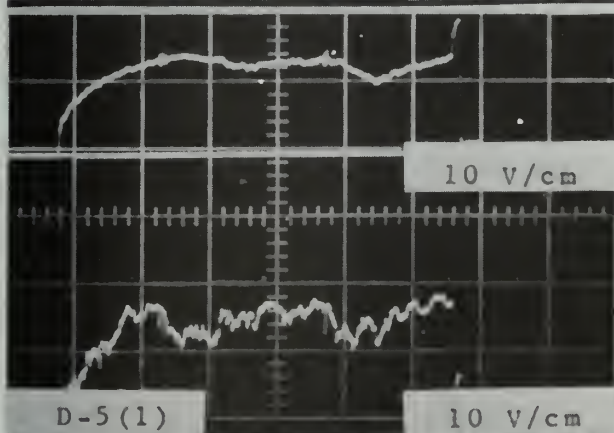
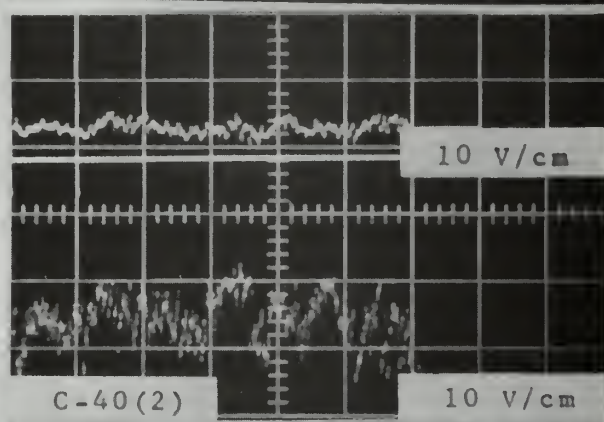
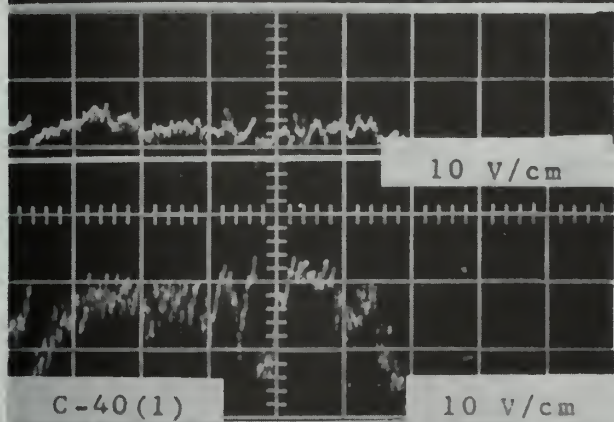
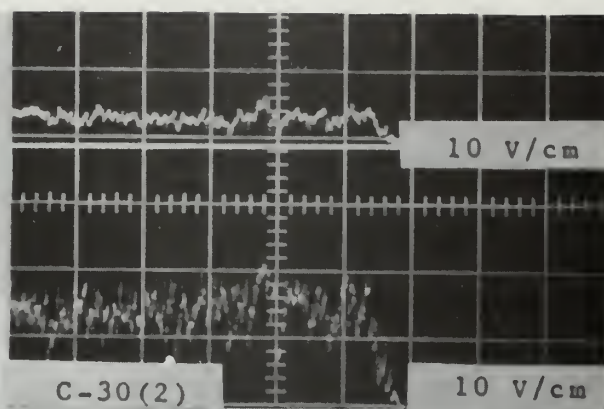
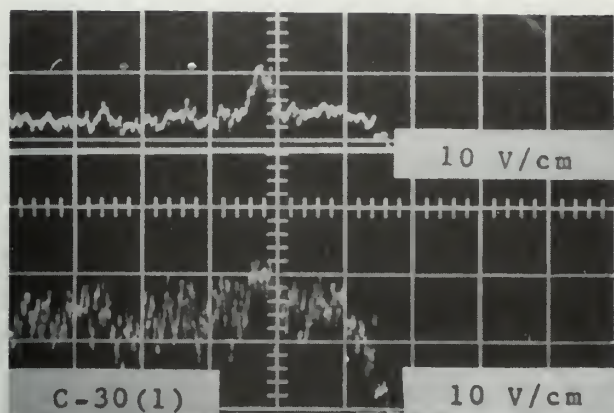




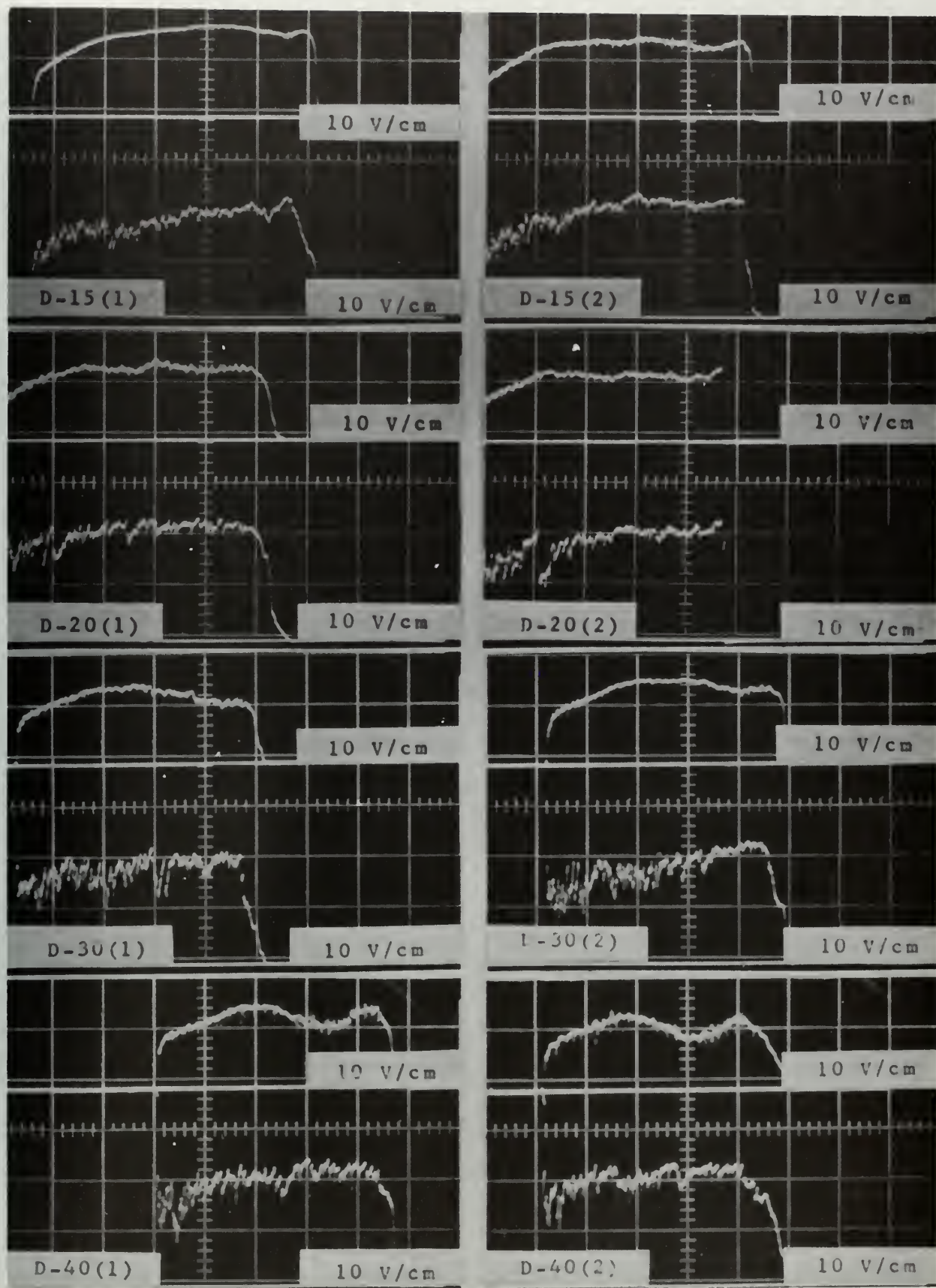






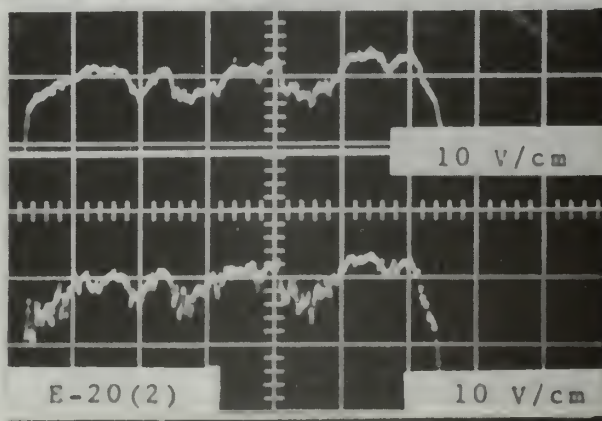
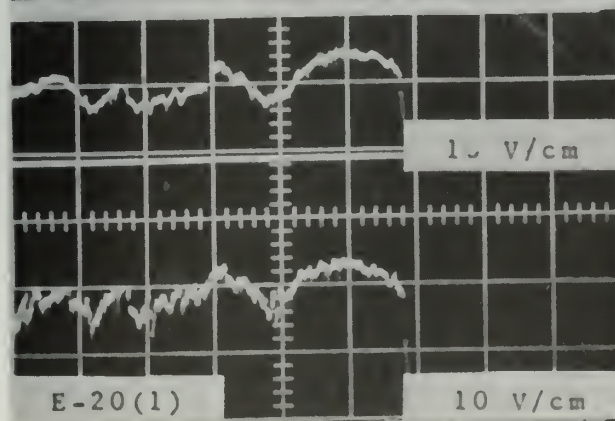
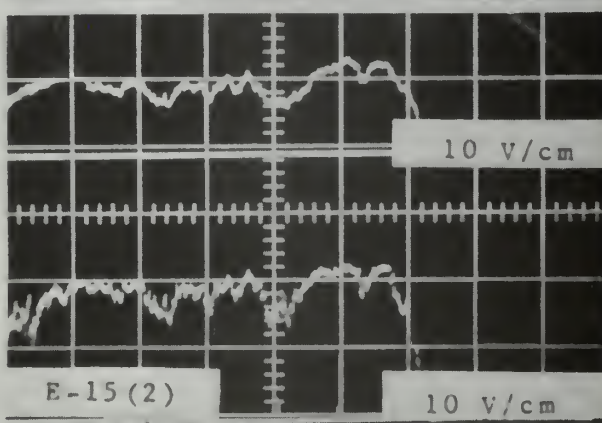
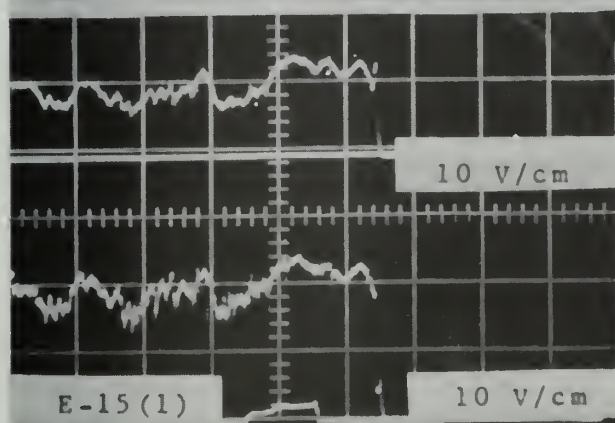
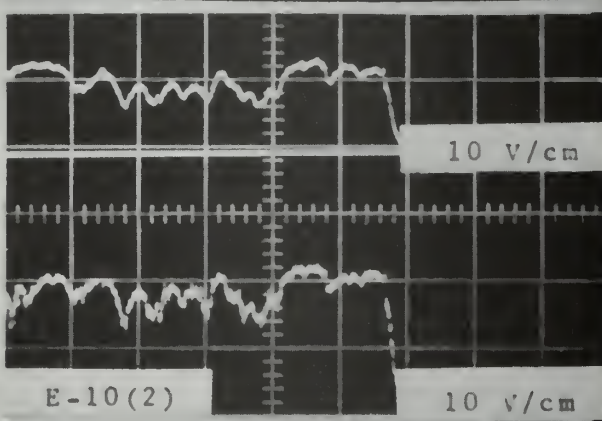
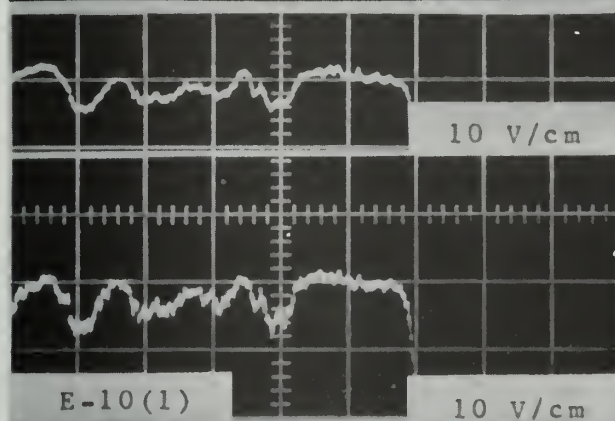
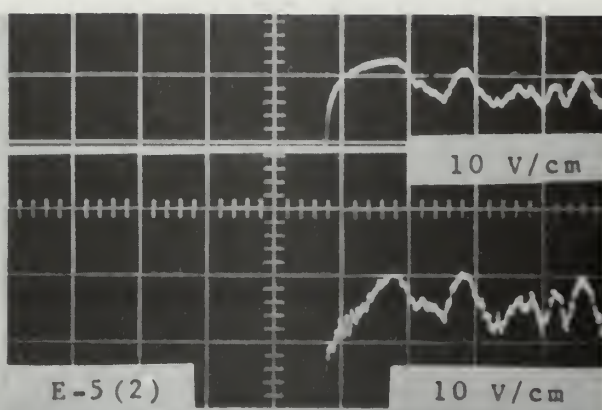
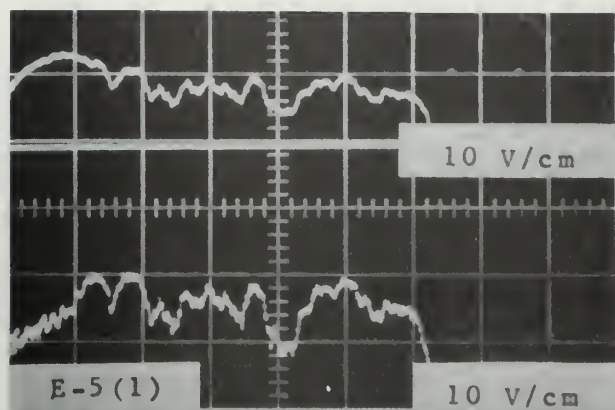






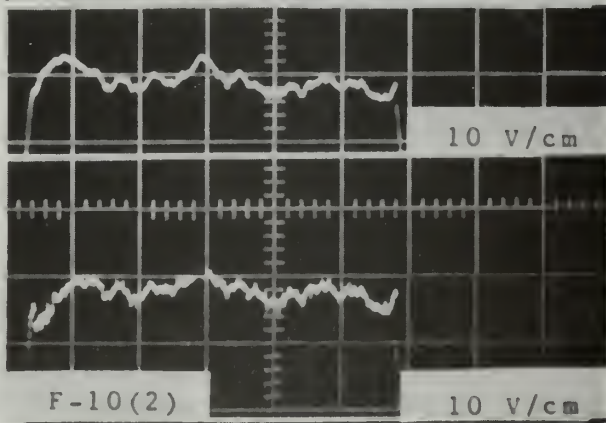
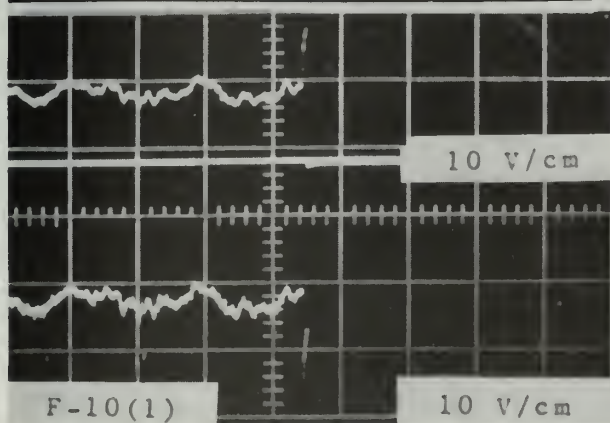
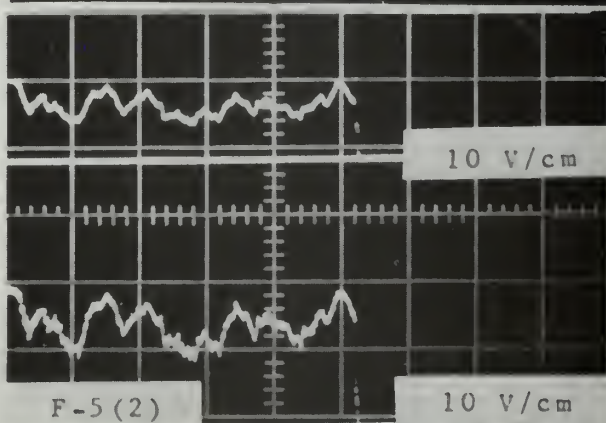
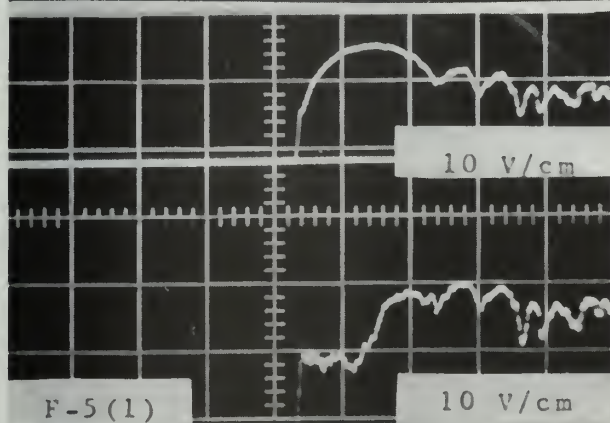
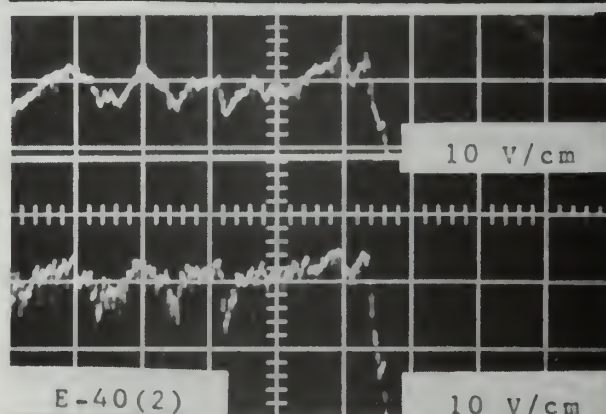
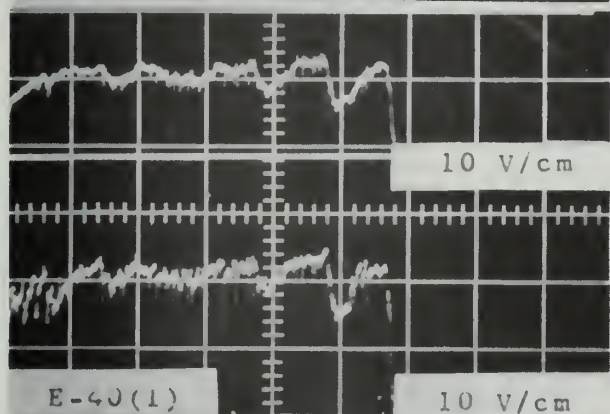
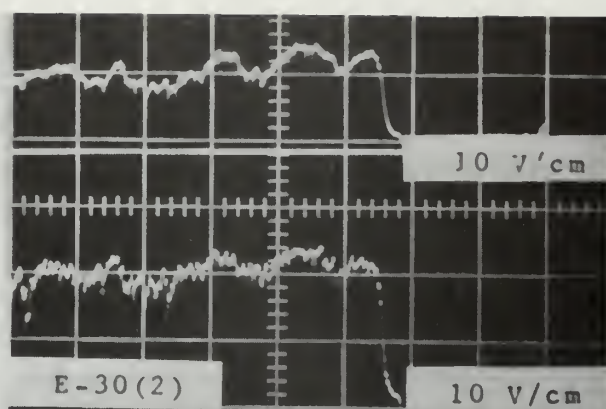
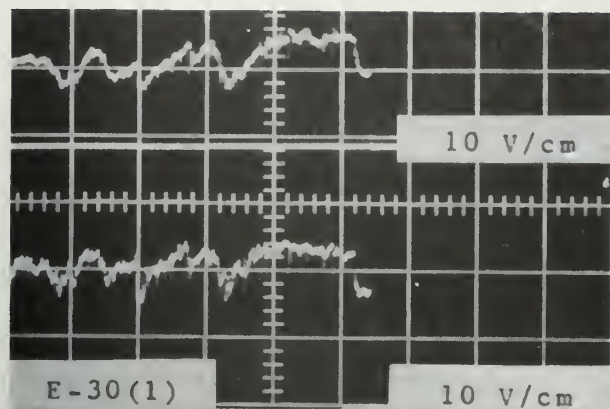




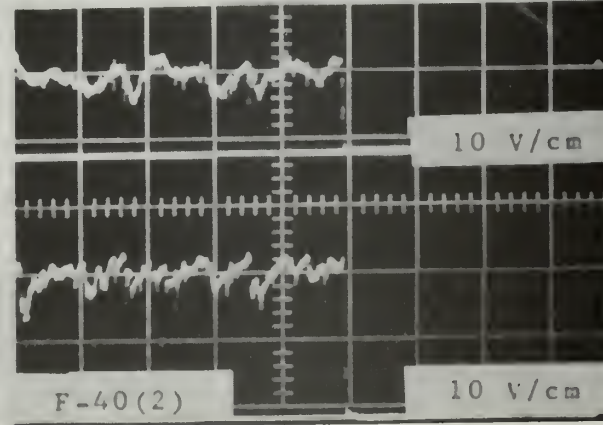
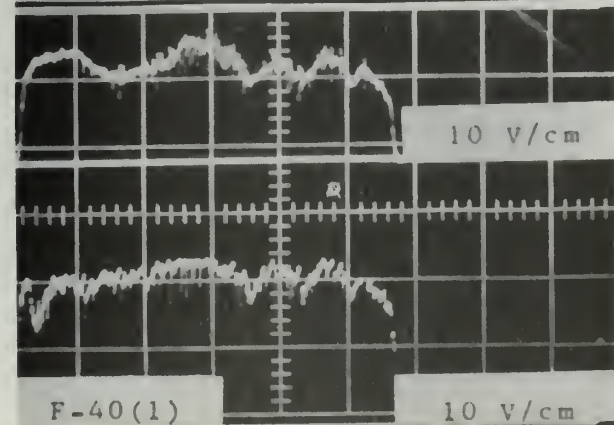
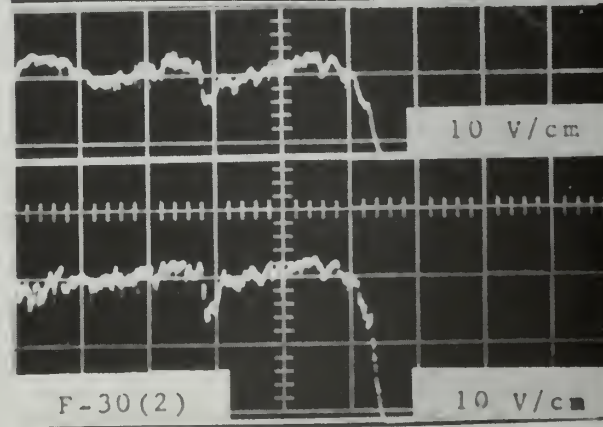
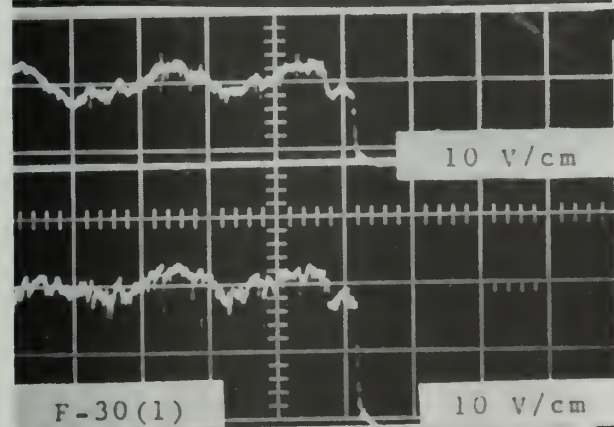
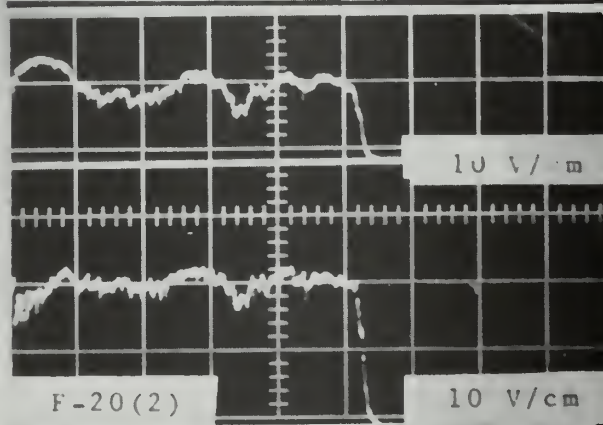
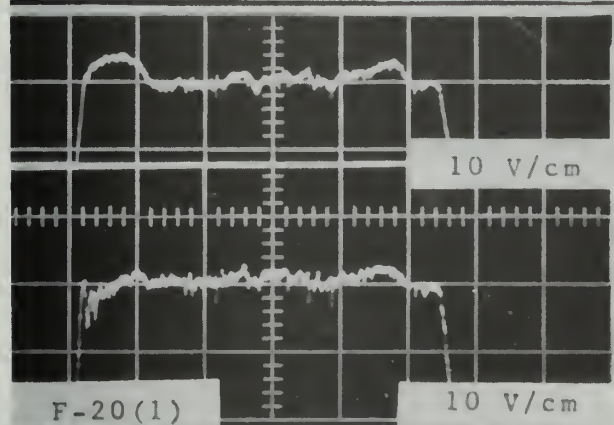
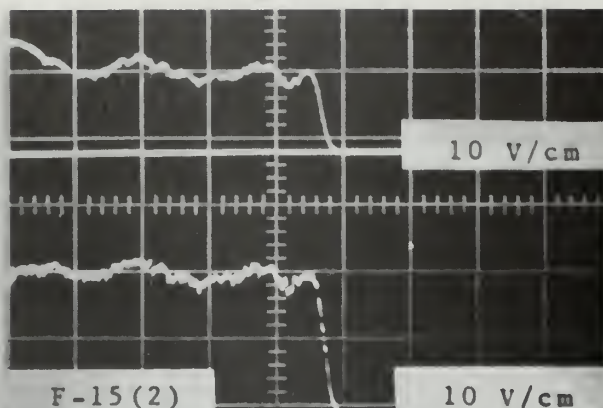
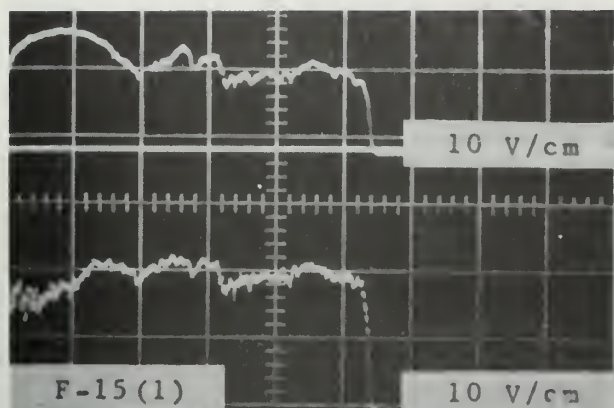






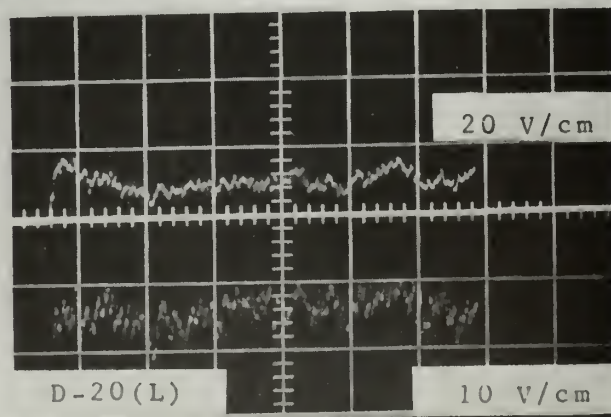
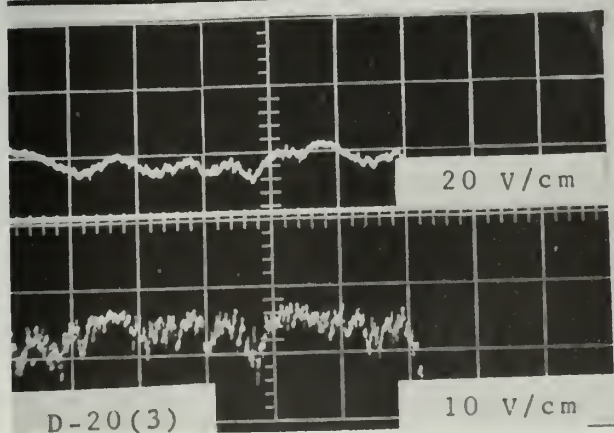
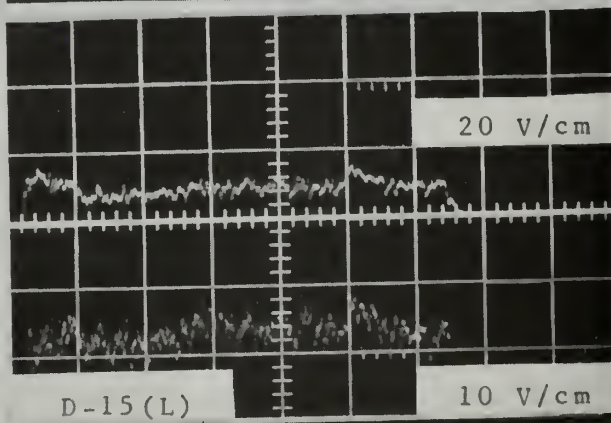
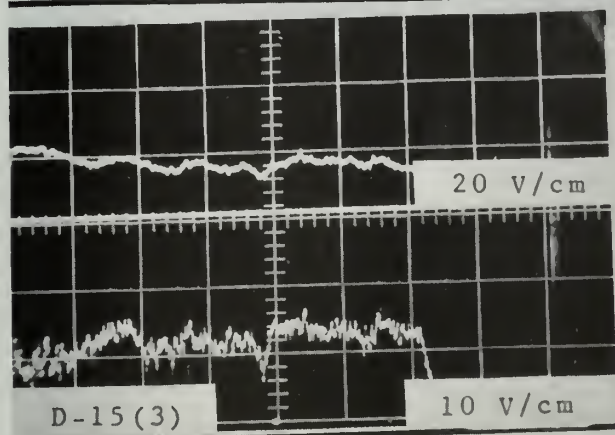
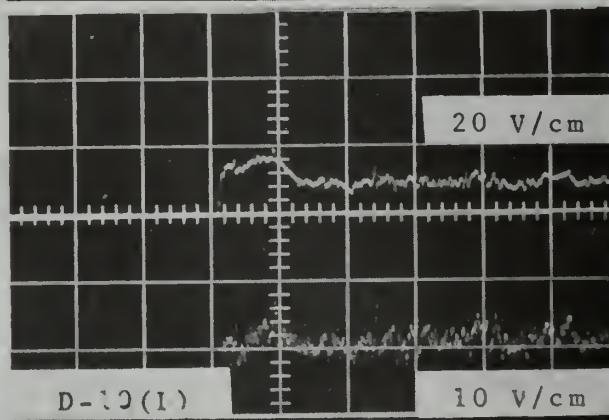
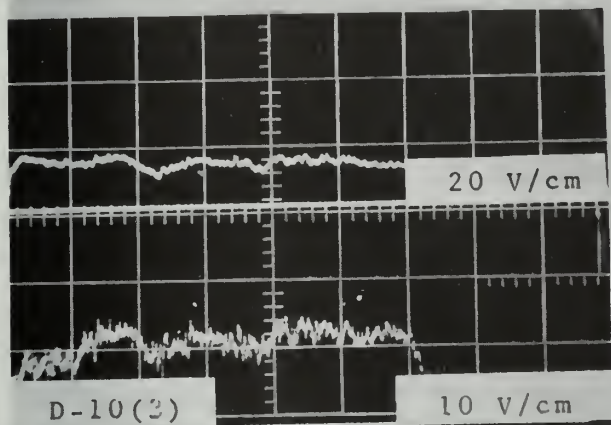
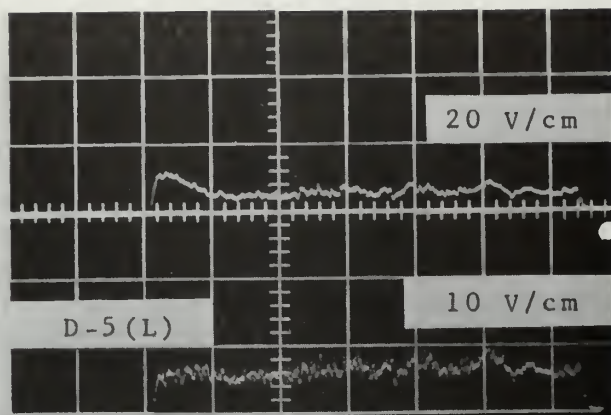
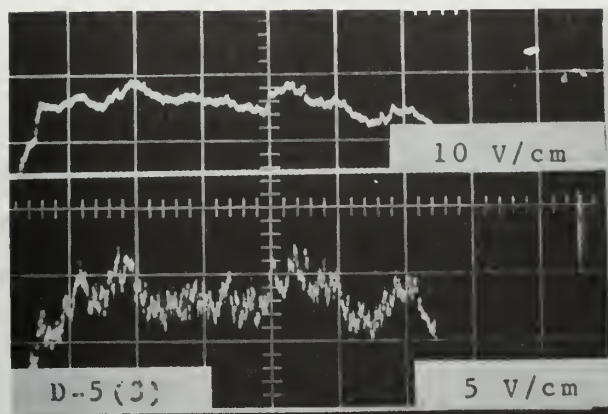




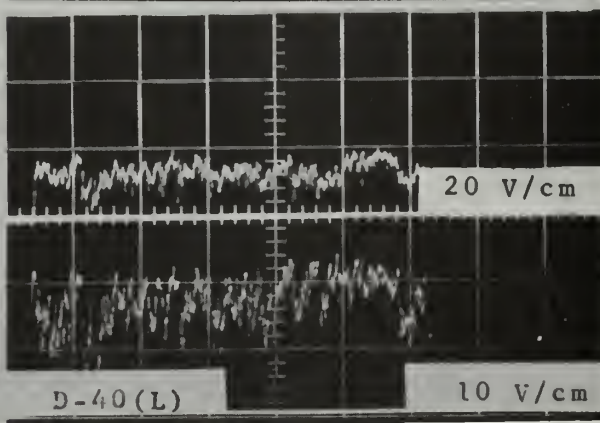
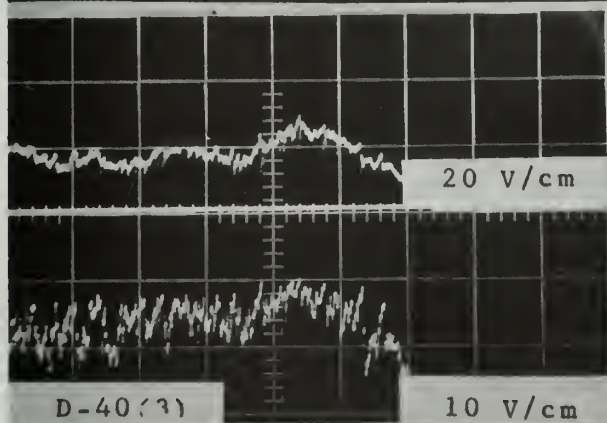
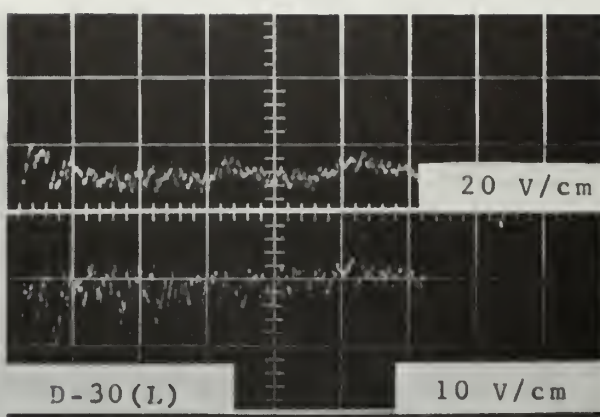
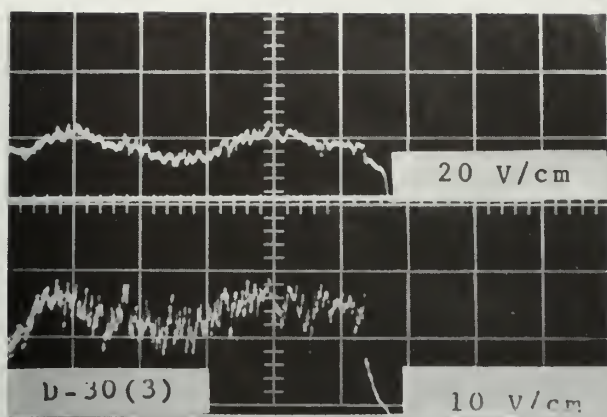
















## APPENDIX IV

### FRICTION TRIAL DATA

Table III contains basic force data computed from the oscilloscope traces displayed in Table IV.

#### TABLE III

##### MAXIMUM FORCE COMPONENTS AND OPERATING DATA FOR THE FRICTION TRIALS

Table III contains basic operating data from the friction trials. The trials are numbered 1 through 14. Trials 1 through 4 measure tool-to-rock friction, dry. Trials 5 through 9 measure tool-to-rock friction, lubricated. Trials 10 through 14 measure rock-to-rock friction, dry. In all cases the speed of the ram was the same as for the cutting trials, 15 feet per minute.

Force components were computed from deflections using the calibration constants recorded in Appendix II.



# Tool-Rock Friction Coefficient

TRIAL	OSCILLOSCOPE SETTINGS		MAXIMUM CHART DEFLECTION, CM		MAXIMUM FORCE COMPONENTS ON CUTTING TOOL, LBS		Measured $\mu = \tan \theta = \frac{F_h}{F_v}$		$\mu_{static}$	$\mu_{dynamic}$
	Sweep Speed, sec/cm	Gain, Ver	V/cm Hor	$D_v$	Static $D_h$	Dy-namic $D_h$	$F_v$	Static $F_h$	Dy-namic $F_h$	
<u>Dry Trials:</u>										
1	50	1	1	.20	.16	.11	20	12.0	8.25	.410
2	50	1	1	.48	.24	.19	48	18.0	14.25	.297
3	50	1	1	.69	.31	.22	69	23.2	16.5	.239
4	50	1	1	1.05	.51	.43	105	38.2	32.2	.307
<u>Lubricated Trials:</u>										
5	50	1	1	.17	.06		17	4.5		.265
6	50	1	1	.30	.12		30	9.0		.300
7	50	1	1	.60	.20	.11	60	15.0	8.25	.143
8	50	1	1	.72	.22	.15	72	16.5	11.25	.156
9	50	1	1	1.01	.39	.19	101	29.2	14.25	.141



# Rock-Rock Friction Coefficient

TRIAL	OSCILLOSCOPE SETTINGS		MAXIMUM CHART DEFLECTION, CM		MAXIMUM FORCE COMPONENTS ON CUTTING TOOL, LBS	
	Sweep Speed, sec/cm	Gain, Ver	V/cm Hor	D <sub>v</sub>	D <sub>h</sub>	F <sub>v</sub> F <sub>h</sub>
<u>Dry Trials:</u>						
10	50	1	1	.12	.10	12 7.5 .625
11	50	1	1	.32	.24	32 18.0 .565
12	50	1	1	.40	.30	40 22.5 .565
13	50	1	1	.71	.60	71 45.0 .635
14	50	1	1	1.12	1.00	112 75.0 .670

$$\mu = \tan \theta = \frac{F_h}{F_v}$$

Measured

NOTE: Static and dynamic friction factors indistinguishable.

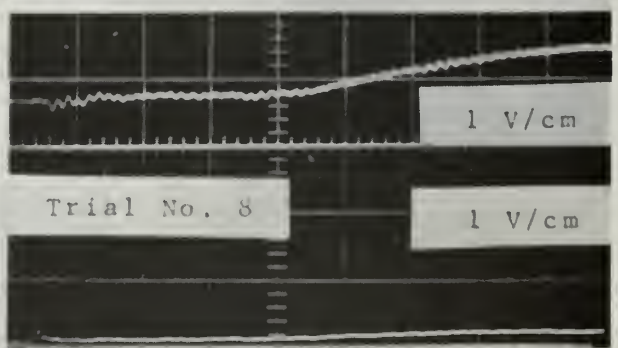
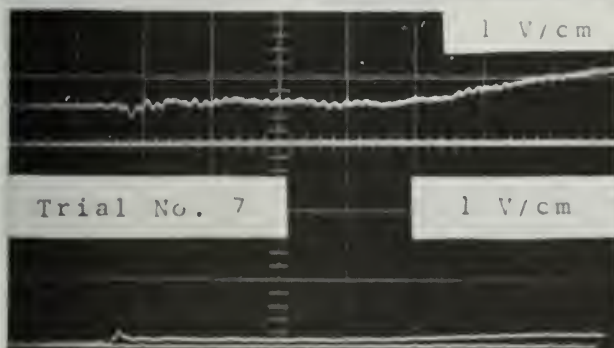
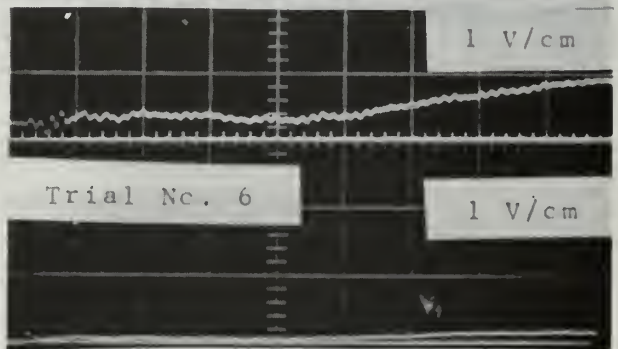
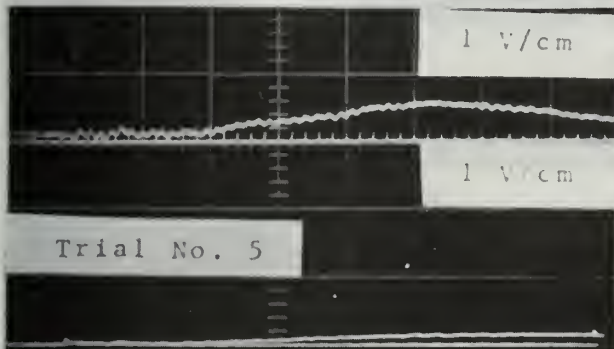
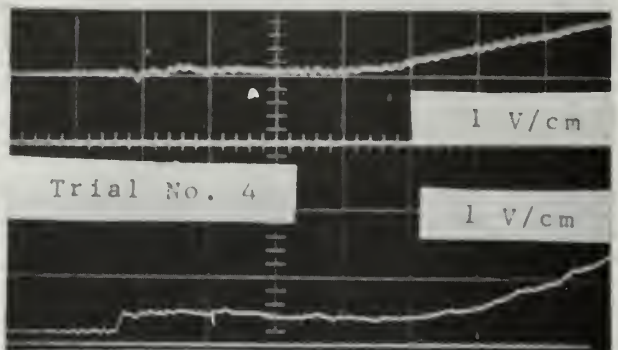
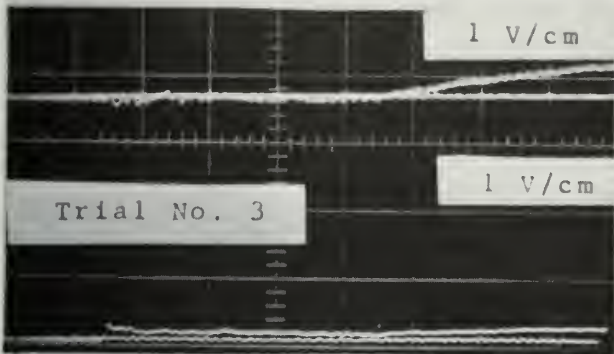
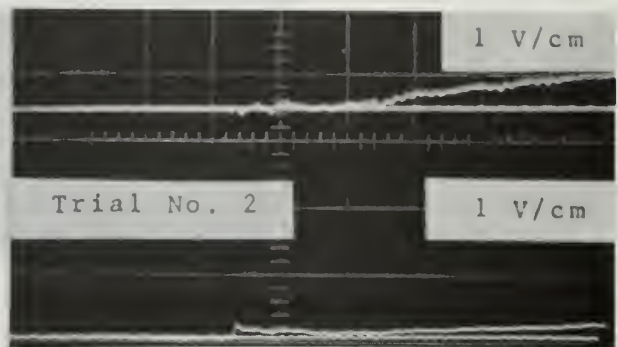
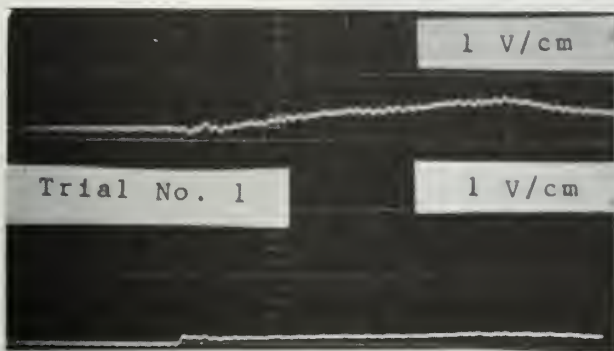


TABLE IV  
OSCILLOSCOPE TRACES FOR THE FRICTION TRIALS

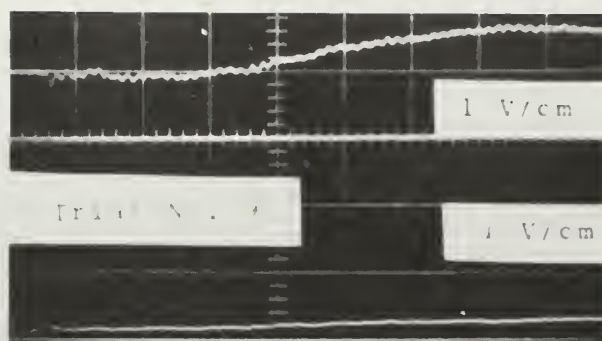
Table IV contains the photographs of the oscilloscope traces from which the data in Table III were reduced. In all cases the uppermost trace is the vertical force and the lower trace is the horizontal force.



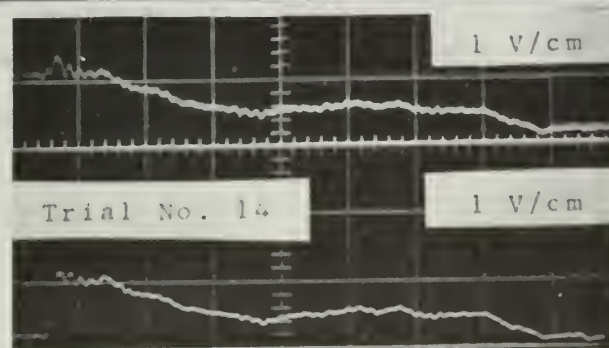
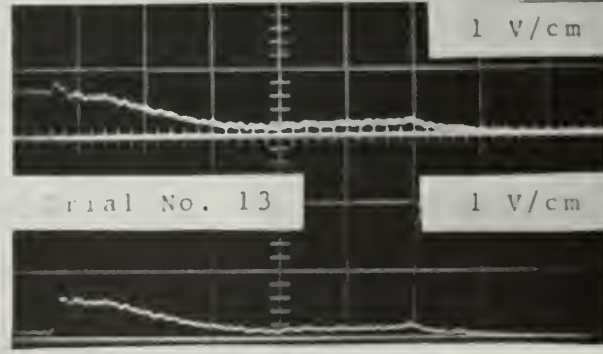
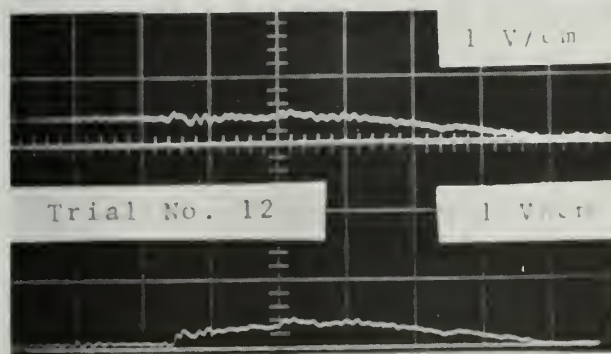
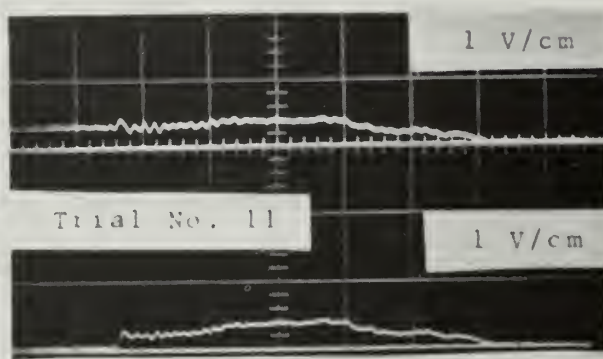
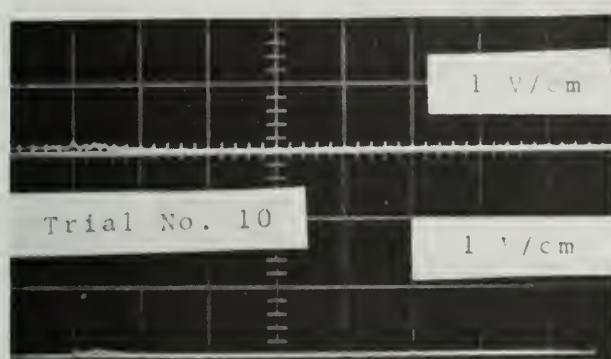








## ROCK-ROCK FRICTION





## VITA

Hugh Albert Crisp was born at Dallas, Texas, on February 15, 1932, the son of Marshall Clayborne and Kathleen Crisp. He attended public schools in Riverdale and University Park, Maryland; Washington, D.C.; Cleveland Heights, Ohio; and Richland and Lynden, Washington; graduating from Lynden High School in 1950. After a year's employment by the Bellingham Coal Mines, he entered Western Washington College of Education at Bellingham, Washington. In 1953 he transferred to the State University of Washington at Pullman, where he received his Bachelor of Science degree in Mining Engineering in 1955.

Following a short period of employment with Allis-Chalmers Manufacturing Company at Milwaukee, Wisconsin, Crisp entered the Navy and was commissioned in the Civil Engineer Corps in October, 1956. He has had duty at the Naval Postgraduate School, Monterey, California; the Naval Communications Station, Adak, Alaska; and the Naval Air Station, North Island, San Diego, California. He was selected for postgraduate education in Petroleum





Engineering and entered the Graduate School of The University of Texas in June, 1962.

Crisp was married to Grace Van Woudenberg on September 18, 1954. They have two children, Kathleen Margaret, age 4, and Marshall Steven, age 2.

Permanent address: % Mrs. K. F. Crisp  
326 West Mercer Street  
Seattle 99, Washington

This thesis was typed by Maxine R. DeButts.

Multilithed by Aztec Printing Company.

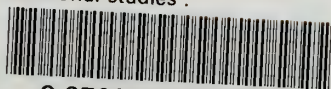






thesC867

Additional studies :



3 2768 001 02460 7  
DUDLEY KNOX LIBRARY